Measured Changes in C-Band Radar Reflectivity of Clear Air Caused by Aircraft Wake Vortices

Anne I. Mackenzie
Langley Research Center • Hampton, Virginia

Contents

Symbols

B	radar receiver bandwidth
C_n^2	refractive index structure constant
c	speed of light
D	antenna diameter
G	antenna gain
k	Boltzmann's constant
L	loss
l_m	Kolmogorov microscale
N	noise power
n	refractive index
P_t	peak transmitted power
P	pressure
R	range
S	signal power
T	temperature
T_s	system equivalent noise temperature
t	number of sample standard deviations away from mean, used in statistical calculations where sample population is small enough that true standard deviation is unknown
V	range cell volume
v	kinematic viscosity
α	angular width of radar target
ε	turbulent eddy dissipation rate
η	volume radar reflectivity
θ	antenna two-sided 3-dB beamwidth
λ	radar wavelength
σ	radar cross section
τ	range gate length

Abstract

Wake vortices from a Lockheed C-130 airplane were observed at the NASA Wallops Flight Facility with a ground-based, monostatic C-band radar and an antenna-mounted boresight video camera. The airplane wake was viewed from a distance of approximately 1 km, and radar scanning was adjusted to cross a pair of marker smoke trails generated by the C-130. For each airplane pass, changes in radar reflectivity were calculated by subtracting the signal magnitudes during an initial clutter scan from the signal magnitudes during vortex-plus-clutter scans. The results showed both increases and decreases in reflectivity on and near the smoke trails in a characteristic sinusoidal pattern of heightened reflectivity in the center and lessened reflectivity at the sides. Reflectivity changes in either direction varied from −131 to −102 dBm^{-1}; the vortex-plus-clutter to noise ratio varied from 20 to 41 dB. The radar recordings lasted 2.5 min each; evidence of wake vortices was found for up to 2 min after the passage of the airplane. Ground and aircraft clutter were eliminated as possible sources of the disturbance by noting the occurrence of vortex signatures at different positions relative to the ground and the airplane. This work supports the feasibility of vortex detection by radar, and it is recommended that future radar vortex detection be done with Doppler systems. (This paper was written in January 1997.)

1. Introduction

From January through May 1995, the Sensors Research Branch of Langley Research Center tested X-band and C-band radars to determine the characteristics of ground-based wake vortex detection at those frequencies. The Radar Wake Vortex Experiment is part of the NASA Reduced Spacing Operation/Terminal Area Productivity (RSO/TAP) program, which seeks to improve aircraft throughput at busy airports while maintaining current safety standards. At present, aircraft, when landing or taking off, are spaced at standard distances according to their relative sizes and weights to prevent the upset or disturbance that can occur when one aircraft flies through the wake vortices produced by another. Radar is a sensor that can determine the presence, location, and longevity of vortices. With information provided by such a sensor, air traffic controllers could space aircraft according to the detected hazard rather than using standard separations which might be longer than necessary.

In an effort to find the best frequency for all-weather wake vortex detection, initial tests were conducted at Wallops Island with a permanently installed C-band radar in conjunction with an experimental X-band radar connected to the inner portion of the nearby Wallops ultrahigh-frequency (UHF) antenna. Because it had already been well established that X-band radars could detect rain by Rayleigh scattering, the Wallops tests were performed in clear weather to test for detection of air turbulence by Bragg scattering.[1] The X-band radar system, the principal one under test, was slaved to the C-band radar antenna; therefore, data were acquired by both systems simultaneously. Both radars scanned across the wake of a Lockheed C-130 airplane for about 2 min after the passage of the airplane. The C-130 had been fitted with smoke pods to give a visual indication of the position of the wake vortices. Although not designed for the purpose of vortex detection, the C-band radar provided auxiliary information that, it was hoped, would assist in validation of the X-band detection of Bragg-scattered signals from the aircraft-generated vortices.

Analysis of the C-band data, which consisted of signal magnitudes at one range gate selected for each pass, showed an identifiable signature that lasted for up to 2 min after passage of the airplane. Particularly evident during azimuth scans across the wake, the vortex-plus-clutter signal magnitude consistently varied from the clutter magnitude in a roughly sinusoidal pattern in the immediate vicinity of the wake. Assuming that the changes in magnitude were caused by vortex backscattering, one sees the vortex effect as an increase or decrease in reflectivity between −131 and −102 dBm^{-1}, more typically between −120 and −110 dBm^{-1}. The following report is organized into sections on previous related work at C-band frequencies, the experimental setup, radar calibrations, clutter tests, and the C-band analysis. Interesting signal returns and simultaneous airplane tracks relative to the radar, weather data, and plots of clutter-variability data are provided in the appendices.

---

[1]In Rayleigh scattering, targets, such as raindrops, have well-defined boundaries and are much smaller than the electromagnetic waves reflected from them. In Bragg scattering, a distributed target, such as turbulent air, reflects electromagnetic waves at half-wave intervals that sum coherently to produce a stronger signal than the reflections from other parts of the target.

2. Background

Since the 1930's, radar meteorologists have studied clear-air turbulence as a natural, meteorological phenomenon (ref. 1). In recent years, some of the theory developed for meteorology has been applied to the study of aircraft wake vortices. For example, Tatarski (ref. 2) related the radar volume reflectivity of turbulent air to the structure constant and the radar wavelength with the equation

$$\eta(\lambda) \approx 0.38 C_n^2 \lambda^{-1/3} \tag{1}$$

where

η = volume radar reflectivity

C_n^2 = structure constant, a measure of variability of refractive index field within inertial subrange

λ = radar wavelength, $\lambda/2$ being included in inertial subrange

According to Kolmogorov's theory (ref. 3), for incompressible,[2] locally isotropic fluids having a sufficiently high Reynolds number, there exists an inertial subrange of turbulent eddy sizes, defined as those sizes of eddies that break down into smaller eddies with no loss of kinetic energy. The low end of the inertial subrange, called the Kolmogorov microscale, is predicted as

$$l_m = \left(\frac{v^3}{\varepsilon}\right)^{1/4} \tag{2}$$

where

l_m = Kolmogorov microscale

v = kinematic viscosity

ε = eddy dissipation rate

Equation (1) has been applied to the estimation of radar reflectivity of aircraft-induced turbulence. Aircraft-wake-vortex-induced C_n^2 depends on such aircraft factors as weight, velocity, and wingspan, as well as on such meteorological factors as temperature (T), pressure (P), partial pressure of water vapor, and prevailing winds. Proctor (ref. 5) has adapted his two-dimensional terminal area simulation system (TASS) to model wake vortices over time, given initial aircraft and atmospheric conditions. Currently this work is being expanded into a three-dimensional model. Among the TASS outputs are T, P, and ε. Marshall and Scales (ref. 6) are using the TASS outputs for various airplanes in varying weather conditions together with Ottersten's theory (ref. 7) and equation (1) to predict C_n^2 and η. These estimates will be improved as assumptions are validated with experimental tests and the vortex atmospheric and radar models are refined.

The two-dimensional TASS model[3] predicted that a C-130 in a standard atmosphere with no crosswind should produce a pair of vortices whose total spatial extent is 80 m in width by 60 m in height 30 sec after passage of the airplane. The core radius, that distance from one vortex center to the location of highest tangential velocity for that vortex, was calculated to be 5 m (ref. 6). Marshall's current work (ref. 6) predicts that the proper scales of turbulence and, therefore, sufficient reflectivity should exist at C-band frequencies to allow wake vortex detection.

In the summer of 1990, W. H. Gilson of the Massachusetts Institute of Technology Lincoln Laboratory conducted a series of clear-air wake vortex radar tests (ref. 8) at Kwajalein Atoll in the Marshall Islands. The experiment employed seven different radars, one of which was the ALCOR C-band Doppler radar. ALCOR transmitted 10-μsec pulses at 3-MW peak power, using a 0.3° antenna beam. Viewing the wake of a Lockheed C-5A cargo airplane at a look angle varying between 45° and 90° from the longitudinal wake axis, ALCOR successfully detected and tracked the wake at ranges up to 17 km. From the ALCOR data, the calculated τ of the wake was -125 dBm^{-1} at 30 km (260 sec) behind the C-5A and 1524 m (5000 ft) altitude. The η value decreased 10 dB at 3048 m (10000 ft) altitude and another 10 dB at 6401 m (21000 ft) altitude.

In early 1991, J. D. Nespor et al. (ref. 9) conducted further C-band, clear-air, wake vortex radar tests for General Electric Company at White Sands Missile Range, using the Multiple Object Tracking Radar (MOTR). MOTR is a phased array, pulsed Doppler radar that, during the tests, transmitted 1-μsec pulses at 1-MW peak power in a 1° antenna beam. Nespor reported detecting the wake from a Ling-Temco-Vought A-7 small attack jet, looking along the longitudinal wake axis behind the airplane at a range of 2.7 km. Nespor calculated vortex C_n^2 values ranging from -135.4 to -116.6 dB. According to equation (1), this calculation would produce η values in the range from -135.3 to -116.6 dBm^{-1}.

In view of these past experiments, it seemed reasonable to expect that the Wallops R5 C-band radar would detect a C-130 wake at 1-km range, using a 0.4° antenna

---

[2]Turbulent airflow on scales of less than 2 km and close to the ground can be considered incompressible (ref. 4).

[3]TASS initialized its wake vortex calculations based on classic elliptical theory (ref. 5). No provisions were made for aircraft flaps. Some of the initializing assumptions were that initial circulation = 340 m^2/sec, vortex core radius = 2 m, vortex height = 180 m, and vortex separation = 24 m.

2

beam and transmitting 1-μsec pulses at 2.2-MW peak power. Based on available C-band radar system parameters, pre-experiment calculations indicated that the radar would be able to detect wake turbulence having a reflectivity of at least -143.6 dBm^{-1}, obtaining a signal to noise ratio (SNR) of 0 dB or greater.

3. Experimental Setup

3.1. Radar 5

The C-band radar that recorded the vortex data described here is a type AN/FPQ-6 monostatic radar permanently located at Wallops Flight Facility and bearing the Wallops designation R5. In past years, R5 has served to observe meteorological phenomena; recently, it tracked Space Shuttle craft and, at the time of these tests, was configured for that use. The radar parameters for this experiment are compiled in table 1.

Table 1. C-Band Radar 5 Characteristics

Receiver and transmitter:

Transmitted carrier frequency, MHz	5765
Peak transmitted power, MW	2.2
Pulse repetition frequency, Hz	640
Pulse length, μsec	0.25
Range gate length, μsec	0.75
Measured noise 3-dB bandwidth, MHz	4.36
Noise level at the receiver, dBm	−100.6
Number of range gates recorded	1
Data recording rate, Hz	10

Antenna:

Beamwidth, deg	0.4
Diameter, m	8.84
Gain, dB	51
1st sidelobe height, dB	−16.5
Polarization	Vertical
Scanning rate, deg/sec	2
Scanning direction	Az-El
Tower height, m	14.98
Two-way line loss, dB	4.9

R5 radiated sufficient power and measured atmospheric reflections with sufficient spatial resolution to detect vortices. However, R5 recorded data in only one 112.5-m-long range cell per airplane pass, which meant that, as the vortices drifted with the wind, rose, or fell, they could be seen only occasionally in the data record, when they happened to be in the correct range cell. The receiver detected signal magnitudes only, without velocity information. Signal levels were recorded in the form of automatic gain control (AGC) values; at the beginning of each experiment day, the radar was calibrated to establish the correspondence between AGC level and SNR. A calibrated sphere track test was performed once, and from the results of that test, the radar system noise was calculated and later multiplied by the SNR value to determine the absolute signal received. The signal data are

presented in appendix A in a two-dimensional format: signal level versus scan angle at the fixed range for that pass.

At the antenna scan rate of 2°/sec and the sample recording rate of 10 samples/sec, each data point represented a spatial "smear" 0.2° in extent. According to the pulse repetition rate of 640 pulses/sec, each sample was obtained by integrating 64 pulses.

For the work described here, the actual vortex pair width should be the same as the apparent width. Taking into account the convolution of beam shape, AGC response shape, and target shape, modeling shows that targets 1° or more in width will appear at their true width, while targets smaller than 1° will appear larger than their true width. For example, targets 0.5° wide will appear to be 0.7° wide and targets 0.2° or less wide will appear to be 0.5° wide. When aircraft vortices are initially formed, their combined width will be slightly larger than the aircraft wingspan. Because the aircraft wingspan at the longest recorded range provides a lower bound of 1.6° for the true angular width, the vortex pair will occupy more than 1° in any R5 scan.

3.2. C-130 Airplane

NASA 427, a research C-130 airplane, was selected as the wake vortex generator. This airplane has a wingspan of 40.4 m and, during experiment flights, weighed between 64 863 kg (143 000 lb) and 48 895 kg (110 000 lb), depending on how much fuel had been burned. Typically, it flew at 64.3 m/sec (125 knots) airspeed with gear and flaps up. Wing-tip-mounted smoke generators were fueled by corvus oil from a tank in the cargo section and were activated for approximately 30 sec as the airplane flew past the radar stations.

3.3. Scanning Strategies and Flight Patterns

The C-130 airplane flew in level, oval patterns past R5 and the X-band radar, which was slaved to R5. These two radars were sited 539 m apart. Appendix A contains numerous plots of the airplane track that show its relation to the R5 tower position and the radar scan. Data were gathered with the following three antenna scanning strategies depicted in figures 1, 2, and 3, respectively:

1. Head-on azimuth scans: The antenna scanned in an azimuthal plane, keeping a fixed 20° elevation while the airplane flew toward the antenna beam and over the antenna.

2. Tail-on azimuth scans: The antenna scanned in an azimuthal plane, keeping a fixed 20° elevation while the airplane flew over the antenna and away from the antenna beam.
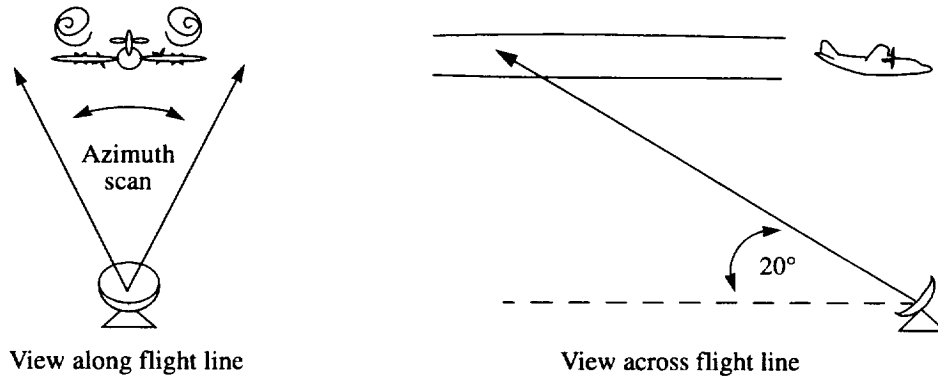
Figure 1. Head-on azimuth-scan configuration for airplane flying toward and over radar beam.
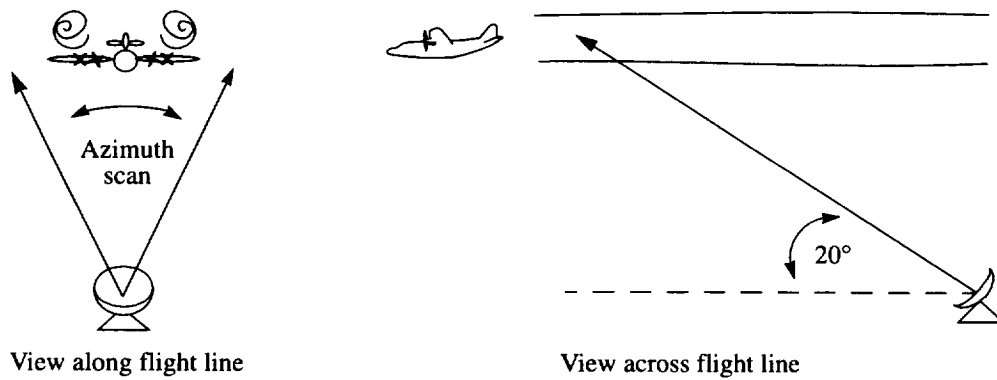
Figure 2. Tail-on azimuth-scan configuration for airplane flying over and away from radar beam.
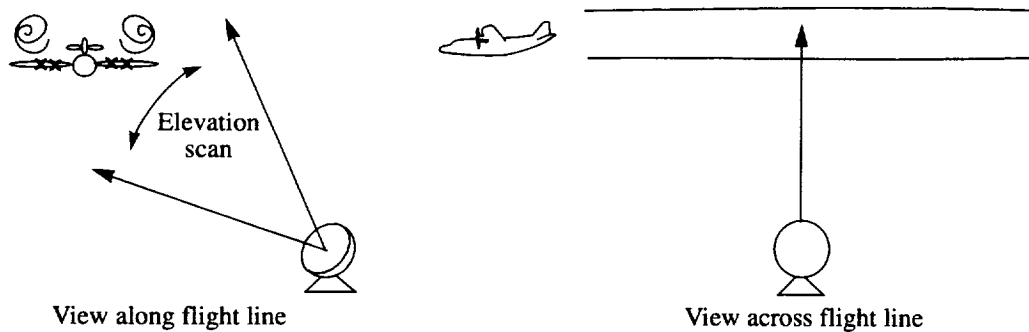
Figure 3. Elevation-scan configuration for airplane flying along side and past radar.

3. Elevation scans: The antenna scanned in an elevation plane, keeping a fixed azimuth while the airplane flew past the antenna to one side of the antenna tower.

The azimuth wake vortex scans provided a view that was partly longitudinal and partly radial from below, while the elevation scans provided a mostly lateral view. In order to accommodate the X-band radar, the airplane flew past at close range, usually about 1 km away, at an

altitude of between 274 and 659 m (899 to 2161 ft) above ground level. At 30 sec before the airplane passed, both radars began data recording. The first scan was a long, clutter scan of about 40° extent. Subsequent scans were shorter, usually about 15° in extent. The antennas were fitted with boresight videotape cameras to enable the ground crew to view the smoke trails emanating from wing-tip-mounted smoke pods on the C-130. The pilot flew along a requested line crossed by the initial antenna

4

scan; the R5 antenna operator adjusted the scanning throughout the radar recording to continue crossing the smoke trails as they drifted across the sky. Data recording continued until 2 min after the airplane had passed.

At the same time as the weather radars were recording the vortices, a C-band tracking radar was recording the position of the airplane. Usually the tracking radar was R10, which was located between R5 and the X-band radar. The proximity of the tracking radar to the flight line resulted in the occasional temporary loss of the radar fix on the airplane as it flew over R10. On occasions when the more distant tracking radar R18 was employed, the tracks were uninterrupted.

3.4. Weather and Local Geography

The vortex data presented here were recorded between January 5 and January 11, 1995. On these days, the sky was blue and sunny, and light winds prevailed. Meteorological data, including temperature, pressure, water vapor mixing ratio, and wind speed, were collected every 2 hr. Those data recorded at the times closest to the vortex radar data are presented in appendix B for an altitude (400 m above ground level) that is representative of the airplane passes.

The terrain of the Wallops Flight Facility, which borders on the Atlantic Ocean, is flat and very marshy. A map of the area surrounding the radar test site is shown in figure 4. C-band R5 is situated in a row of radars which includes tracking Radar 10 and the X-band radar that operated in conjunction with R5 during the experiment. This group of radars is about 6 mi south of the airfield and tracking Radar 18 (not pictured in the figure). Within 1 km of the R5 tower, there are grassy fields, numerous clumps of trees, a body of open water between the mainland and the island, and occasional metal towers and buildings housing other radar stations. Even in the absence of rain or wake vortices, substantial variations (up to 18 dBm) were seen over time in the combined radar reflections from the ground and atmosphere when looking at the same point in space. There were also signal variations of up to 30 dBm over angular space from the varying ground clutter at different azimuths and elevations.

4. Signal Level Calculations

4.1. Recording Lag Correction

Initial studies indicated that there was a consistent lag between position and signal level recordings made by R5 when the antenna was scanning. Comparison of the apparent positions of a strong fixed target as the antenna scanned upward and downward past it during elevation scanning at the 2°/sec scan rate led to the deduction that the recorded position was 0.5° "ahead" of the correct position for the target. This error also occurred during clockwise and counterclockwise azimuth scanning and was corrected for by adding or subtracting 0.5°, as appropriate, to the angular position at all recorded data points.

4.2. AGC to SNR Interpolation

Because the direct output of the recording system was AGC values, it was necessary to collect calibration data to establish the relationship between AGC level and SNR. At least once on each experiment day, usually at the beginning, the radar was calibrated with a series of test signals from a nearby tower; the signal ranged in 5-dB steps from 0 to 65 dB above the radar noise level observed at the receiver. Thirty seconds worth of AGC data were averaged at each SNR level. In postrecording processing, SNR levels were determined for every recorded AGC data point by linear interpolation between the appropriate SNR values. In general, most radar returns lay within the calibrated region of the SNR scale. The recorded signal level was observed to exceed the scale only when the airplane was close to the radar and the recorded range gate was centered at 814 m, one of the closer recorded ranges.

4.3. Calibrated Sphere Track and Noise Calculation

On May 1, 1995, a calibrated sphere track test was performed to provide data for calculating the radar system noise seen by the receiver. During the test, R5 was configured in the same way it had been during the wake vortex recordings. The receiver bandwidth was set at the nominal value 4.8 MHz, for which the previously measured noise bandwidth had been 4.36 MHz. A metallic sphere with a radar cross section (RCS) of 0.0182 m^2 (6-in. diameter) was attached to a balloon and released from the ground. As the balloon and sphere ascended, R5 tracked the sphere until it was 50 km away, recording AGC level versus range. From these data, SNR versus range was calculated. At each of three ranges, 13.167 km, 26.335 km, and 45.720 km, noise power was calculated according to the radar equation

$$\frac{S}{N} = \frac{P_t G^2 \lambda^2 \sigma}{(4\pi)^3 R^4 L_{2\text{-way}} N} \tag{3}$$

5
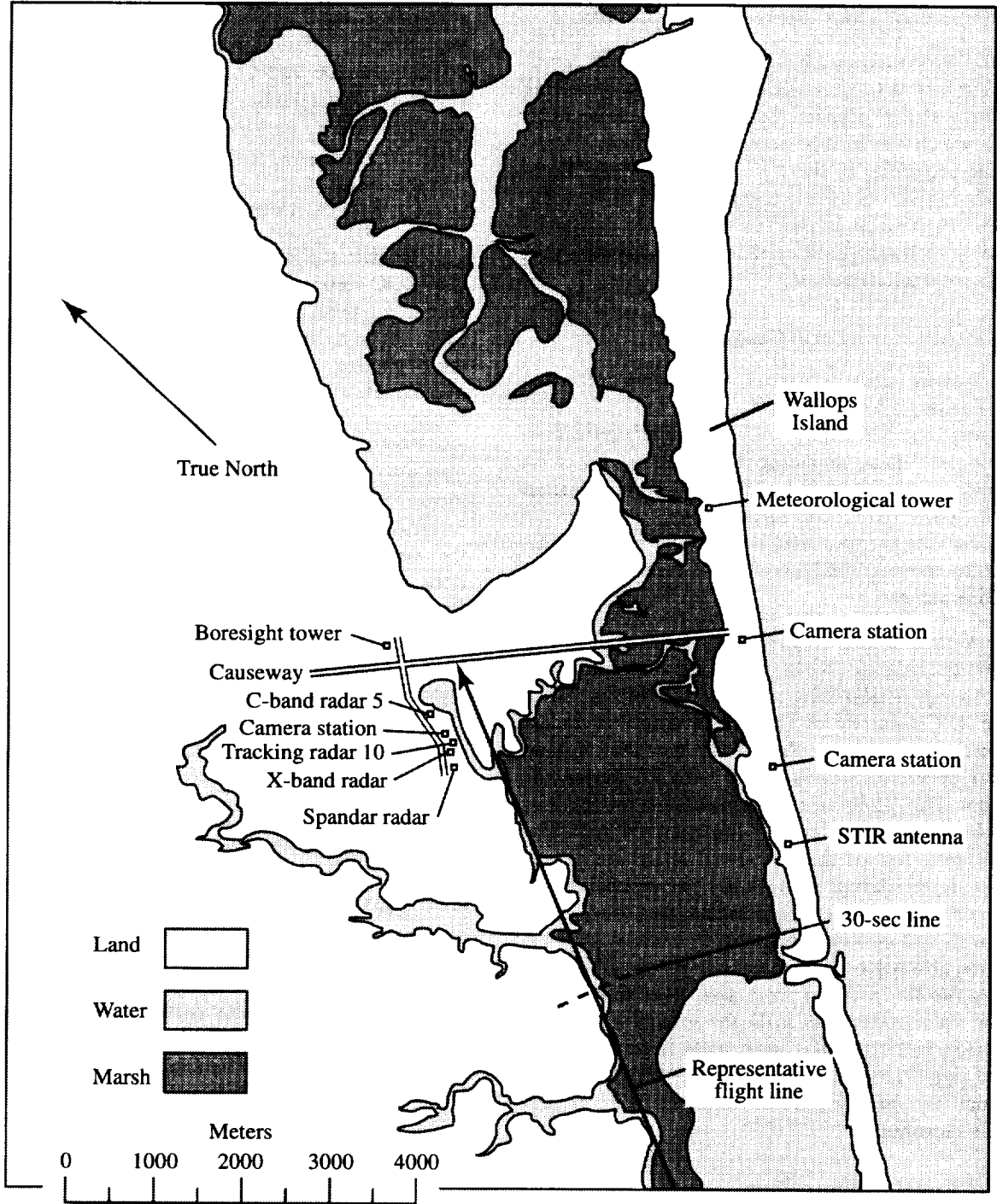
Figure 4. Map of experiment site at Wallops Flight Facility, Wallops Island, Virginia. C-band Radar 5 is situated in a row of radars which include tracking Radar 10 and the X-band radar that operated in conjunction with R5 during the experiment. This group of radars is about 6 miles south of the airfield and tracking Radar 18 (not pictured). During azimuth-scan passes, the C-130 flew directly over the radars; during elevation-scan passes, the aircraft flew past the radars as pictured.

6

where

S/N = interpolated SNR

P_t = peak transmitted power

G = antenna gain

λ = radar wavelength

σ = RCS

R = range

$L_{2\text{-way}}$ = 2-way line losses + atmospheric
losses = 4.9 dB + $R \cdot$ 0.015 dB/km

The average of the three resulting noise values was −100.58 dBm. Using B = 4.36 MHz in the equation

$$N = kT_S B \qquad (4)$$

where k = Boltzmann's constant, 1.38×10^{-23} J/K, one obtains the resulting noise temperature 1454 K, which is equivalent to a noise figure of 7.8 dB.

All experimental SNR values were multiplied by the noise power to obtain the plotted power values seen at the receiver.

5. Clutter-Only Recordings

Because the nonvortex returns varied so much over time, it was infeasible to do clutter subtraction with a single clutter map; instead, a clutter scan would be needed for each pass. As used here, the term "clutter" includes atmospheric and ground returns. It was decided that some statistical data on clutter collected in the absence of aircraft would help in deciding which disturbances in the vortex data sets were the result of vortices. A data collection time was selected when the weather was clear and the mean weather conditions were fairly constant. By the time a clutter-only recording could be done using R5 on such a day, it was November 28, 1995, 6 months after the experiment. Several data sets were obtained with different antenna scans, including the following whose results are discussed herein:

100 azimuth scans from 10° to 50°, at 20° elevation and 1369-m range

100 elevation scans from 20° to 50°, at 141° azimuth and 1409-m range

The other radar parameters were set, as before, according to table 1.

Because the vortex data would be considered on the basis of signal level differences relative to one initial clutter scan per pass, the clutter itself was characterized by finding the nonvortex signal level variations over time at many antenna positions. The clutter signal levels were calculated in mW and interpolated, together with their detection times, at regular 0.25° intervals. At each angular position so determined, available pairs of dBm signal powers and their corresponding detection times were subtracted to produce sets of signal power difference values for various time intervals ranging from 2 sec to 8 min. For each set of between 46 and 98 signal power difference samples representing a given time lag, the average and standard deviation of all the signal power differences were determined in dBm. A smoothed, abbreviated, wire mesh representation of the results is shown in figures 5 and 6, including lag times up to 3 min, a time period slightly longer than the flight passes. Tables C2 and C3 in appendix C contain the unsmoothed numerical results together with the number of samples in each set used to find the sample standard deviations.

At any one position and for a given time lag, the distribution of signal power differences was roughly Gaussian about a mean of no change. (The vortex data sets showed that the mean clutter level varied very greatly from day to day.) The clutter was particularly variable at some positions (e.g., at 40.5° during the azimuth scans and 22.5° during the elevation scans). The signal level changes also increased somewhat with longer time lags, although the effect was much less striking than the change with position. For the azimuth scans, the sample standard deviation of the signal level varied from 1.4 dBm (30.75°, 145 sec) to 3.7 dBm (40.5°, 36 sec). For the elevation scans, the standard deviation varied from 1.5 dBm (37.5°, 25 sec) to 3.6 dBm (22.5°, 149 sec).

One may determine the expected range of clutter power variations at any particular position and time lag by applying the t-test (ref. 10). For all the data in tables C2 and C3, the smallest number of degrees of freedom is 46, which has a $t_{.05}$ value of 1.68 (ref. 10). So, an upper limit for the expected range of signal level variations caused by change in clutter alone may be determined (with 95-percent confidence) at any position by multiplying the standard deviation of the signal power differences by 1.68. For example, at 25° azimuth and 20° elevation, there is a 95-percent chance that, after 36 sec, the clutter power level will have changed less than 4.9 dBm. At 35° azimuth and 20° elevation, there is a 95-percent chance that, after 36 sec, the clutter level will have changed less than 3.6 dBm. At 141° azimuth and 25° elevation, there is a 95-percent chance that, after 37 sec, the clutter power level will have changed less than 4.5 dBm.

Although these numbers represent only one range gate on one day, they give an idea of the variability one could encounter with such a radar. Clearly, the variability at single points is quite large over a few minutes time even when no unusual disturbances, such as vortices, are
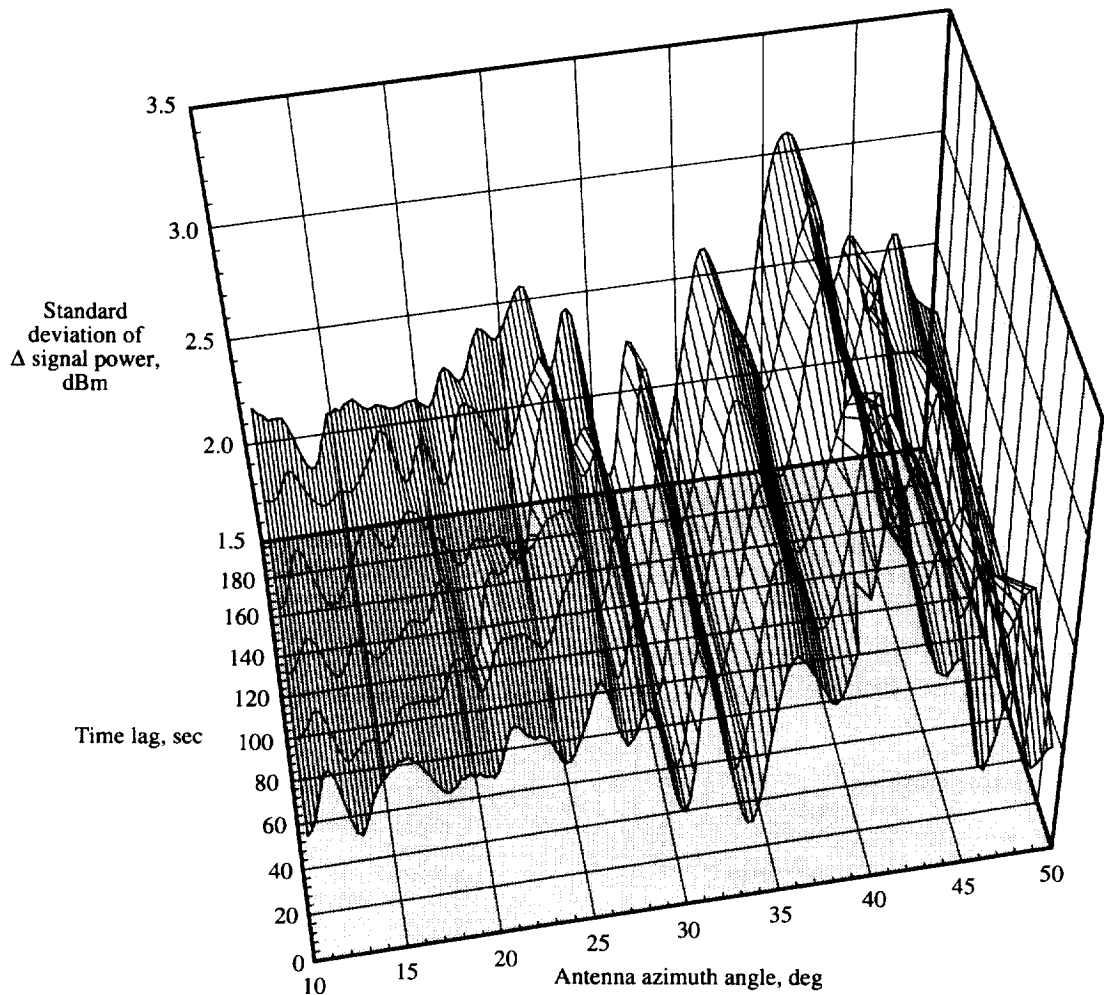
Figure 5. Variability of received clutter power with azimuth direction; Wallops R5 elevation = 20° on 11/28/95 (data smoothed). At any given angular position and time lag, mean signal level change was negligible. Standard deviation of signal level change varied from 1.4 to 3.7 dBm before smoothing.

encountered. As it turned out, the signal level changes caused by vortices were often of the same order of magnitude as the changes from unknown causes. For this reason, it was decided to search for vortex patterns extended over space, rather than for fluctuations at individual points.

6. Vortex Data Analysis Method

6.1. Selection of Passes

Out of the 209 airplane passes for which azimuth-scan or elevation-scan R5 recordings were available, 13 azimuth-scan passes and 10 elevation-scan passes were chosen for detailed analysis for possible wake vortex detection. Staring-mode passes were ignored because vortex detection would be enabled by the signal level contrasts seen spatially, as well as temporally, in

scanning mode. Where concurrent airplane tracking data were available, flight paths of the C-130 were examined in conjunction with the R5 scans to select passes where the recorded volume was initially within about 50 m of the airplane wake, in any direction. The passes were further screened for proper functioning of the airplane wing-tip smokers and availability of videotapes that showed the smoke trails. Finally, it was desired, for each pass, to have an initial clutter scan recorded at the same positions as the vortex data of interest. Data from the 23 passes that met these criteria are shown in appendix A.

Appendix A contains one plot per pass of the airplane track and the radar range cell track across the ground. At the top of the corresponding radar data plots is additional information, such as radar range, airplane altitude, and the time when the airplane flew over the range cell track. This intersection was determined by

8
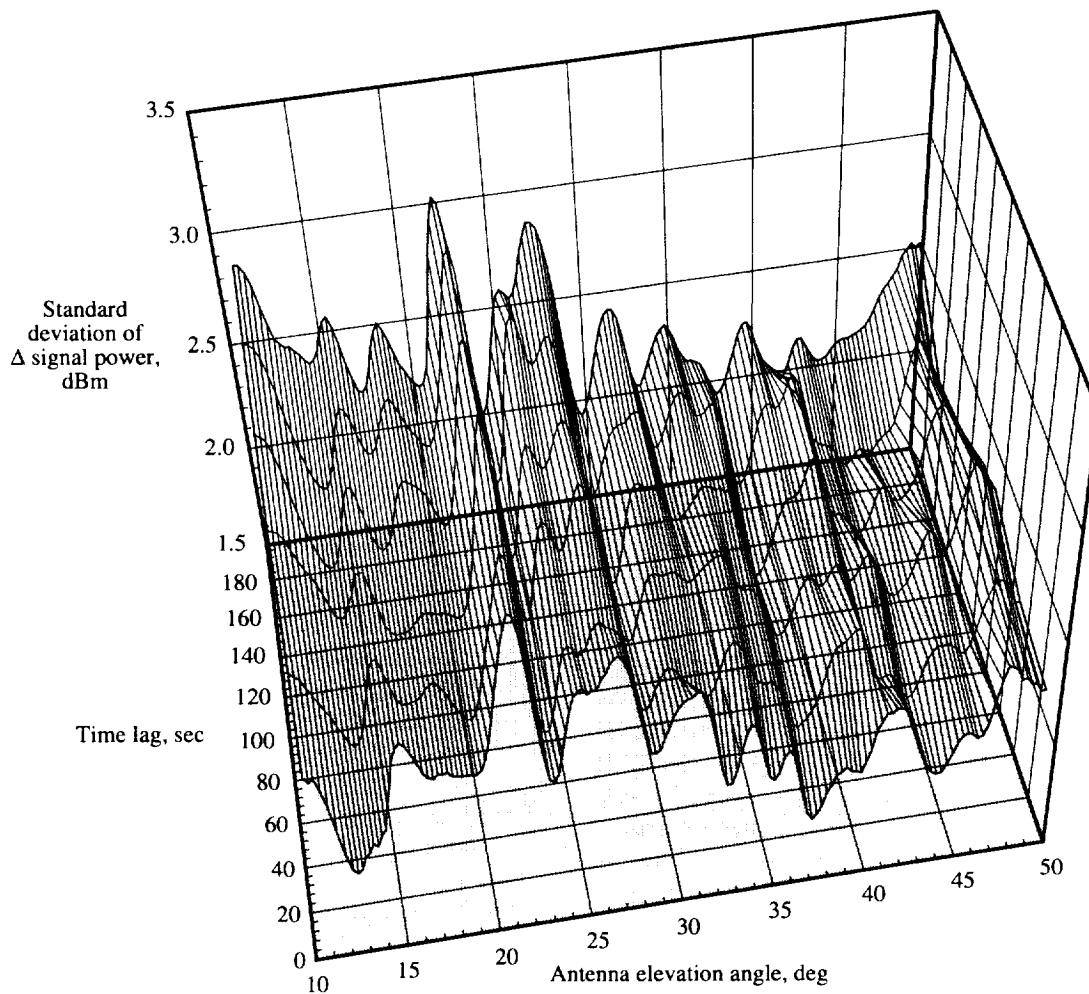
Figure 6. Variability of received clutter power with elevation direction; Wallops R5 at azimuth = 141° on 11/28/85 (data smoothed). At any given angular position and time lag, mean signal level change was negligible. Standard deviation of signal level change varied from 1.5 to 3.6 dBm before smoothing.

graphic interpolation between the airplane tracking data points, which were provided at 1-sec intervals. Some of the airplane track plots contain dotted lines where the tracking information dropped out.

6.2. Database and Programming Languages

After the signal power values had been interpolated for each vortex data pass, they were loaded into a database created with Informix software on a Sun SPARCstation 2, running Sun Operating System version 4.1.3_U1. Also in the database were radar-pointing and aircraft-tracking data. Much of the initial sorting was done with Informix-Sequel Query Language (ISQL) queries and plots made by Tecplot. An ISQL-C program allowed logarithmic and trigonometric calculations to be done in C language on values selected by ISQL queries; this program performed clutter subtraction and volume reflectivity calculations. The clutter statistics were

calculated through the use of FORTRAN code on an ASCII file that contained the radar clutter data.

6.3. Criteria for Recognizing Wake Vortices

In studying signal plots for evidence of vortex detection, a number of questions were asked.

1. Is the variation larger than that which would have occurred because of variations in atmospheric and ground clutter alone?

2. Does the signal disturbance have a nonrandom shape?

3. Is the signal disturbance coincident with the smoke trails?

4. Does the disturbance appear at different positions not associated with any particular ground clutter feature?

9

5. Does the signal disturbance appear at different times not tied to any particular position of the airplane?

6. Is the indicated physical size of the vortex reasonable?

7. Is the implied volume reflectivity of the vortex in keeping with previous observations?

In the end, the answers to these questions were "not necessarily" to the first question and "yes" to the others. Because the clutter variability was so large and it was not known in advance what a vortex would look like, the vortex search was carried out visually by inspection of signal level plots and videotapes of the smoke trails. Possible sidelobe detection of the airplane was a major concern, so plots of the position of the airplane have been included in this report with notations to show where the airplane was at times of interest in the radar recordings.

6.4. Clutter Subtraction

In each vortex data pass, one antenna scan was designated as the clutter scan. This clutter scan was recorded less than a minute before the passage of the airplane and included those positions of interest during the rest of the pass. In order to detect changes possibly caused by wake vortices, the received signal levels in succeeding scans were compared to the signal levels at the same positions in the clutter scan. Both increases and decreases in signal level were noted in the vicinity of the vortices.

6.5. Volume Reflectivity

Where deviations in signal level from the clutter level were found, the change in reflectivity was calculated as

$$\Delta \eta = \frac{|\Delta S|(4\pi)^3 R^4 L_{2\text{-way}}}{P_t G^2 \lambda^2 V} \tag{5}$$

where

$\Delta \eta$ = change in volume reflectivity, RCS/volume[4]

ΔS = change in received signal power

V = range cell volume

For R in the near field (less than 1266 m), the range cell volume was calculated as that of a cylinder of diameter equal to the antenna, so that

$$V = \frac{\pi D^2 c\tau}{8} = 6905 \text{ m}^3 \tag{6}$$

---

[4]In this report, η is expressed in units of dB m^{-1}. Another common form of the unit is dB s m/m^3.

10

where

D = antenna diameter

c = speed of light

τ = range gate length

For R in the far field (greater than or equal to 1266 m), the volume was calculated as that of a conic section, so that

$$V = \frac{\pi \theta^2}{12}(R_{\text{far}}^3 - R_{\text{near}}^3) \tag{7}$$

where

θ = 3-dB beamwidth (radians)

R_{far} = range at far edge of range cell

R_{near} = range at near edge of range cell

During the majority of R5 vortex recordings, the value of V was the near-field value, 6905 m^3; for the entire experiment, the maximum value of V was 8885 m^3. For the purpose of reflectivity calculation, it was assumed that the vortices would fill one range cell. For any one calculation, it was not known how much of the radar range cell would be filled by the wake vortices; however, it was expected that early in each pass recording the range cell would be partly filled, while later in that recording the range cell would be completely filled. Therefore, $\Delta \eta$ may at times be underestimated. The value $\Delta \eta$ has been calculated from the magnitude of the signal change so that it is always a positive number of m^{-1} and can be expressed logarithmically. Because $\Delta \eta$ is less than 1 m^{-1}, it is always a negative number of dBm^{-1}. However, one may deduce from the signal plots whether the reflectivity has increased or decreased, according to whether the vortex-plus-clutter scan lies above or below the clutter scan.

7. Vortex Data Analysis Results

7.1. Data Plot Description

The vortex data analysis results are presented in appendix A in the form of signal level plots and tracking data plots. The plots are presented in order of airplane pass numbers, which were assigned chronologically throughout the testing.

For each pass included in this report, two or more antenna scans of interest have been selected. Because absolute signal power has been plotted, SNR may be calculated at any point by adding 100.58 dB to the dBm signal power value. Where the boresight videotape indicated that the radar beam was crossing the smoke trails, portions of the vortex-plus-clutter scans on or between the two smoke trails of the airplane are represented as

solid circles. In a few cases, the smoke position is not marked because there was no videotape available showing when the antenna boresight crossed the smoke trails. Places of interest are identified with an arrow pointing to a particular data point; the time of day (hours, minutes, seconds) and change in reflectivity are given for that data point.

In the tracking data plots, the axes are marked in degrees of latitude and longitude as if they were rectangular coordinates, with the scaling done so that degrees of latitude are the correct "length" relative to degrees longitude for that location in the center of the "map." The direction of flight of the airplane around its loop, indicated by an arrow, was counterclockwise except for passes 52, 54, 56, and 64. The times of interest marked on the signal level plots are also marked along the airplane tracks. The distance between any two points in kilometers may be estimated by converting each 0.01° of the distance marked off along the latitude axis to 1.11 km.

7.2. Screening for Airplane Detection

It seemed quite possible that the airplane might interfere with vortex detection by creating an extra unpredictable sidelobe target in the clutter scan or in the vortex-plus-clutter scans. With this problem in mind, 10 head-on and 10 tail-on clutter scans were compared to see if they displayed substantially different features. Passes 99, 100, 103, and 104 were head-on passes recorded at $R = 1364$ m. Passes 106, 107, 108, 109, 117, and 118 were head-on passes recorded at $R = 1111$ m. Passes 51, 52, 54, 122, and 123 were tail-on passes recorded at $R = 1366$ m. Passes 56, 60, 61, 64, and 127 were tail-on passes recorded at $R = 1110$ m. Comparison of head-on and tail-on clutter scans recorded on the same day at the same range revealed no obvious distinction in the features. Therefore, it appeared that proximity of the airplane was not affecting the clutter scans. Because there were very few days when good head-on and tail-on clutter scans were both available for comparison, it was not possible to establish a firm conclusion. It appeared that the date was much more important than the direction of flight in determining the clutter signal levels. At the same range, clutter recordings made on different days varied as much as 18 dB in amplitude but showed similar features (i.e., peaks at the same pointing angles). Of course, there was a very noticeable difference both in the signal level and in the general shape of clutter scans recorded at different ranges on the same day.

7.3. Evidence of Vortex Detection

The most convincing evidence of vortex detection lay in passes where a signal disturbance could be seen coincident with the smoke in several succeeding scans. Such passes were 52, 54, 99, 100, 103, 104, 107, 108, 117, 122, 123, 132, 137, and 141, which included both azimuth-scan and elevation-scan passes. In the azimuth-scan passes, the coincidence of the vortex signature with the smoke trails as they drifted across the scan during the pass indicated that the signal disturbance was not the effect of ground clutter. At places of interest, the signal disturbance represented a target of spatial extent considerably more than the 0.5° resolution, the disturbance usually being between 100 and 150 m wide. This size is consistent with the TASS-modeled vortex pair width of 80 m at 30 sec, assuming further expansion of the vortices after 30 sec. One may estimate the width of any feature in the scans as $2R \tan(\alpha/2)$, where α is the angular extent of the feature.

The single-range-cell recording allowed a curved strip image 112.5 m in depth, rather than a plan view picture, to be created. Even if this strip passed through a vortex, it did not show what was happening on all sides of the vortex. Another difficulty was that, during the recording, the vortices, as indicated by smoke trails, were twisting around in the sky and could not be expected to form a neat radar image at all times. However, visual inspection of many data plots often revealed a characteristic sinusoidal pattern of the vortex-plus-clutter scan about the clutter scan in the vicinity of the smoke trails. Good examples of this shape may be seen in azimuth scans, such as pass 56, scan 8; pass 100, scan 12; pass 107, scans 5 and 22; pass 117, scan 19; pass 122, scan 11; and pass 123, scan 4. Longer scans sometimes showed a volume of increased reflectivity bounded by two volumes of decreased reflectivity. In volumes of increased reflectivity, the vortex-plus-clutter to noise ratio was typically between 20 and 41 dB, while the vortex to clutter ratio was between 0.1 and 7.9 dB.

In these scans, the smoke trail was sometimes in the portion of the scan where there was an increase in reflectivity and sometimes in the portion showing a decrease in reflectivity. The changes in reflectivity in either direction varied from −131 to −102 dBm^{-1}. The smoke trails frequently remained quite close together, the distance across both trails spanning as little as 40 or 50 m, which is about the same as the expected initial distance across both vortices from a C-130. This could mean either that the vortices did not expand but did influence the reflectivity of the air mass surrounding them or, more likely, that the vortex system expanded outside the smoke trails. In the absence of a more complete spatial representation or velocity information, it is not possible to say which parts of the vortex system produced elevations in reflectivity. In any case, it is safe to say that the smoke alone did not change the reflectivity of the air.

The time lags between the passage of the airplane and the examples of vortex detection shown in this report vary from 10.4 to 120.1 sec. Because signal disturbances were seen coincident with the smoke and irrespective of the position of the airplane, it is unlikely that the disturbances were instances of airplane detection.

7.4. Clutter Limitations to Vortex Detection

In addition to signal level fluctuations in the vicinity of the smoke trails, there were often equally large signal changes in other regions of the scan. Sometimes, as in pass 52, a nonrandom signal disturbance was noted, but the vortex-plus-clutter scan power level never increased above the clutter scan power level. This clutter level fluctuation would make it difficult to write an automated detection algorithm on the basis of signal magnitudes alone, unless the clutter could be substantially reduced.

Currently, no evidence of vortex detection has been found in the X-band data sets recorded at Wallops concurrently with the R5 data. This result is thought to be caused by the high sidelobe clutter power recorded by that system.

8. Concluding Remarks and Recommendations

This study confirms the work of previous researchers who reported that wake vortices could be detected with C-band radars in clear air. Although the measured vortex-induced changes in received signal level were often similar to the expected clutter variation at individual points, the experimental data are convincing evidence of wake detection because the signal level changed in a nonrandom pattern at the locations of the smoke trails. The wake was detected numerous times at a variety of positions relative to the airplane and radar, the calculated size and increased reflectivity of the wake lying within the ranges expected from previous experiments and modeling.

To reiterate the essential characteristics of the radar, R5 transmitted 2.2 MW and integrated over 64 pulses, recording noise at −100.58 dBm and vortex-plus-clutter signals at 20 to 41 dB above the noise level. The results of the research reported herein indicate that, by reducing the receiver noise level and increasing the number of pulses integrated, it should be possible to detect vortices at the same range (1364 m) using much less power. For example, the theoretical Swerling Case 1 target requires a signal to noise ratio (SNR) of 7.2 dB for a probability

of detection of 0.9 and probability of false alarm of 10^{-4} when 64 pulses are integrated. If 256 pulses are integrated, the required SNR decreases to 3.8 dB, an improvement of 3.4 dB. By reducing the receiver noise by 8 dB and increasing the integration improvement factor by 3.4 dB, it should be possible to reduce the transmitted power 27.6 dB to 3.8 kW and still obtain a SNR of 3.8 dB.

Portions of the structure of the vortex system were revealed by the limited recording of one range cell. It appeared that there was a central volume of heightened atmospheric reflectivity, with volumes of lessened atmospheric reflectivity on each side. At present, it is not known why some parts of the vortices in this experiment showed decreased reflectivity. Although the vortex-plus-clutter signals were visible above the clutter signals, it would be of great value to reduce the proportion of ground clutter level in the received signal by antenna modification or pointing. This would make the patterns more predictable, heighten the contrast between vortex and nonvortex information, and improve the probability of vortex detection at low elevations. Detection of vortices by magnitude information alone required pattern recognition and a clutter map recorded as soon as possible before the vortex recording.

For future work toward Reduced Spacing Operation/ Terminal Area Activity (RSO/TAP) program goals, Doppler processing is undoubtedly necessary to sort out clutter targets with confidence, to identify various parts of the vortex system, and to quantify the hazard to airplanes in terms derived from wind velocities. Spatial resolution will have to be improved over the R5 system so that the sample volumes are smaller than individual vortices, on the order of 5 m in diameter. Keeping the previous numerical example, the needed improvement in resolution would be 13 dB, which could be achieved by pulse compression and would require increasing the transmitted power once again. Ultimately, a three-dimensional target representation will be needed to locate and track vortices from origin through decay; this information must be obtained by scanning in both azimuth and elevation and by recording data from a range of distances.

Appendix A

Signal Level Plots and Track Plots

This appendix presents the vortex data analysis results in the form of signal level plots and tracking data plots, ordered according to pass numbers. Note that, above each signal level plot, text labels give additional R5 pointing information and the time and airplane position when the airplane crossed the R5 recorded range cell track. All angles are given relative to R5; times are given in coordinated universal time (UTC) code; altitude is given above ground level (AGL).

Figures A1, A2, A3, and A4 contain three elevation scans and the ground tracks for pass 14. In scan 7, a signal increase is seen just above the aircraft elevation, while a signal decrease is seen just below the aircraft elevation. Between scans 7 and 18, the signal decrease has descended 4° or 89 m over a period of 95 sec.

Radar settings: R = 1268 m, Az = 145.0°, El = scanning
Airplane crossing at time = 20:38:44.3, R = 1288 m, Az = 145.0°, El = 30.0°, Alt = 659 m AGL

——————— Scan 1–clutter
O   Scan 7–vortex plus clutter (no video available)

20:39:06.2, $\Delta\eta$ = –123.9 dBm^{-1}
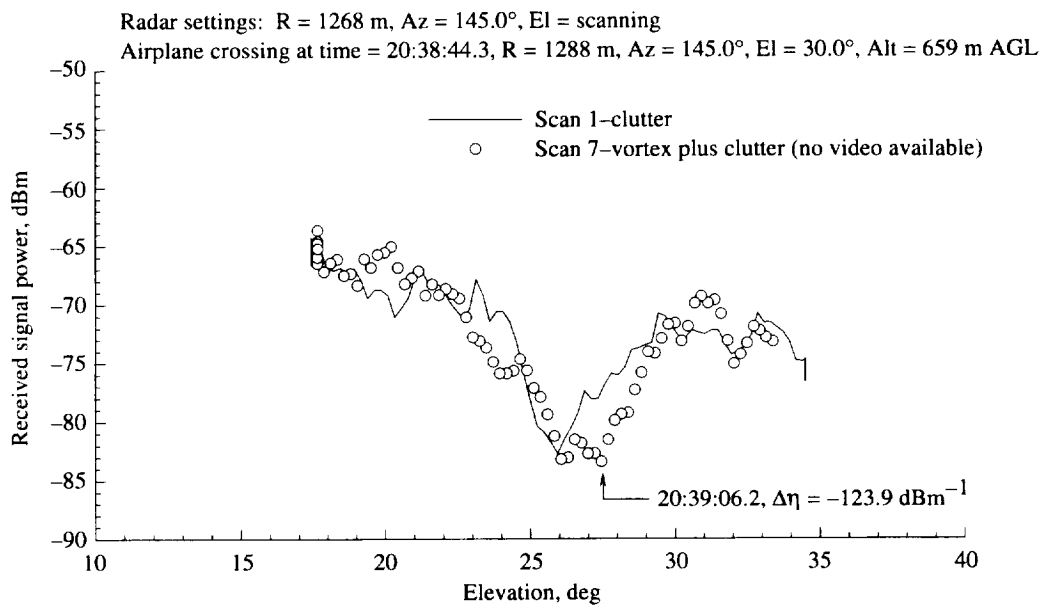
Figure A1. Total signal level vs. antenna elevation angle compared with clutter scan for pass 14, elevation scan 7, on 01-05-95.

Radar settings: R = 1268 m, Az = 145.0°, El = scanning
Airplane crossing at time = 20:38:44.3, R = 1288 m, Az = 145.0°, El = 30.0°, Alt = 659 m AGL

——— Scan 1–clutter
o   Scan 14–vortex plus clutter (no video available)

20:40:08.1, $\Delta\eta = -123.1$ dBm^{-1}
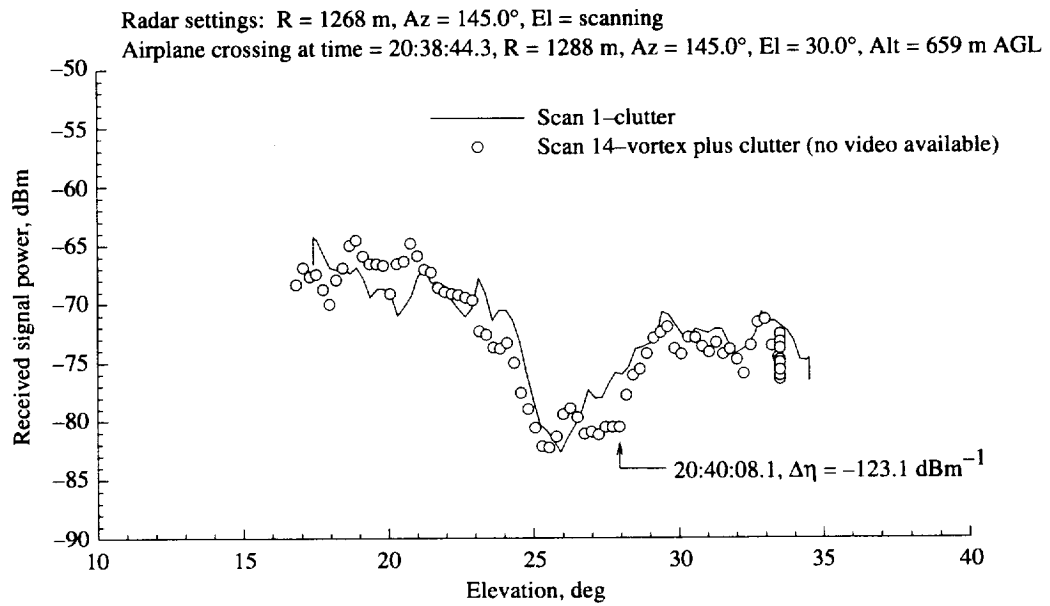
Figure A2. As for figure A1, except for elevation scan 14.

Radar settings: R = 1268 m, Az = 145.0°, El = scanning
Airplane crossing at time = 20:38:44.3, R = 1288 m, Az = 145.0°, El = 30.0°, Alt = 659 m AGL

——— Scan 1–clutter
o   Scan 18–vortex plus clutter (no video available)

20:40:41.5, $\Delta\eta = -115.8$ dBm^{-1}

Figure A3. As for figure A1, except for elevation scan 18.
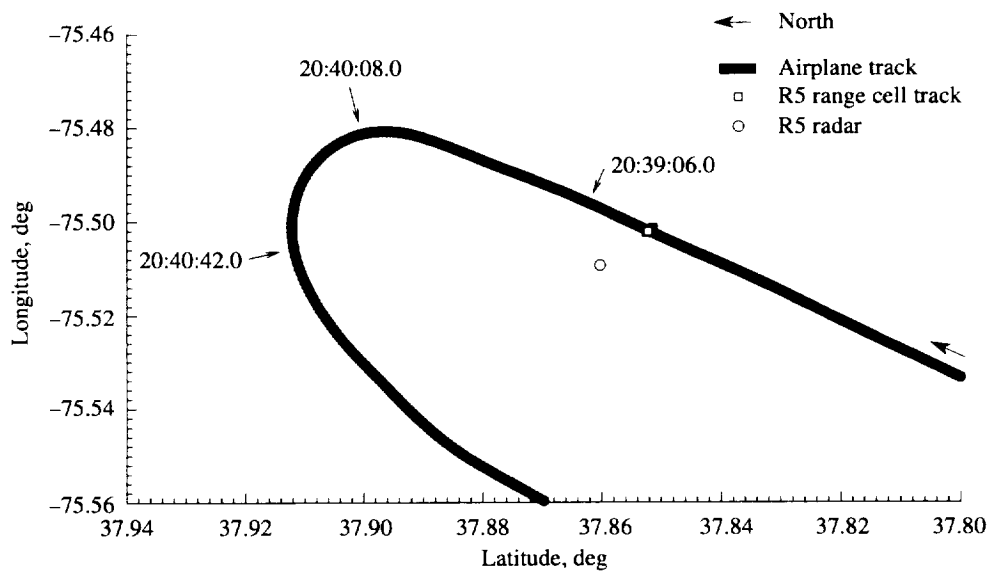
Figure A4. Pass 14 airplane and Radar 5 ground tracks; lateral radar view of airplane wake.

Figures A5 and A6 contain one elevation scan and the ground tracks for pass 21. In scan 7, a signal increase is seen just above the aircraft elevation, while a signal decrease is seen at and below the aircraft elevation.
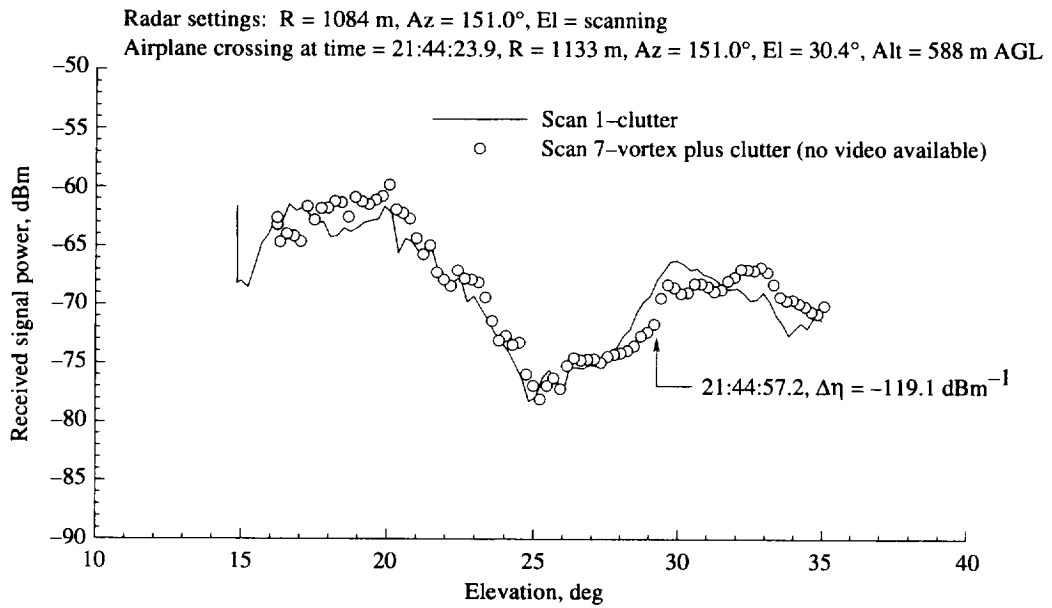
Figure A5. Total signal level vs. antenna elevation angle compared with clutter scan for pass 21, elevation scan 7, on 01-05-95.
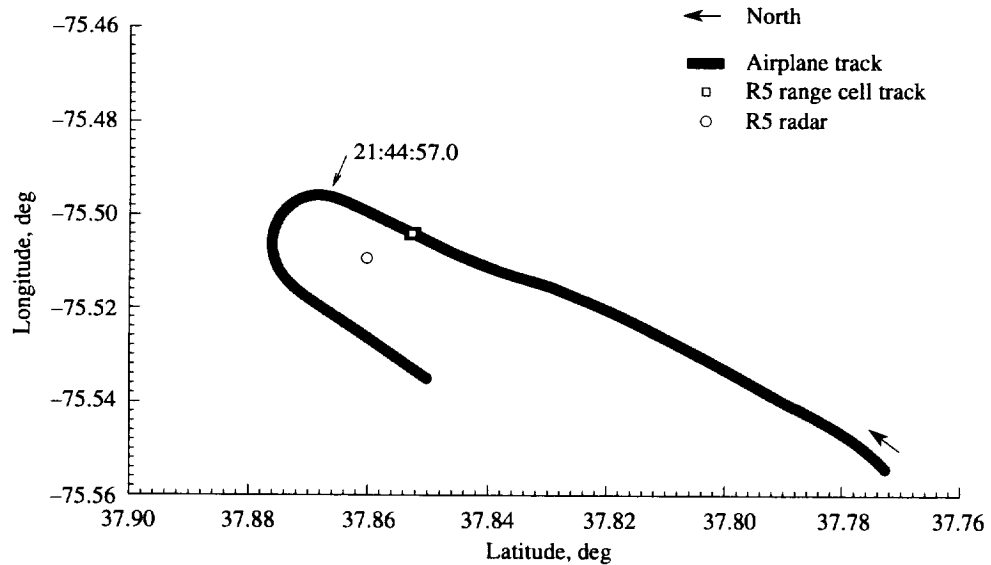
Figure A6. Pass 21 airplane and Radar 5 ground tracks; lateral radar view of airplane wake.

Figures A7, A8, and A9 contain two azimuth scans and the ground tracks for pass 52. During this pass, the signal level was generally higher during the clutter scan than during any of the succeeding scans, implying possible contamination by the aircraft. Nevertheless, some local variation is visible around the smoke trails in scans 10 and 14; the contrast between high and low points is more marked than in the clutter scan.

Radar settings: R = 1366 m, Az = scanning, El = 20.0°
Airplane crossing at time = 19:48:37.1, R = 1359 m, Az = 33.0°, El = 19.4°, Alt = 467 m AGL

—————— Scan 1–clutter
o   Scan 10–vortex plus clutter
•   Scan 10–vortex plus clutter with smoke

19:49:21.7, $\Delta\eta = -108.0$ dBm^{-1}

Figure A7. Total signal level vs. antenna azimuth angle compared with clutter scan for pass 52, azimuth scan 10, on 01-09-95.

Radar settings: R = 1366 m, Az = scanning, El = 20.0°
Airplane crossing at time = 19:48:37.1, R = 1359 m, Az = 33.0°, El = 19.4°, Alt = 467 m AGL

—————— Scan 1–clutter
o   Scan 14–vortex plus clutter
•   Scan 14–vortex plus clutter with smoke

19:49:32.4, $\Delta\eta = -107.9$ dBm^{-1}

Figure A8. As for figure A7, except for azimuth scan 14.

17

Figure A9. Pass 52 airplane and Radar 5 ground tracks; tail-on radar view of airplane wake.

Figures A10, A11, A12, and A13 contain three azimuth scans and the ground tracks for pass 54. In scans 8, 12, and 14, a signal increase is seen at the location of the smoke trails. The signal increase is most obvious in scan 12, 63 sec after the aircraft crosses the radar track.

Radar settings: R = 1366 m, Az = scanning, El = 20.0°
Airplane crossing at time = 19:59:58.3, R = 1364 m, Az = 31.5°, El = 19.6°, Alt = 473 m AGL

Figure A10. Total signal level vs. antenna azimuth angle compared with clutter scan for pass 54, azimuth scan 8, on 01-09-95.

Radar settings: R = 1366 m, Az = scanning, El = 20.0°
Airplane crossing at time = 19:59:58.3, R = 1364 m, Az = 31.5°, El = 19.6°, Alt = 473 m AGL

Figure A11. As for figure A10, except for azimuth scan 12.

Radar settings: R = 1366 m, Az = scanning, El = 20.0°
Airplane crossing at time = 19:59:58.3, R = 1364 m, Az = 31.5°, El = 19.6°, Alt = 473 m AGL

20:01:11.1, $\Delta\eta = -115.3$ dBm^{-1}

Scan 1–clutter
○ Scan 14–vortex plus clutter
● Scan 14–vortex plus clutter with smoke

Azimuth, deg

Received signal power, dBm

Figure A12. As for figure A10, except for azimuth scan 14.

20:01:11.0
20:01:02.0
20:00:45.0

← North
■ Airplane track
□ R5 range cell track
○ R5 radar

Longitude, deg

Latitude, deg
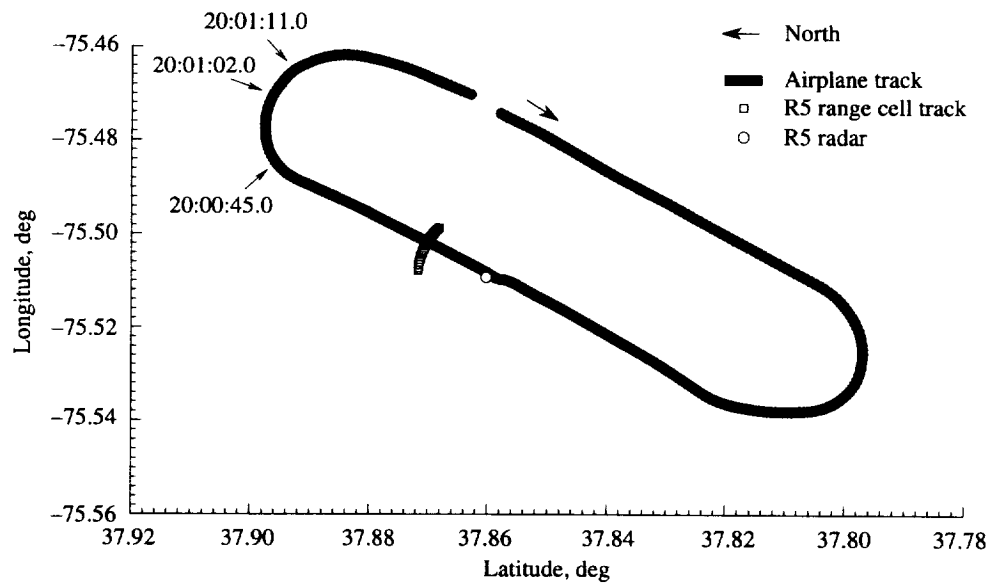
Figure A13. Pass 54 airplane and Radar 5 ground tracks; tail-on radar view of airplane wake.

Figures A14 and A15 contain one azimuth scan and the ground tracks for pass 56. In scan 8, a signal increase and a signal decrease are seen side by side at the location of the smoke trails.

Radar settings: R = 1111 m, Az = scanning, El = 20.0°
Airplane crossing at time = 20:11:18.5, R = 1167 m, Az = 33.0°, El = 18.1°, Alt = 373 m AGL
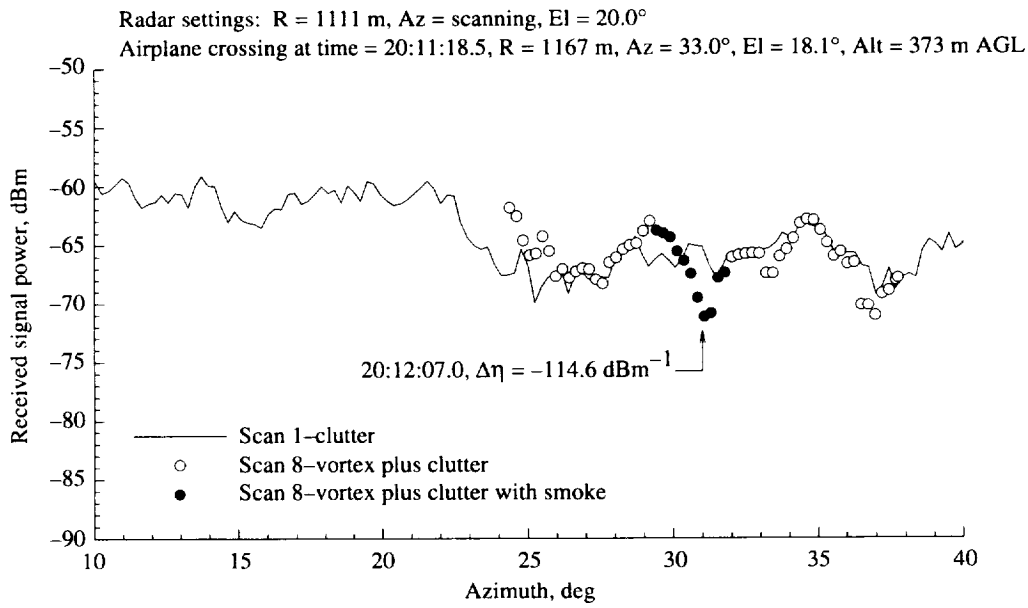
Figure A14. Total signal level vs. antenna azimuth angle compared with clutter scan for pass 56, azimuth scan 8, on 01-09-95.
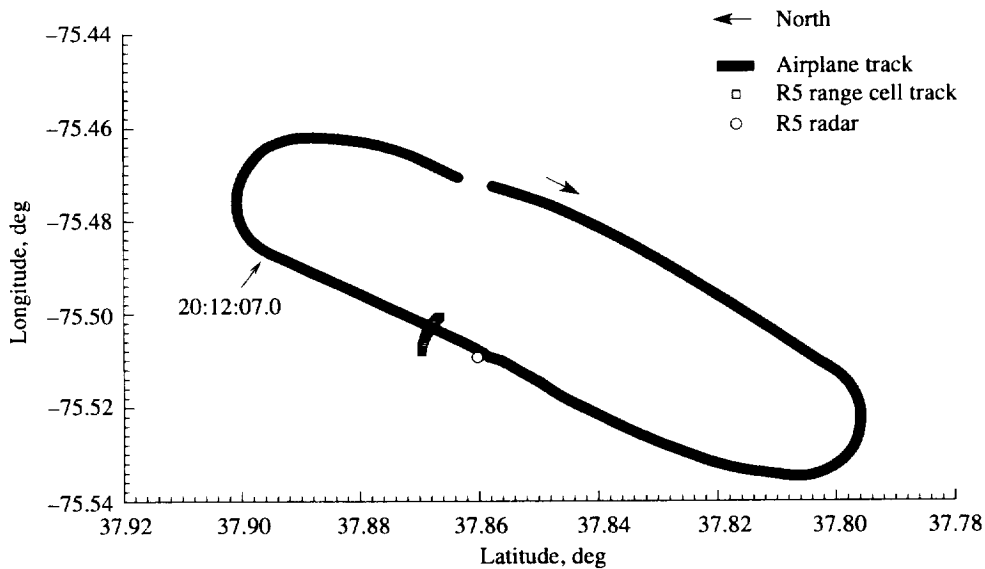
Figure A15. Pass 56 airplane and Radar 5 ground tracks; tail-on radar view of airplane wake.

Figures A16 and A17 contain one azimuth scan and the ground tracks for pass 64. In scan 9, a signal increase is seen at 29° azimuth, the location of the smoke trails. An equally large increase is seen at 35°.

Radar settings: R = 1111 m, Az = scanning, El = 20.0°
Airplane crossing at time = 20:57:42.0, R = 1076 m, Az = 28.5°, El = 13.9°, Alt = 274 m AGL

Figure A16. Total signal level vs. antenna azimuth angle compared with clutter scan for pass 64, azimuth scan 9, on 01-09-95.

Figure A17. Pass 64 airplane and Radar 5 ground tracks; tail-on radar view of airplane wake.

Figures A18, A19, A20, and A21 contain three azimuth scans and the ground tracks for pass 99. In scans 4 and 10, a signal increase is seen at the location of the smoke trails. In scan 35, 120 sec after the aircraft crosses the radar track, the signal increase is still present but the smoke has dissipated.

Radar settings: R = 1364 m, Az = scanning, El = 20.0°
Airplane crossing at time = 19:47:17.7, R = 1296 m, Az = 24.6°, El = 21.5°, Alt = 490 m AGL

———————— Scan 1–clutter
o   Scan 4–vortex plus clutter
●   Scan 4–vortex plus clutter with smoke

19:47:31.4, $\Delta\eta = -125.1$ dBm^{-1}

Figure A18. Total signal level vs. antenna azimuth angle compared with clutter scan for pass 99, azimuth scan 4, on 01-10-95.

Radar settings: R = 1364 m, Az = scanning, El = 20.0°
Airplane crossing at time = 19:47:17.7, R = 1296 m, Az = 24.6°, El = 21.5°, Alt = 490 m AGL

———————— Scan 1–clutter
o   Scan 10–vortex plus clutter
●   Scan 10–vortex plus clutter with smoke

19:47:52.4, $\Delta\eta = -127.0$ dBm^{-1}

Figure A19. As for figure A18, except for azimuth scan 10.
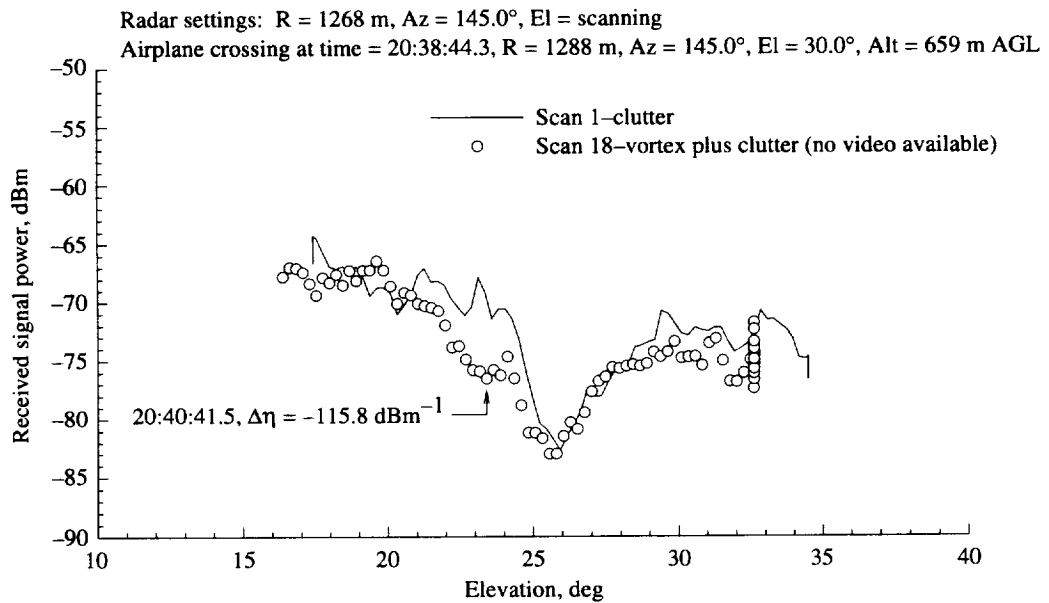
23

Figure A20. As for figure A18, except for azimuth scan 35.

Figure A21. Pass 99 airplane and Radar 5 ground tracks; head-on radar view of airplane wake.

Figures A22, A23, and A24 contain two azimuth scans and the ground tracks for pass 100. In scans 6 and 12, a signal decrease is seen at the location of the smoke, while a signal increase is seen 4° or 95 m clockwise.

Figure A22. Total signal level vs. antenna azimuth angle compared with clutter scan for pass 100, azimuth scan 6, on 01-10-95.

Figure A23. As for figure A22, except for azimuth scan 12.

Figure A24. Pass 100 airplane and Radar 5 ground tracks; head-on radar view of airplane wake.

Figures A25, A26, A27, and A28 contain three azimuth scans and the ground tracks for pass 103. During this pass, a crosswind was blowing the smoke trails across the field of view to the left. In scans 8, 17, and 23, a signal increase is seen at or near the smoke trails.

Radar settings: R = 1364 m, Az = scanning, El = 20.0°
Airplane crossing at time = 20:05:36.0, R = 1358 m, Az = 24.2°, El = 19.9°, Alt = 478 m AGL

Figure A25. Total signal level vs. antenna azimuth angle compared with clutter scan for pass 103, azimuth scan 8, on 01-10-95.

Radar settings: R = 1364 m, Az = scanning, El = 20.0°
Airplane crossing at time = 20:05:36.0, R = 1358 m, Az = 24.2°, El = 19.9°, Alt = 478 m AGL

Figure A26. As for figure A25, except for azimuth scan 17.

Radar settings: R = 1364 m, Az = scanning, El = 20.0°
Airplane crossing at time = 20:05:36.0, R = 1358 m, Az = 24.2°, El = 19.9°, Alt = 478 m AGL

Scan 1–clutter
Scan 23–vortex plus clutter
● Scan 23–vortex plus clutter with smoke

20:07:14.0, $\Delta\eta = -124.3$ dBm^{-1}

Figure A27. As for figure A25, except for azimuth scan 23.

← North

■ Airplane track
□ R5 range cell track
○ R5 radar

20:07:14.0

20:06:41.0

20:06:03.0

Figure A28. Pass 103 airplane and Radar 5 ground tracks; head-on radar view of airplane wake.

28

Figures A29, A30, A31, and A32 contain three azimuth scans and the ground tracks for pass 104. In scans 5, 11, and 15, a signal increase is seen 2° counterclockwise from the smoke trails. The strongest increase is seen in scan 11, 48 sec after the aircraft crosses the radar track.

Radar settings: R = 1364 m, Az = scanning, El = 20.0°
Airplane crossing at time = 20:10:16.2, R = 1431 m, Az = 20.2°, El = 19.4°, Alt = 490 m AGL

——————— Scan 1–clutter
o   Scan 5–vortex plus clutter
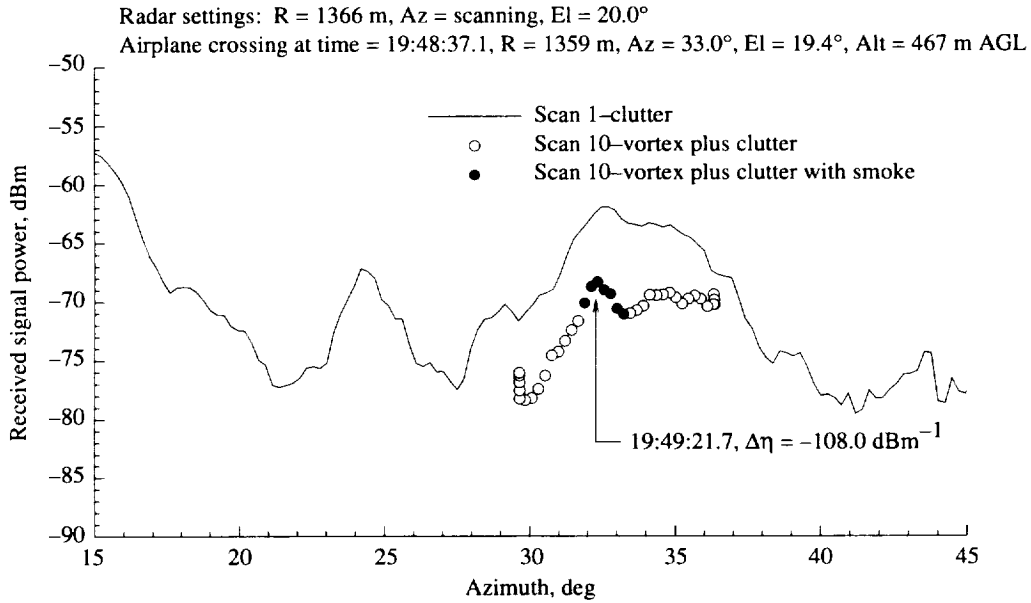•   Scan 5–vortex plus clutter with smoke

20:10:35.9, Δη = −129.2 dBm^{-1}
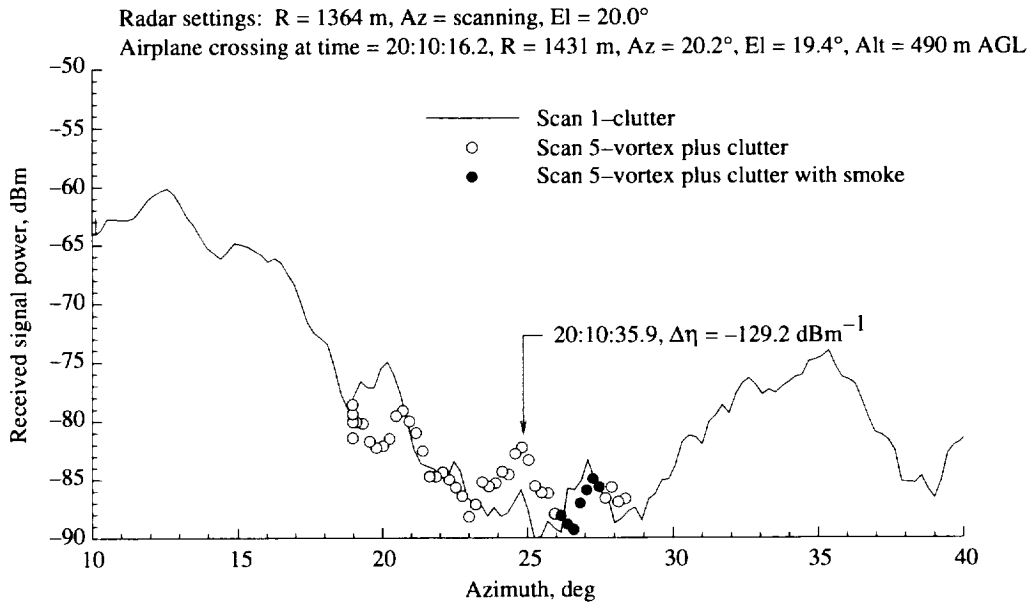
Figure A29. Total signal level vs. antenna azimuth angle compared with clutter scan for pass 104, azimuth scan 5, on 01-10-95.

Radar settings: R = 1364 m, Az = scanning, El = 20.0°
Airplane crossing at time = 20:10:16.2, R = 1431 m, Az = 20.2°, El = 19.4°, Alt = 490 m AGL

——————— Scan 1–clutter
o   Scan 11–vortex plus clutter
•   Scan 11–vortex plus clutter with smoke

20:11:04.3, Δη = −126.7 dBm^{-1}
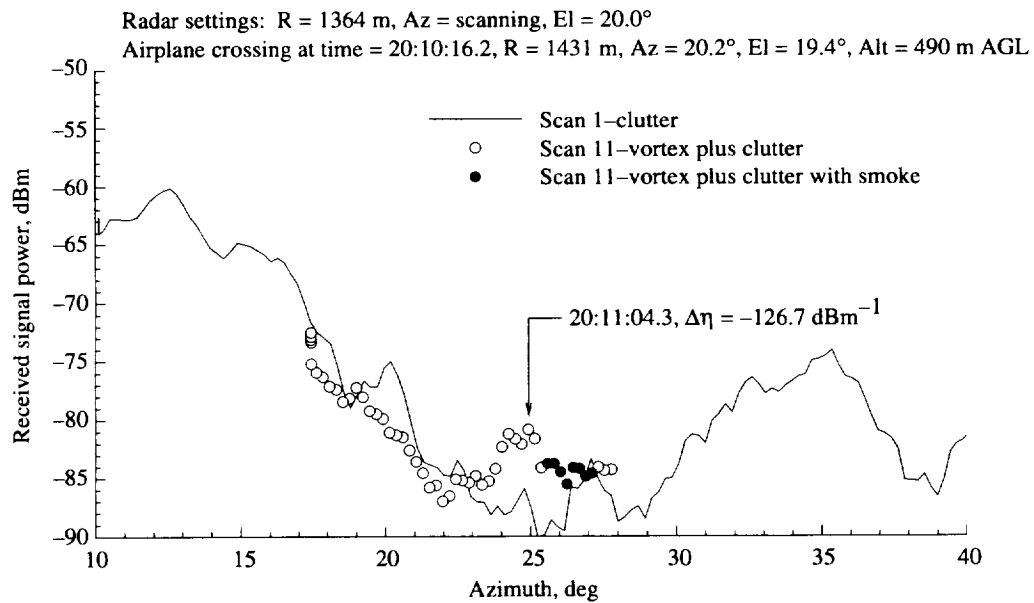
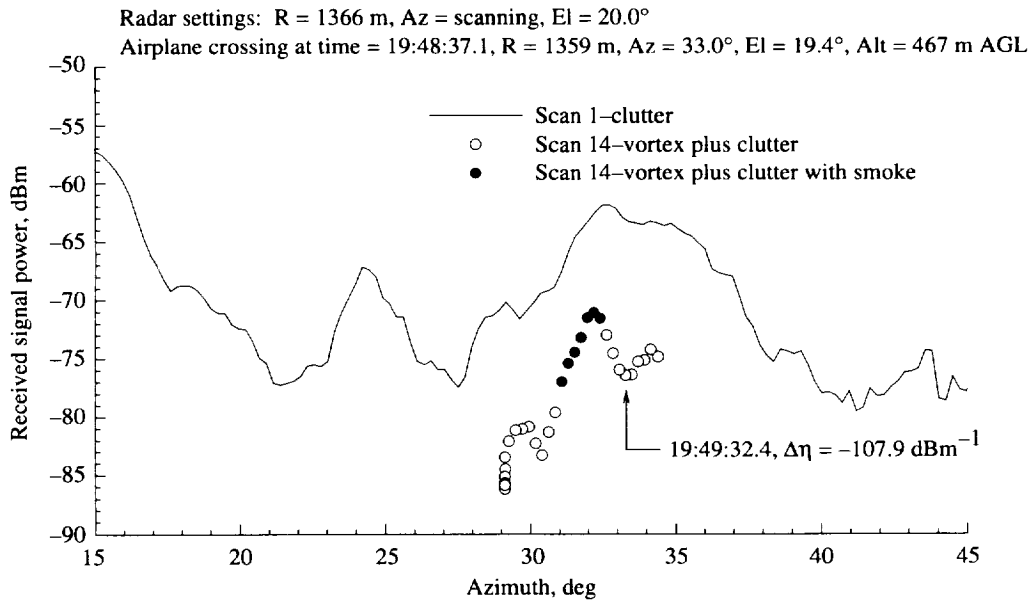Figure A30. As for figure A29, except for azimuth scan 11.

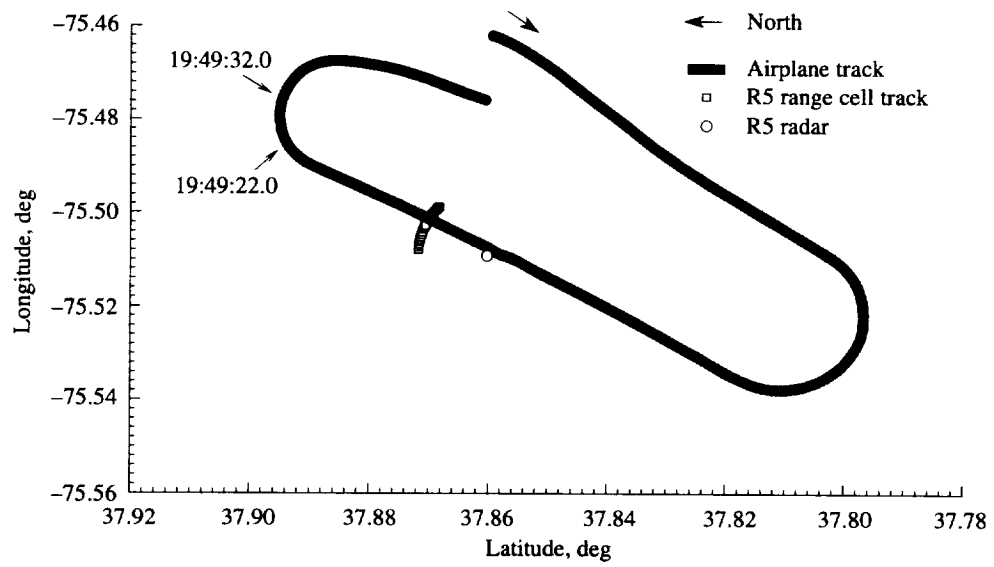Figure A31. As for figure A29, except for azimuth scan 15.
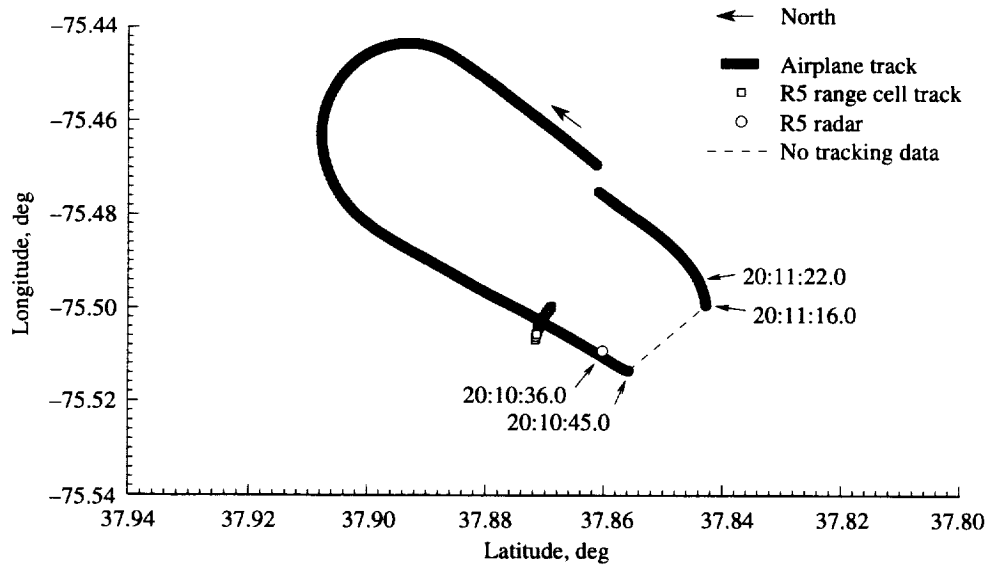
Figure A32. Pass 104 airplane and Radar 5 ground tracks; head-on radar view of airplane wake.

Figures A33, A34, A35, and A36 contain three azimuth scans and the ground tracks for pass 106. Following the smoke trails from right to left, one sees a signal increase in scan 5, a decrease in scan 12, and an increase and a decrease in scan 22.

Radar settings: R = 1111 m, Az = scanning, El = 20.0°
Airplane crossing at time = 20:19:45.25, R = 1110 m, Az = 26.4°, El = 20.1°, Alt = 396 m AGL

20:20:09.0, $\Delta\eta$ = -120.0 dBm^{-1}

————— Scan 1-clutter
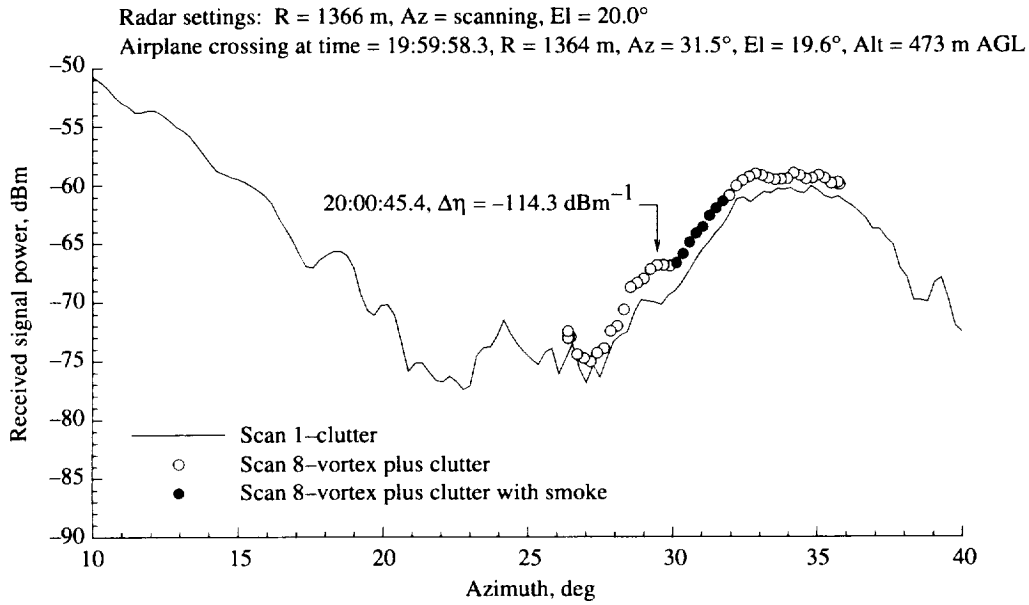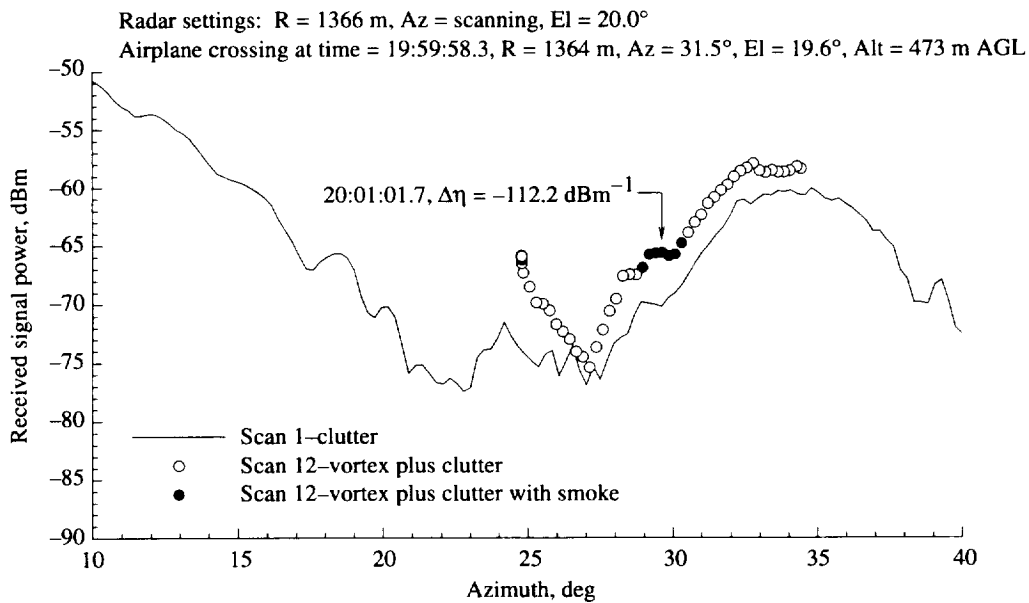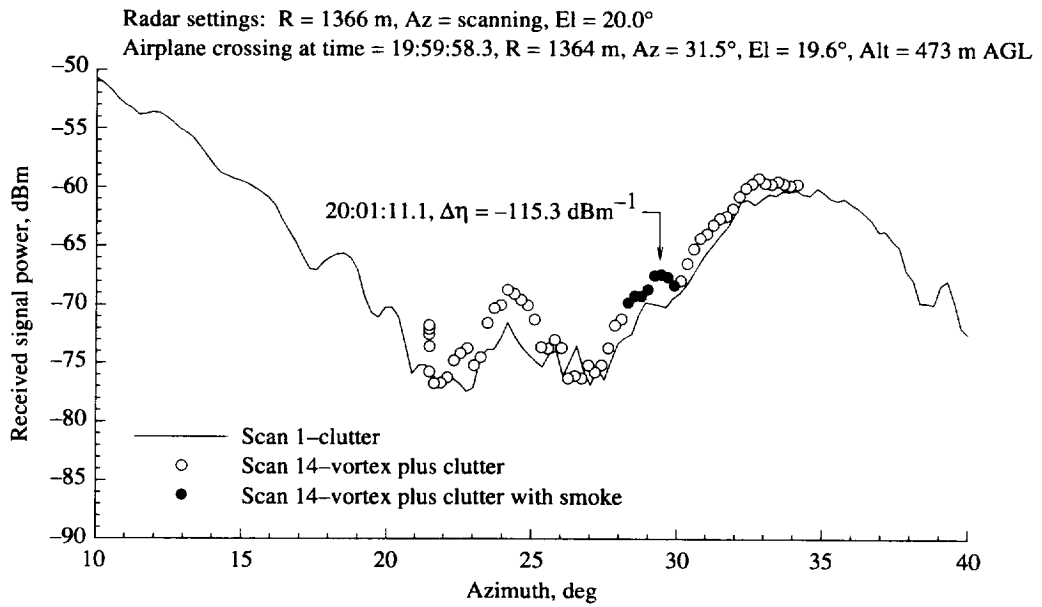   o   Scan 5-vortex plus clutter
   •   Scan 5-vortex plus clutter with smoke

Figure A33. Total signal level vs. antenna azimuth angle compared with clutter scan for pass 106, azimuth scan 5, on 01-10-95.

Radar settings: R = 1111 m, Az = scanning, El = 20.0°
Airplane crossing at time = 20:19:45.25, R = 1110 m, Az = 26.4°, El = 20.1°, Alt = 396 m AGL

————— Scan 1-clutter
   o   Scan 12-vortex plus clutter
   •   Scan 12-vortex plus clutter with smoke

20:20:38.1, $\Delta\eta$ = -121.3 dBm^{-1}

Figure A34. As for figure A33, except for azimuth scan 12.

Radar settings: R = 1111 m, Az = scanning, El = 20.0°
Airplane crossing at time = 20:19:45.25, R = 1110 m, Az = 26.4°, El = 20.1°, Alt = 396 m AGL

20:21:19.6, $\Delta\eta$ = −114.1 dBm^{-1}

——— Scan 1–clutter
○ Scan 22–vortex plus clutter
● Scan 22–vortex plus clutter with smoke

Figure A35. As for figure A33, except for azimuth scan 22.

◄— North
▬ Airplane track
□ R5 range cell track
○ R5 radar
– – – No tracking data

20:21:20.0

20:20:45.0

20:20:05.0
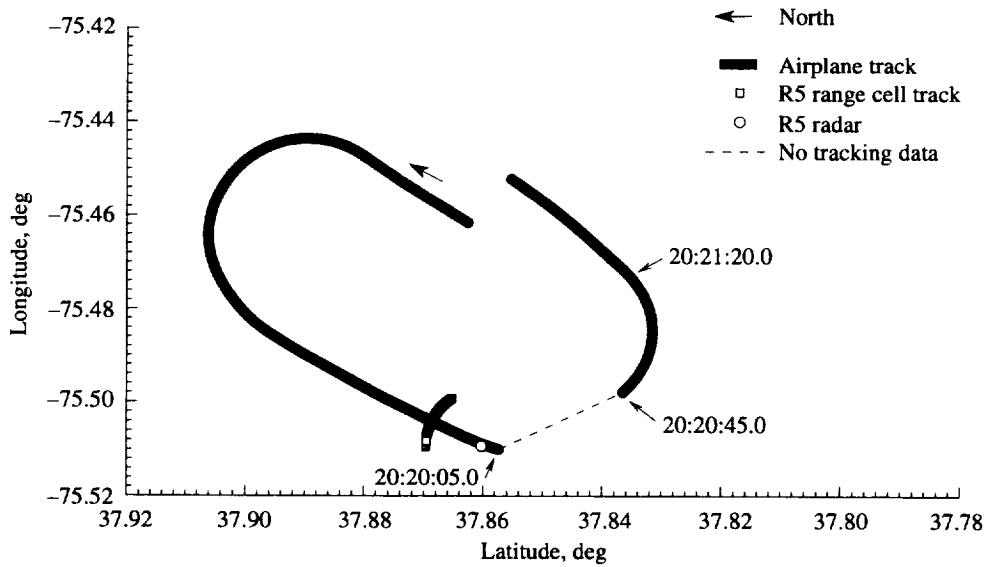
Figure A36. Pass 106 airplane and Radar 5 ground tracks; head-on radar view of airplane wake.

Figures A37, A38, A39, and A40 contain three azimuth scans and the ground tracks for pass 107. In scan 5, a signal decrease is seen at the location of the smoke trails, immediately adjacent to a signal increase. In scan 8, a signal decrease is seen at the smoke trails. In scan 22, a signal increase is seen at the smoke trails, immediately adjacent to a signal decrease. The videotape showed that, by this time, the shape of the smoke trail leftmost in the field of view had changed from a straight line to a corkscrew pattern.

Radar settings: R = 1111 m, Az = scanning, El = 20.0°
Airplane crossing at time = 20:24:39.5, R = 1053 m, Az = 20.6°, El = 23.2°, Alt = 427 m AGL

20:25:08.0, $\Delta\eta = -110.9 \ dBm^{-1}$

Scan 1–clutter
○ Scan 5–vortex plus clutter
● Scan 5–vortex plus clutter with smoke
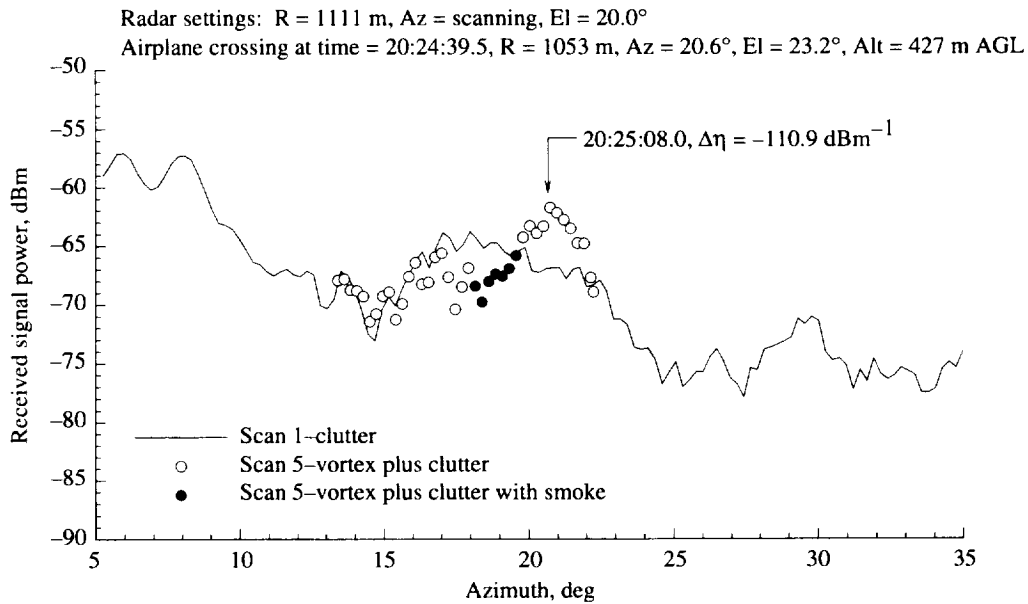
Figure A37. Total signal level vs. antenna azimuth angle compared with clutter scan for pass 107, azimuth scan 5, on 01-10-95.

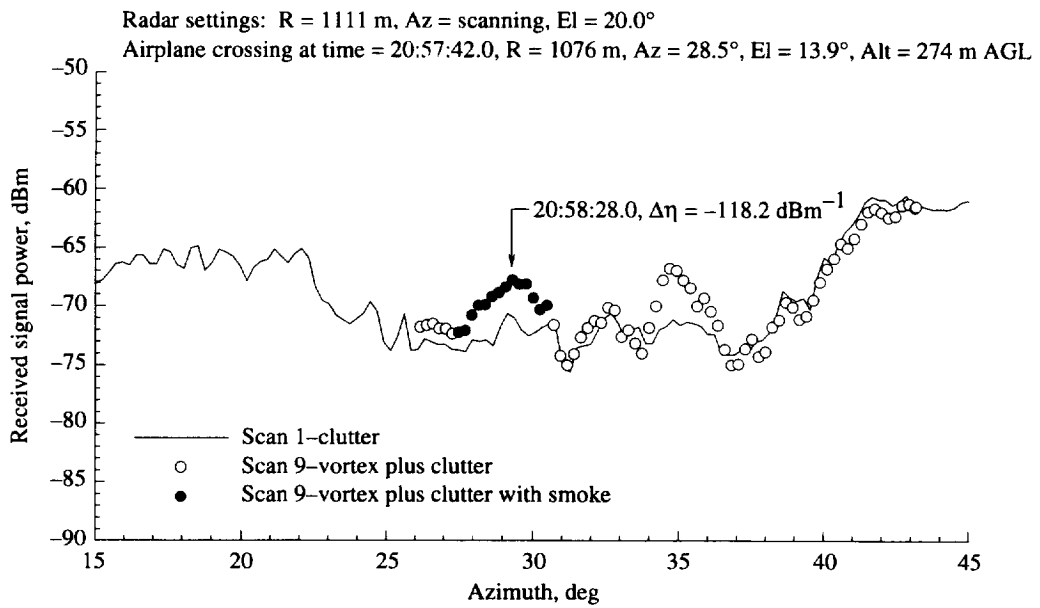Radar settings: R = 1111 m, Az = scanning, El = 20.0°
Airplane crossing at time = 20:24:39.5, R = 1053 m, Az = 20.6°, El = 23.2°, Alt = 427 m AGL

Scan 1–clutter
○ Scan 8–vortex plus clutter
● Scan 8–vortex plus clutter with smoke

20:25:20.9, $\Delta\eta = -112.6 \ dBm^{-1}$
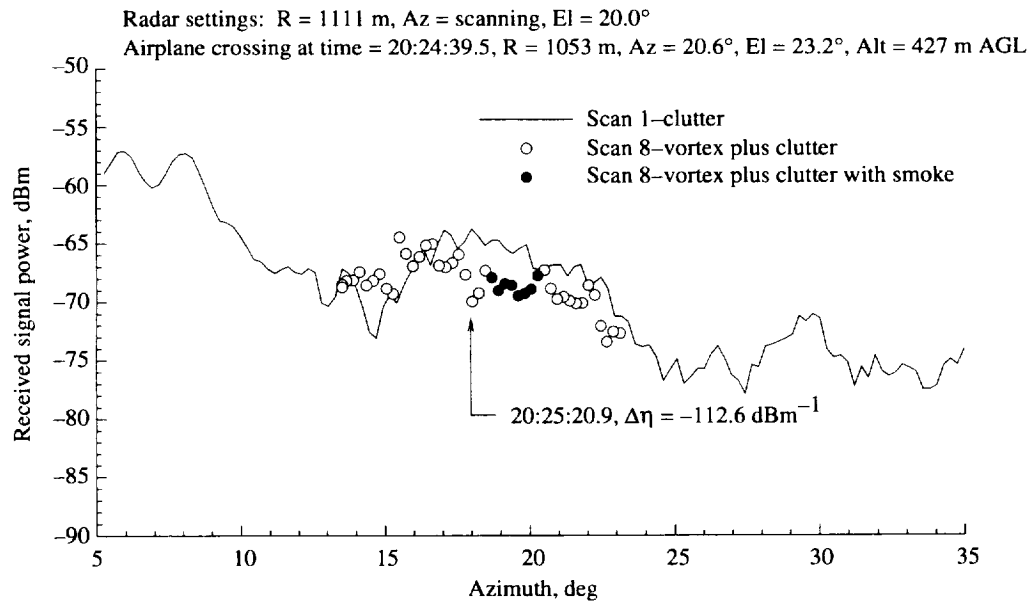
Figure A38. As for figure A37, except for azimuth scan 8.

Figure A39. As for figure A37, except for azimuth scan 22.
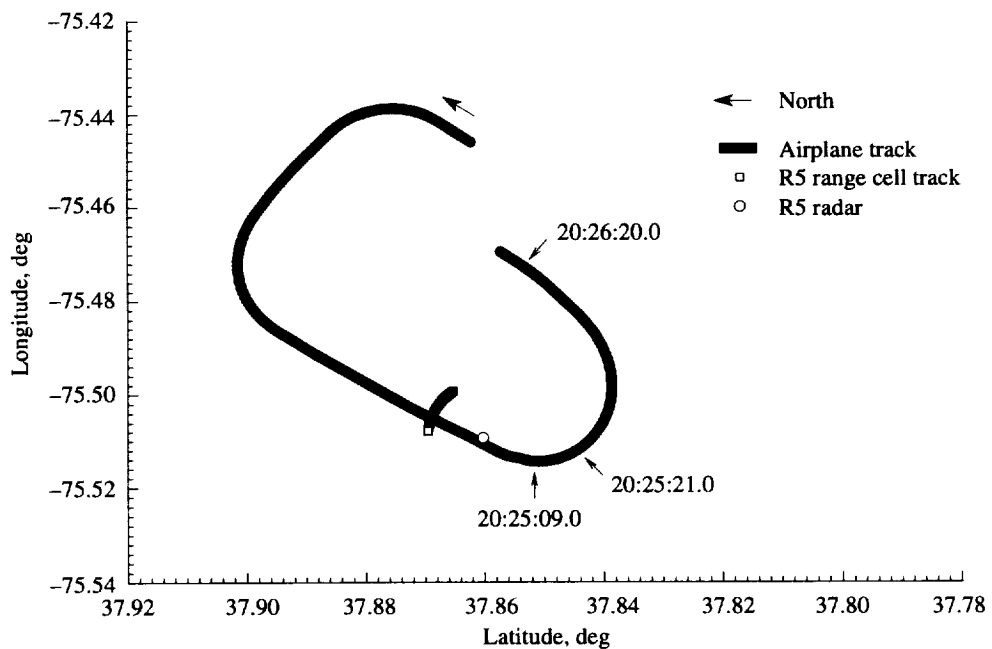
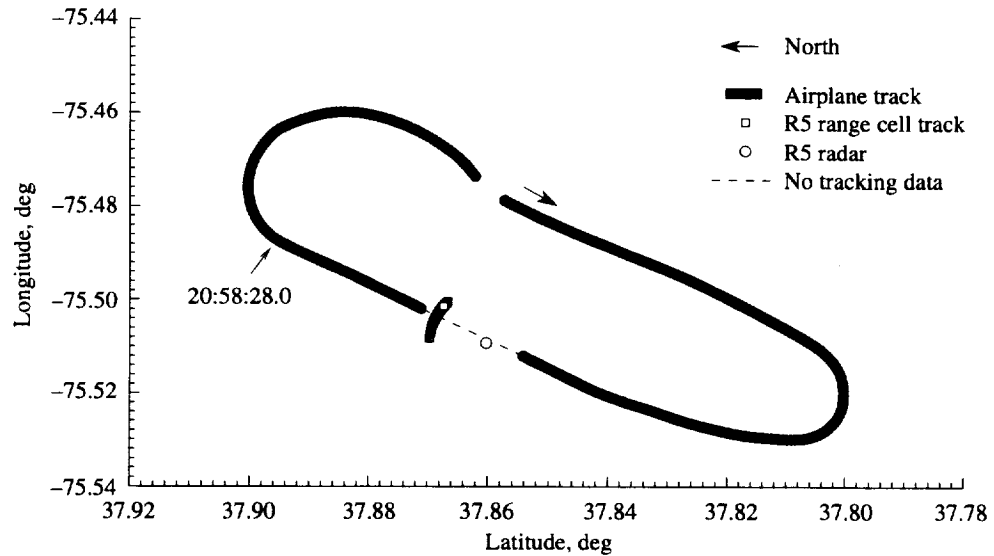

Figure A40. Pass 107 airplane and Radar 5 ground tracks; head-on radar view of airplane wake.

Figures A41, A42, and A43 contain two azimuth scans and the ground tracks for pass 108. In scan 7, a signal increase is seen 4° clockwise or 78 m from the smoke trails. In scan 14, a signal increase is seen at the smoke trails with a signal decrease on either side.

Radar settings: R = 1111 m, Az = scanning, El = 20.0°
Airplane crossing at time = 20:29:19.5, R = 1109 m, Az = 21.3°, El = 20.7°, Alt = 407 m AGL

20:29:52.5, $\Delta\eta$ = -112.4 dBm^{-1}

Scan 1–clutter
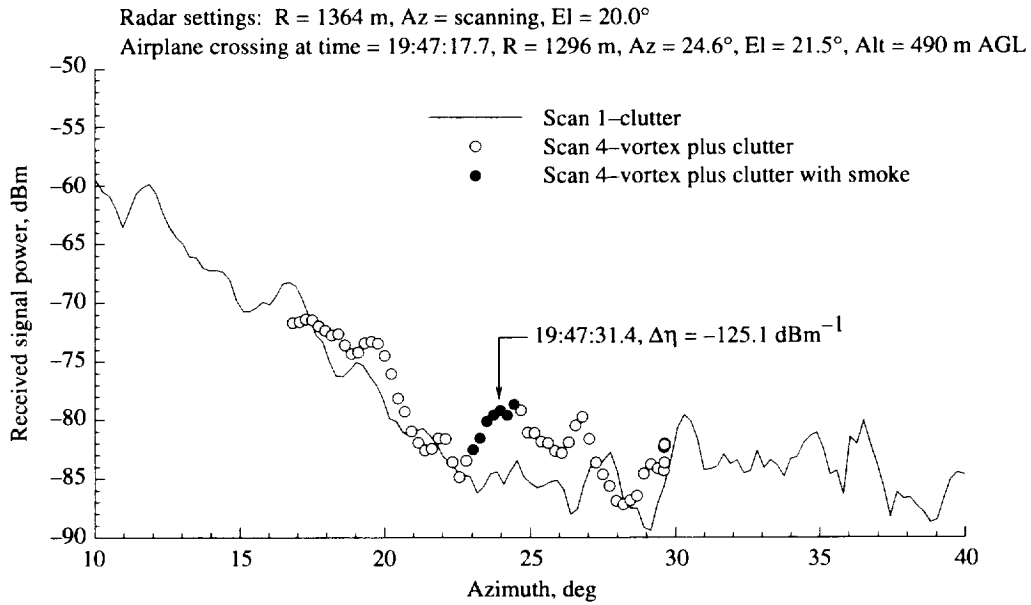o Scan 7–vortex plus clutter
● Scan 7–vortex plus clutter with smoke
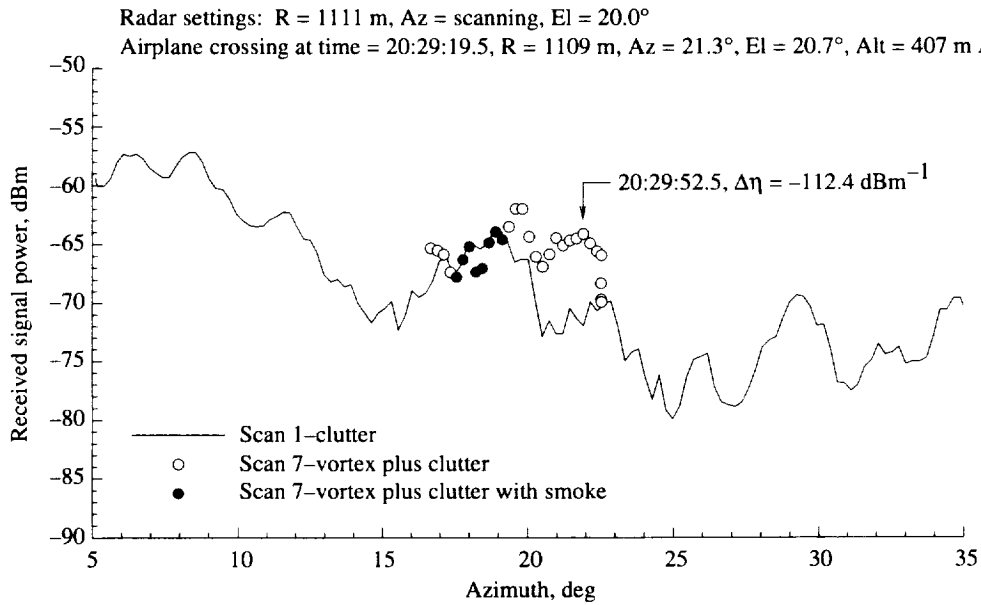
Figure A41. Total signal level vs. antenna azimuth angle compared with clutter scan for pass 108, azimuth scan 7, on 01-10-95.
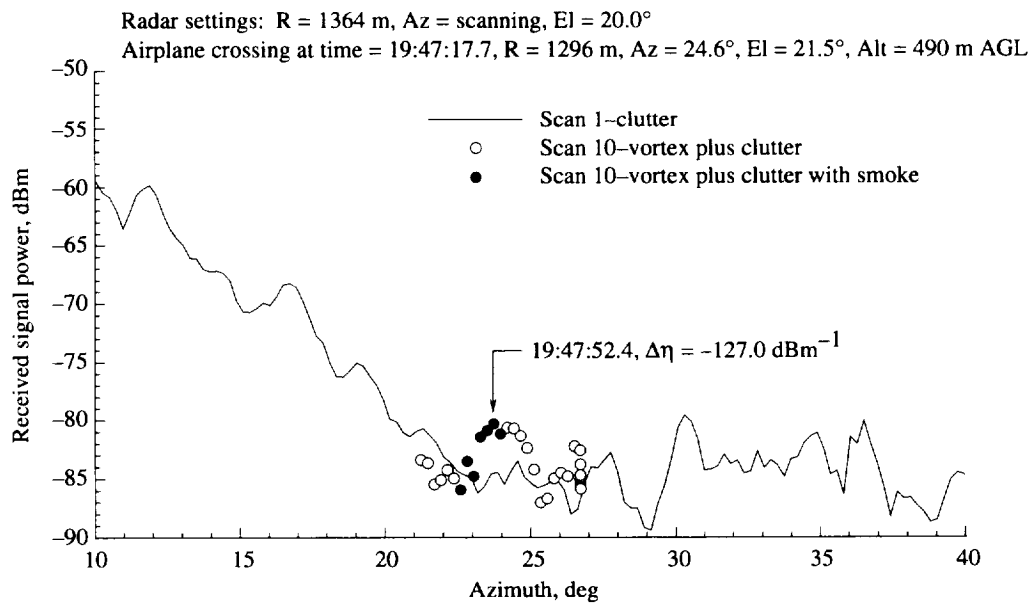
Radar settings: R = 1111 m, Az = scanning, El = 20.0°
Airplane crossing at time = 20:29:19.5, R = 1109 m, Az = 21.3°, El = 20.7°, Alt = 407 m AGL

20:30:37.0, $\Delta\eta$ = -118.8 dBm^{-1}

Scan 1–clutter
o Scan 14–vortex plus clutter
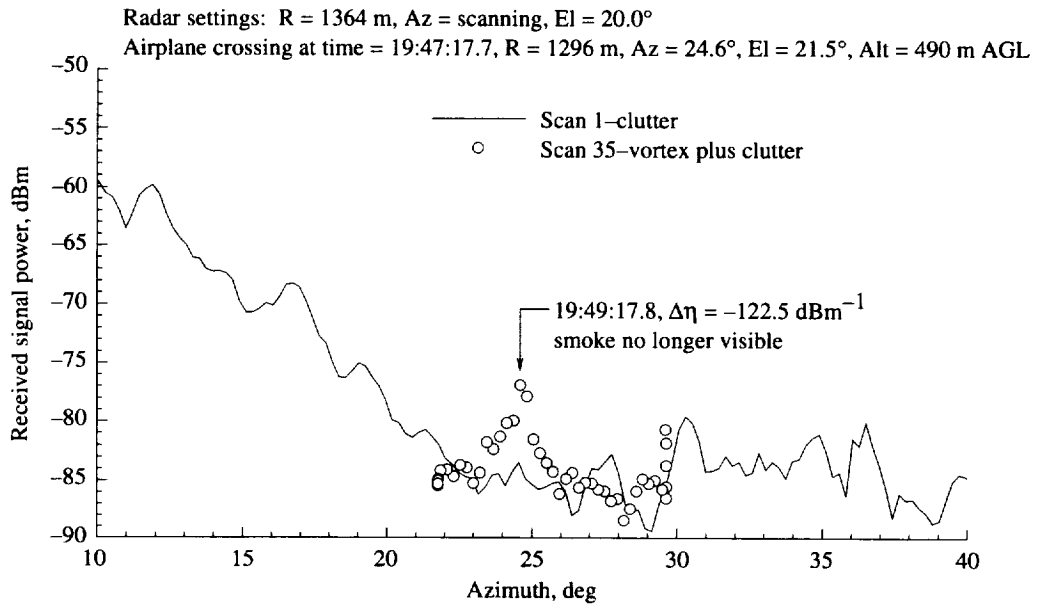● Scan 14–vortex plus clutter with smoke

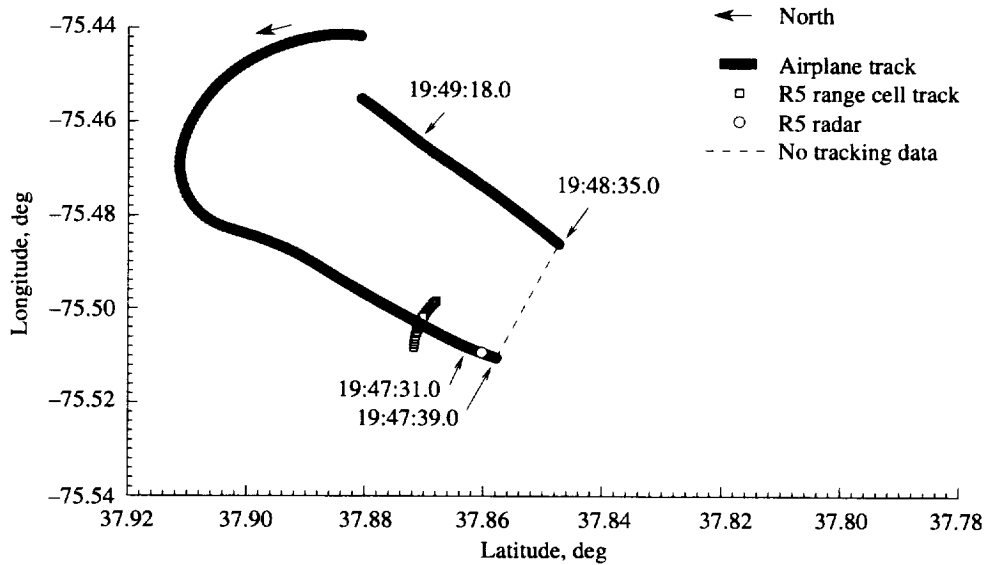Figure A42. As for figure A41, except for azimuth scan 14.

35
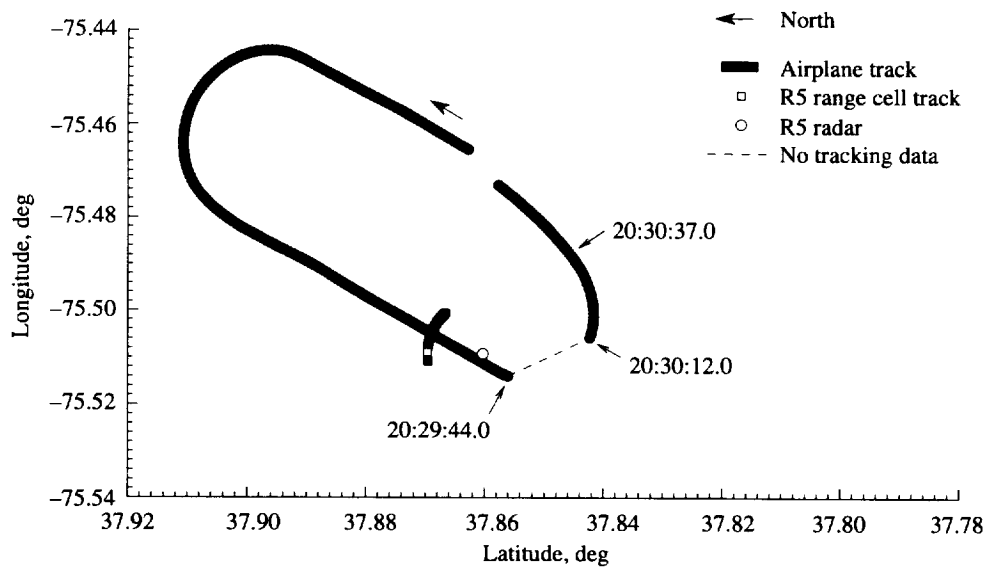
Figure A43. Pass 108 airplane and Radar 5 ground tracks; head-on radar view of airplane wake.

Figures A44, A45, and A46 contain two azimuth scans and the ground tracks for pass 109. During this pass, the antenna was scanning slightly above the elevation of the aircraft track and the smoke trails could not be seen on the bore-sight videotape. In scans 4 and 5, 21 sec and 54 sec after the aircraft crosses the radar track, a large signal increase is seen at 43° azimuth, 155 m from the aircraft track.
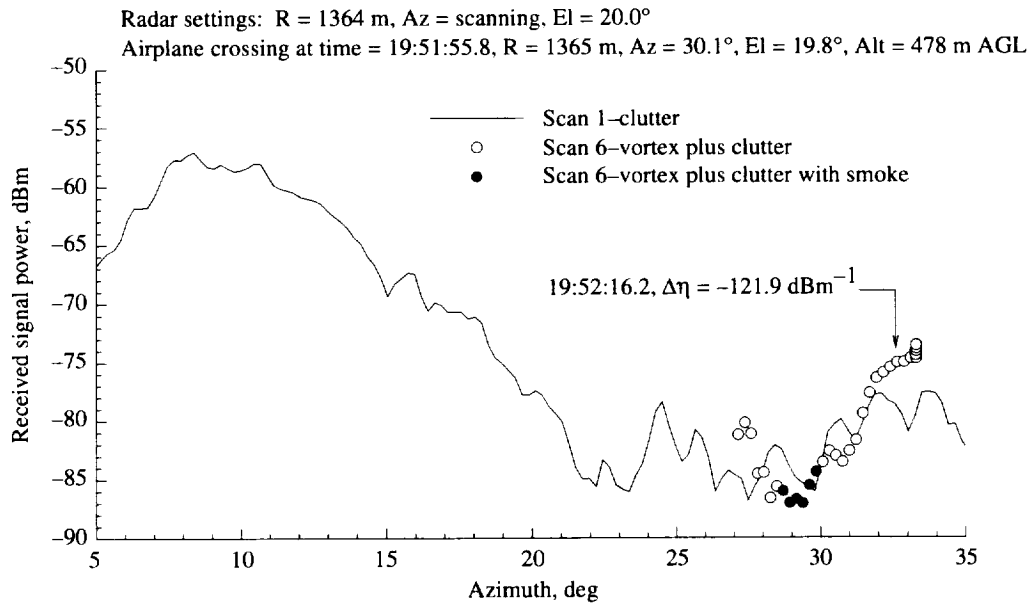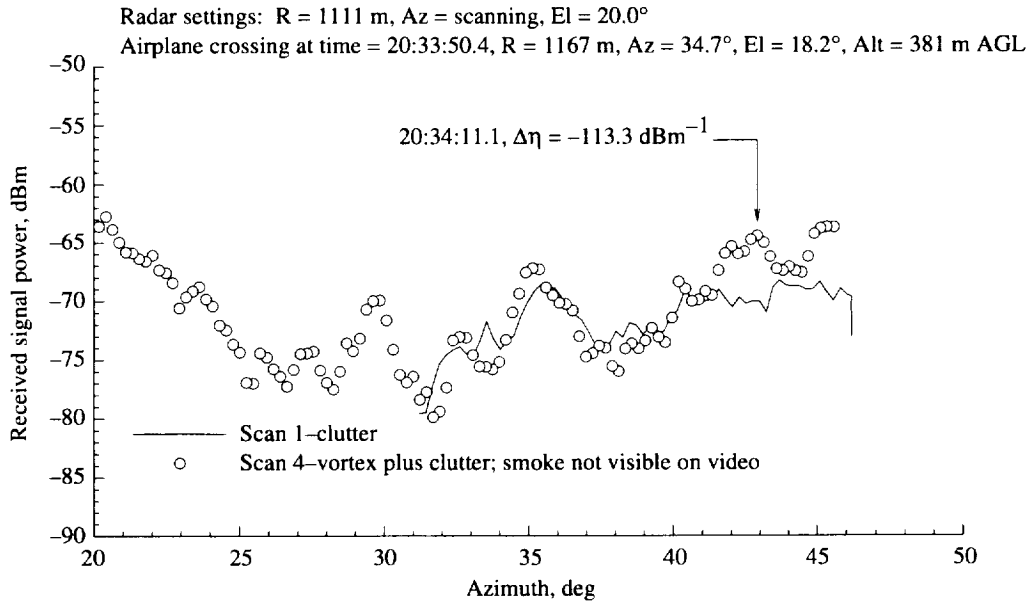

Figure A44. Total signal level vs. antenna azimuth angle compared with clutter scan for pass 109, azimuth scan 4, on 01-10-95.
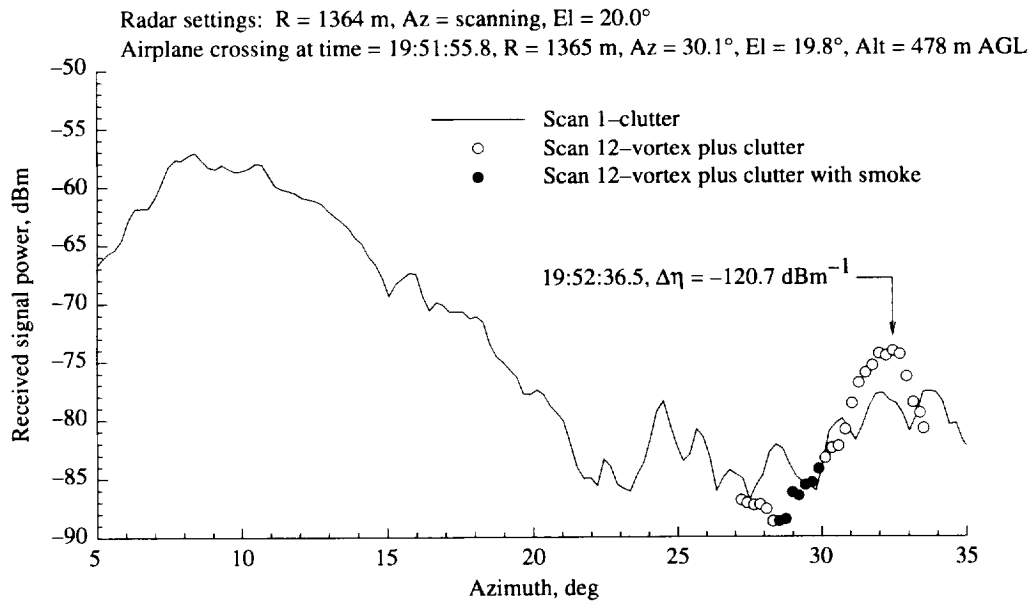

Figure A45. As for figure A44, except for azimuth scan 5.
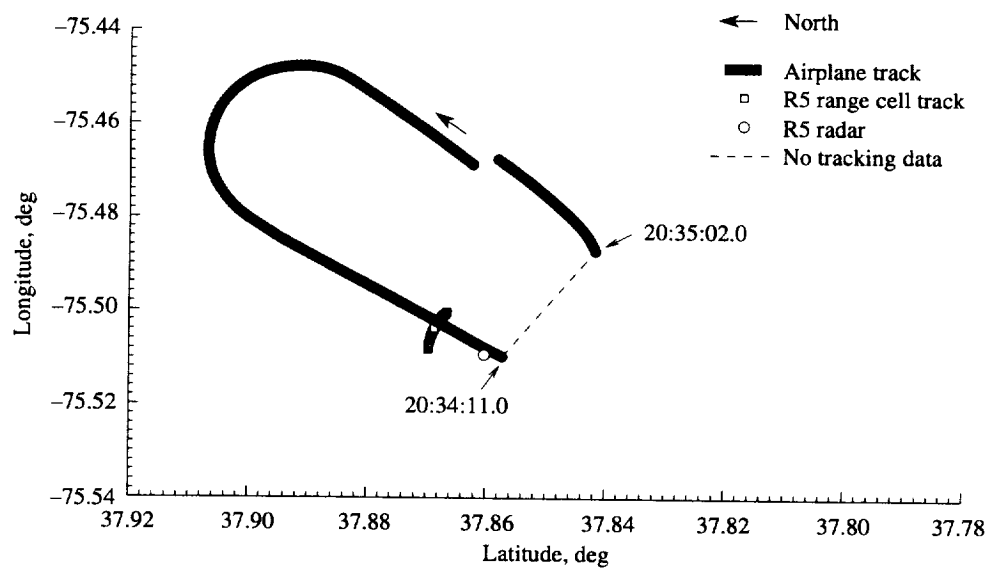
Figure A46. Pass 109 airplane and Radar 5 ground tracks; head-on radar view of airplane wake.

Figures A47, A48, A49, and A50 contain three azimuth scans and the ground tracks for pass 117. In scans 11, 18, and 19, a signal increase is seen accompanied by a signal decrease on either side. The signal disturbance follows the smoke trails as they drift from right to left.
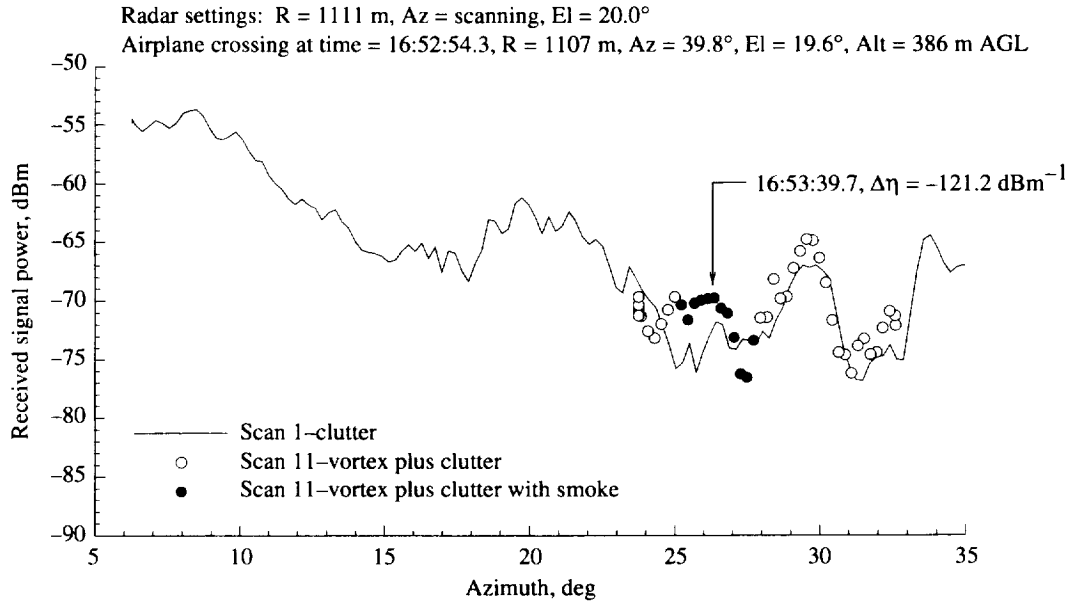
Figure A47. Total signal level vs. antenna azimuth angle compared with clutter scan for pass 117, azimuth scan 11, on 01-11-95.
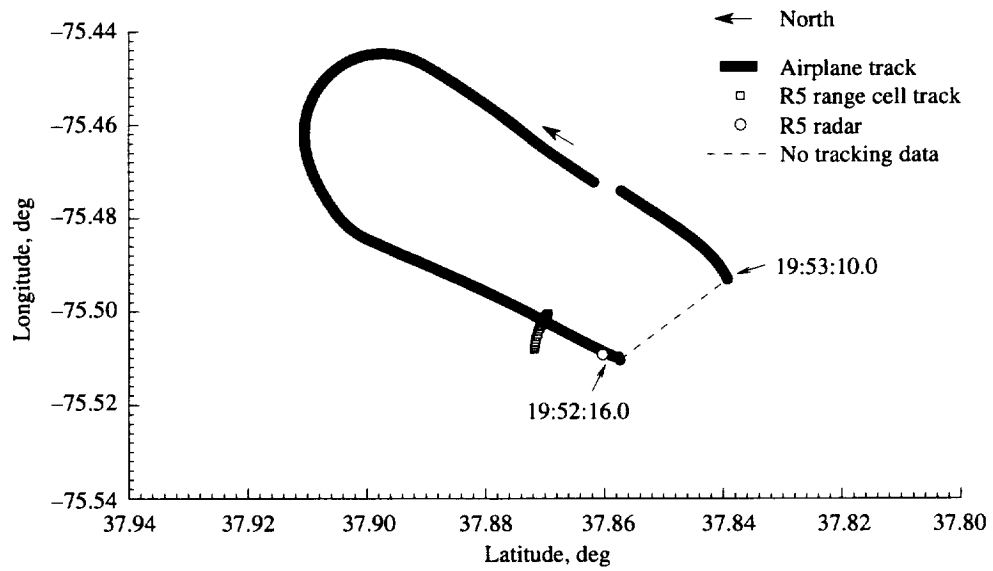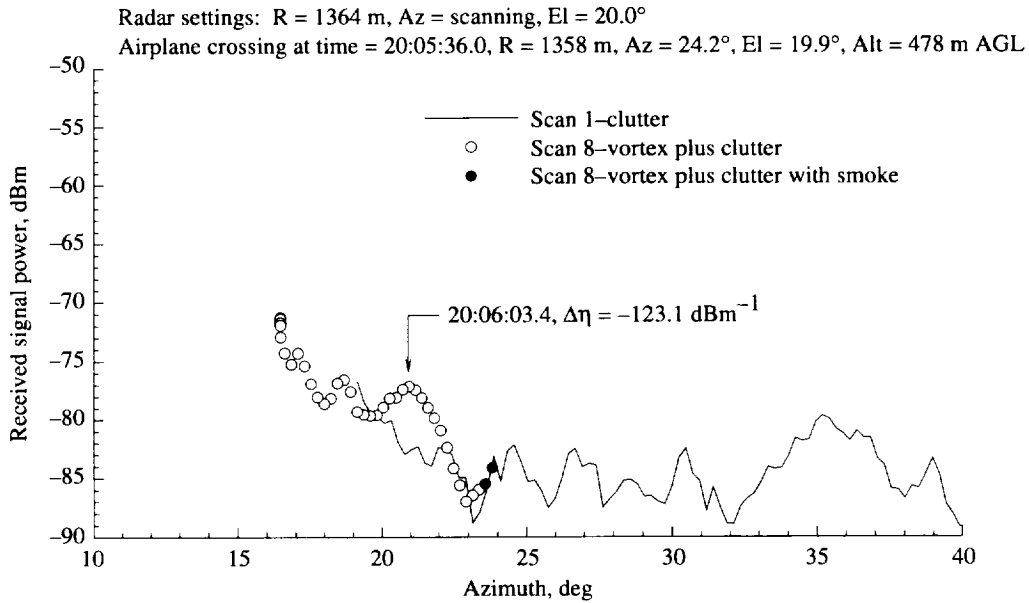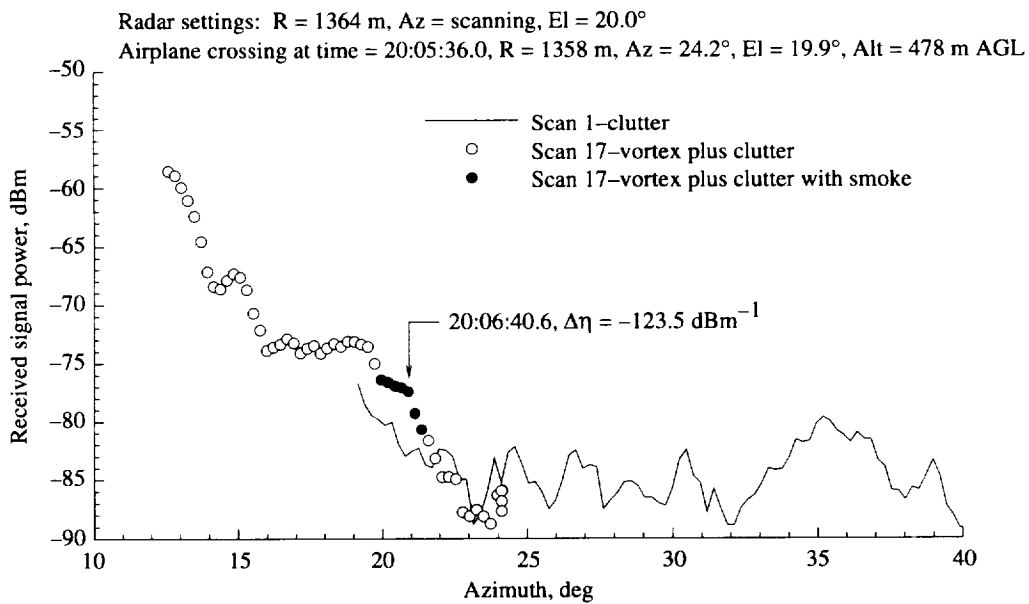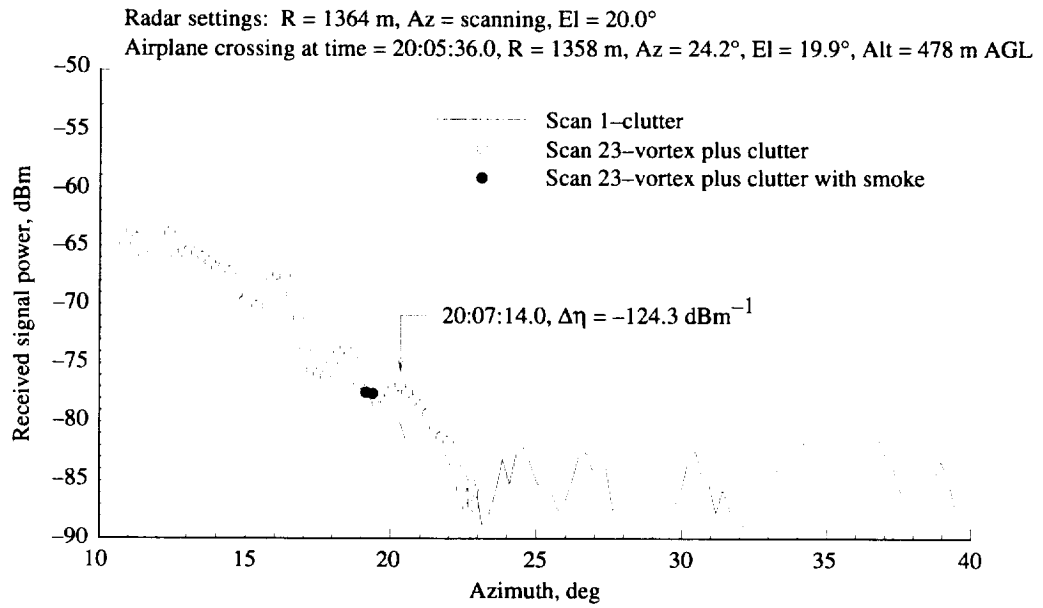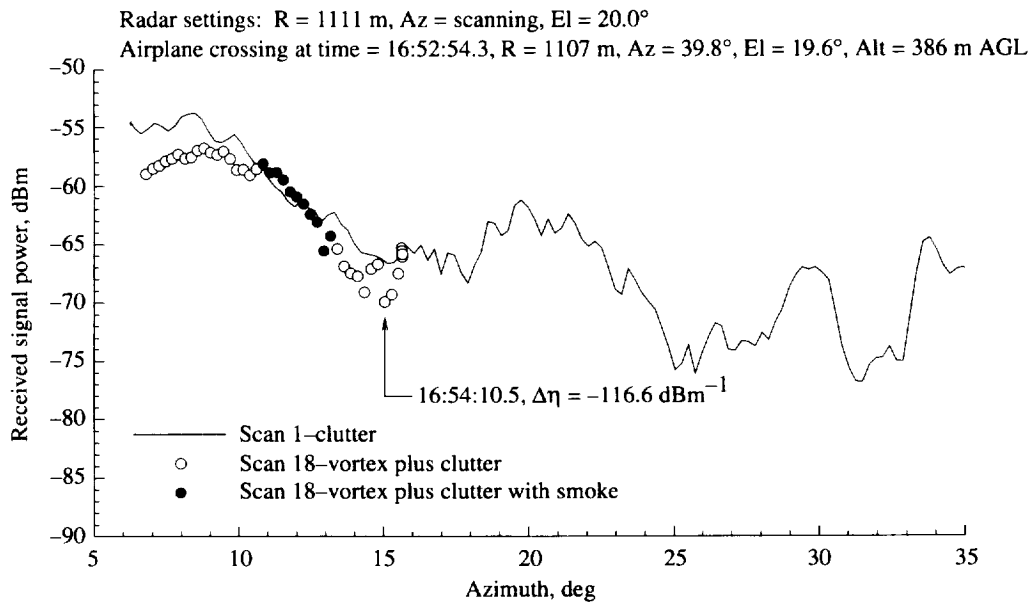

Figure A48. As for figure A47, except for azimuth scan 18.
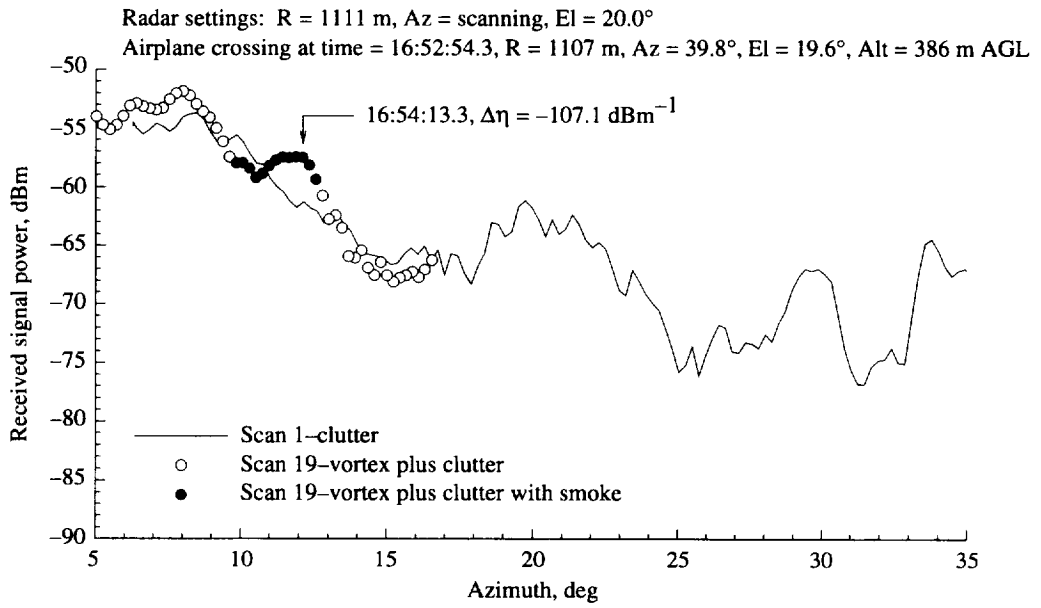
Figure A49. As for figure A47, except for azimuth scan 19.
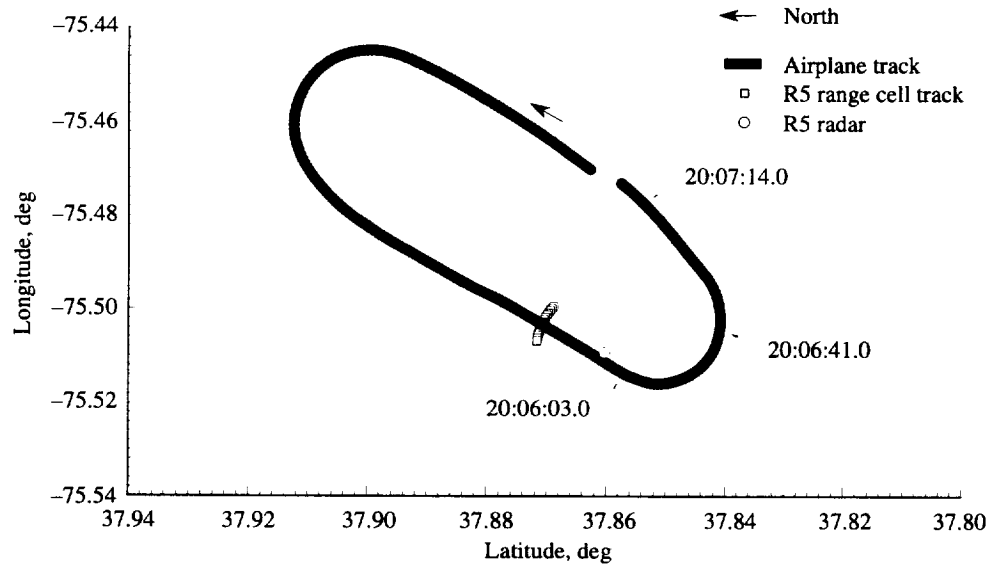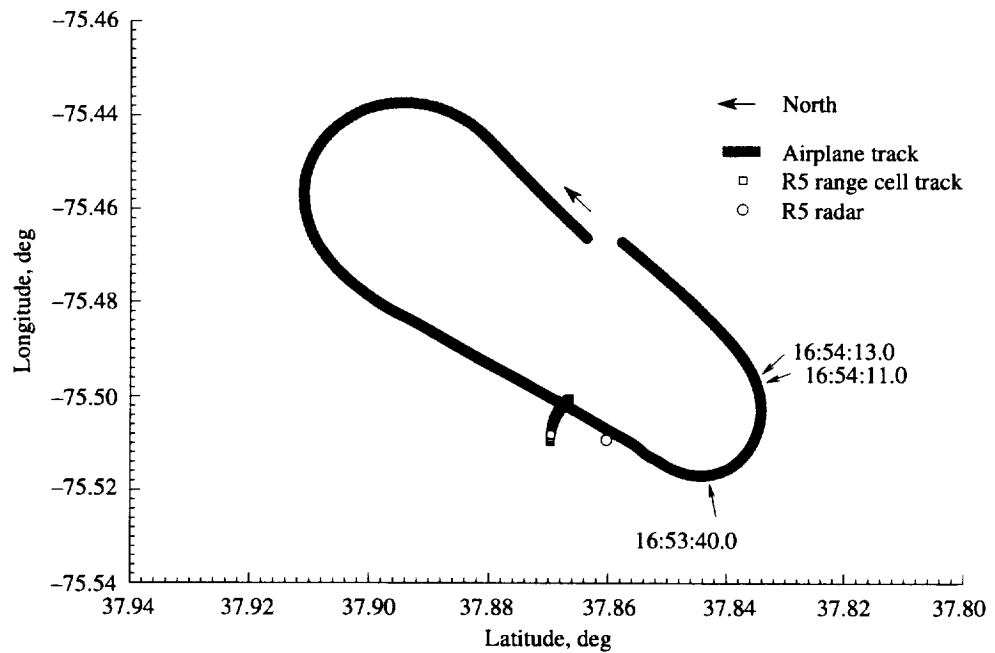

Figure A50. Pass 117 airplane and Radar 5 ground tracks; head-on radar view of airplane wake.

Figures A51, A52, A53, A54, and A55 contain four azimuth scans and ground tracks for pass 122. In scan 4, signal increases are seen on either side of the smoke trails. In scans 5, 10, and 11, a signal increase moves with the smoke trails from right to left. The videotape showed that the smoke trails had been blown diagonal to the camera view by 17:21:48.0, which implies that the wake should occupy an increased angular span, compared to the wake in most of the passes.

Radar settings: R = 1366 m, Az = scanning, El = 20.0°
Airplane crossing at time = 17:21:31.7, R = 1367 m, Az = 27.2°, El = 20.0°, Alt = 481 m AGL

—————— Scan 1–clutter
○   Scan 4–vortex plus clutter
●   Scan 4–vortex plus clutter with smoke

17:21:53.3, $\Delta\eta = -122.8$ dBm^{-1}

Azimuth, deg

Received signal power, dBm
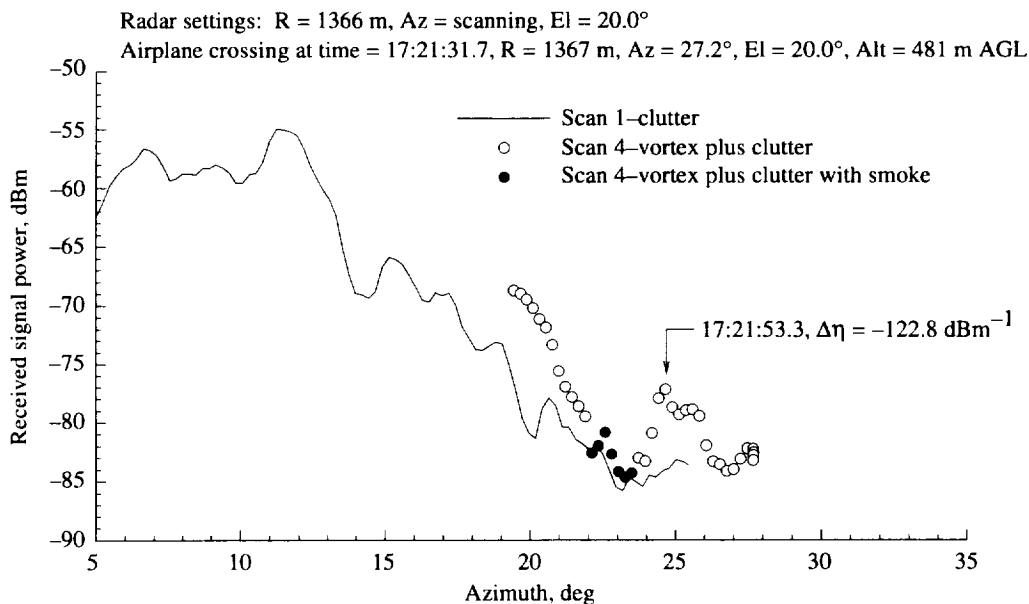
Figure A51. Total signal level vs. antenna azimuth angle compared with clutter scan for pass 122, azimuth scan 4, on 01-11-95.

Radar settings: R = 1366 m, Az = scanning, El = 20.0°
Airplane crossing at time = 17:21:31.7, R = 1367 m, Az = 27.2°, El = 20.0°, Alt = 481 m AGL

—————— Scan 1–clutter
○   Scan 5–vortex plus clutter
●   Scan 5–vortex plus clutter with smoke

17:21:56.8, $\Delta\eta = -124.8$ dBm^{-1}

Azimuth, deg

Received signal power, dBm
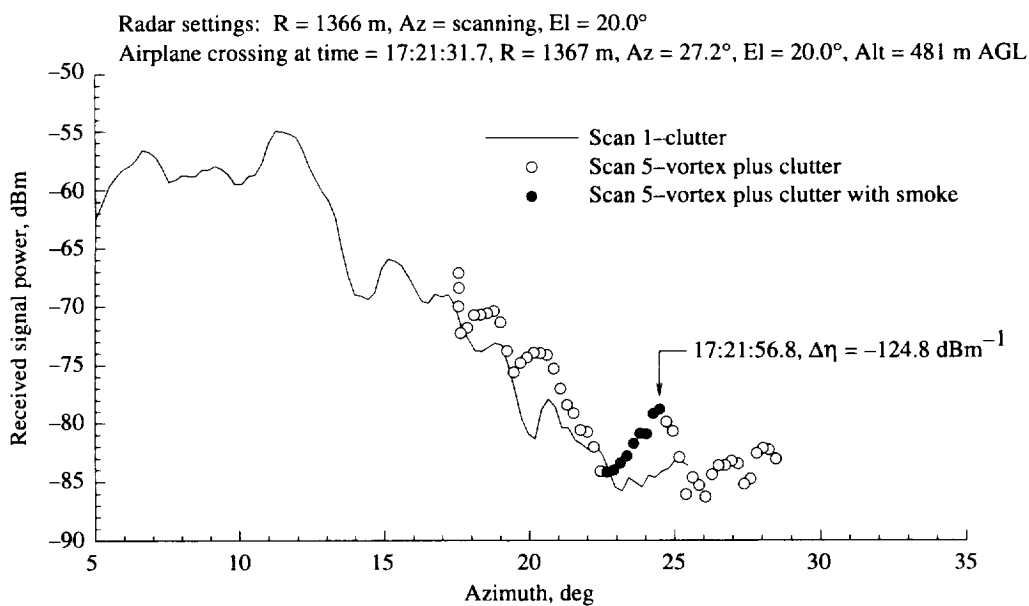
Figure A52. As for figure A51, except for azimuth scan 5.

Radar settings: R = 1366 m, Az = scanning, El = 20.0°
Airplane crossing at time = 17:21:31.7, R = 1367 m, Az = 27.2°, El = 20.0°, Alt = 481 m AGL

17:22:18.6, $\Delta\eta$ = −104.7 dBm^{-1}

——— Scan 1–clutter
○ Scan 10–vortex plus clutter
● Scan 10–vortex plus clutter with smoke
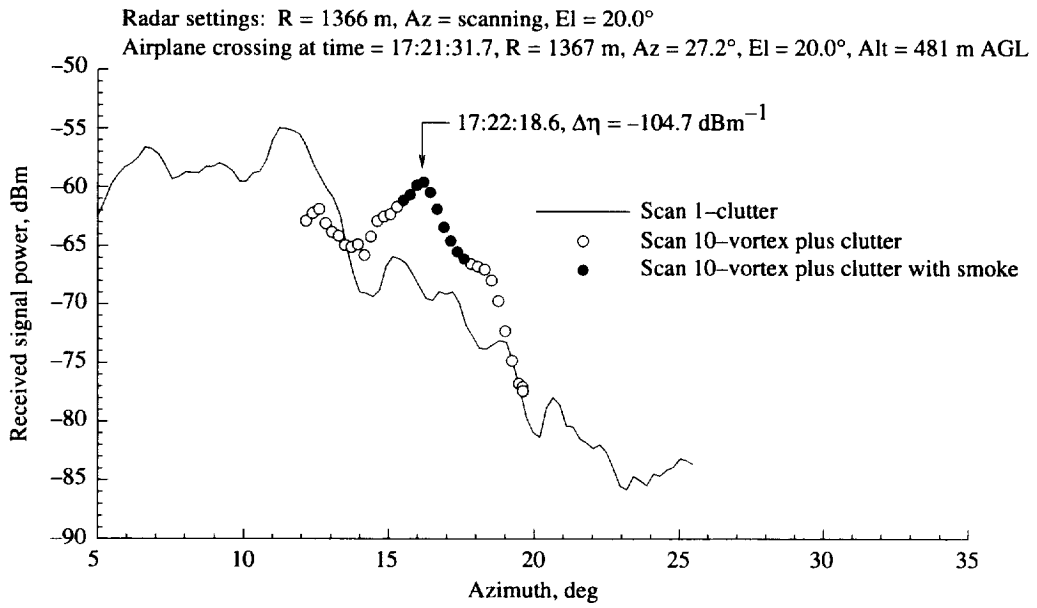
Figure A53. As for figure A51, except for azimuth scan 10.

Radar settings: R = 1366 m, Az = scanning, El = 20.0°
Airplane crossing at time = 17:21:31.7, R = 1367 m, Az = 27.2°, El = 20.0°, Alt = 481 m AGL

17:22:22.3, $\Delta\eta$ = −106.2 dBm^{-1}

——— Scan 1–clutter
○ Scan 11–vortex plus clutter
● Scan 11–vortex plus clutter with smoke
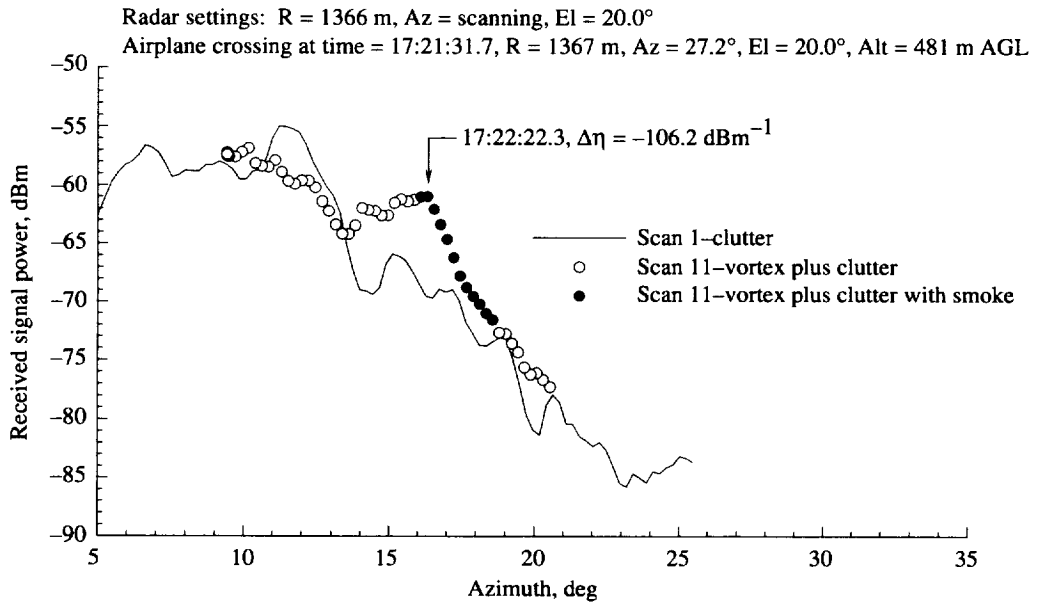
Figure A54. As for figure A51, except for azimuth scan 11.
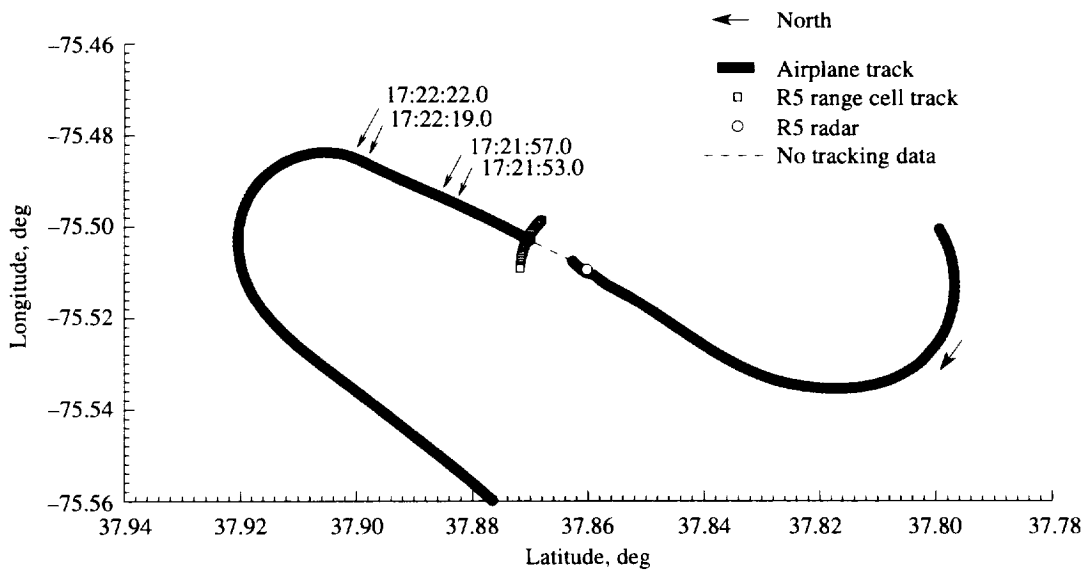
Figure A55. Pass 122 airplane and Radar 5 ground tracks; tail-on radar view of airplane wake.

Figures A56, A57, A58, and A59 contain three azimuth scans and the ground tracks for pass 123. In scan 4, a signal increase is seen coincident with the smoke trails, immediately adjacent to a signal decrease. In scan 7, a signal increase is seen between two signal decreases. In scan 123, a signal decrease is seen coincident with the smoke trails, adjacent to a signal increase. Over a 48 sec period, the signal disturbance moves with the smoke from right to left.
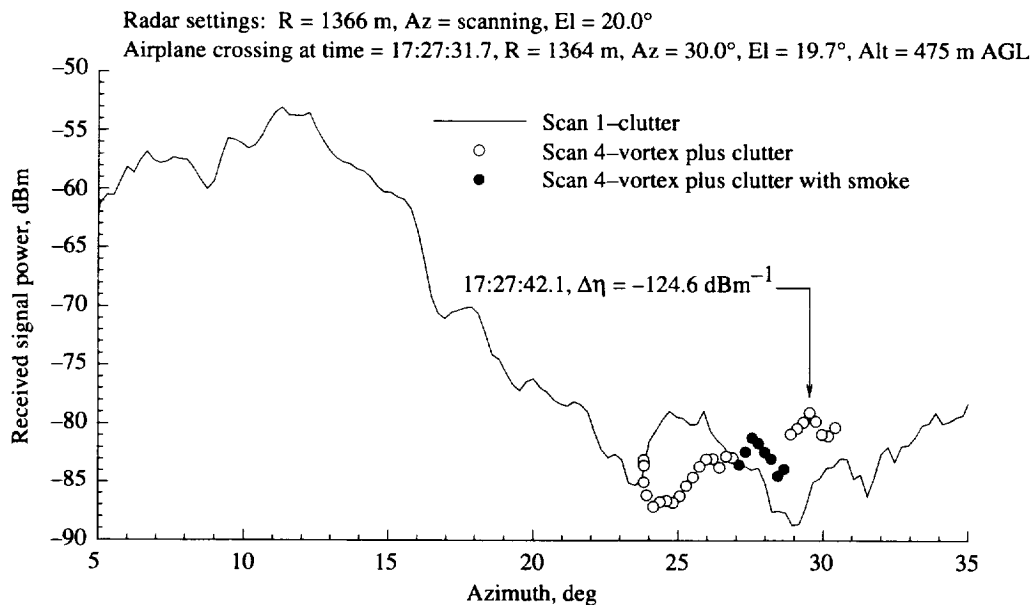
Figure A56. Total signal level vs. antenna azimuth angle compared with clutter scan for pass 123, azimuth scan 4, on 01-11-95.
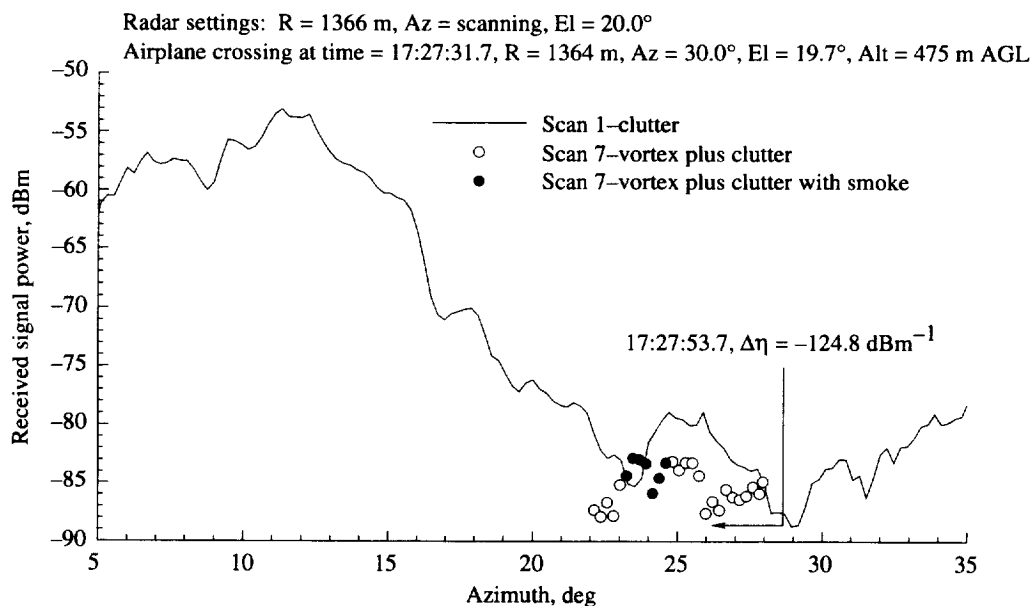
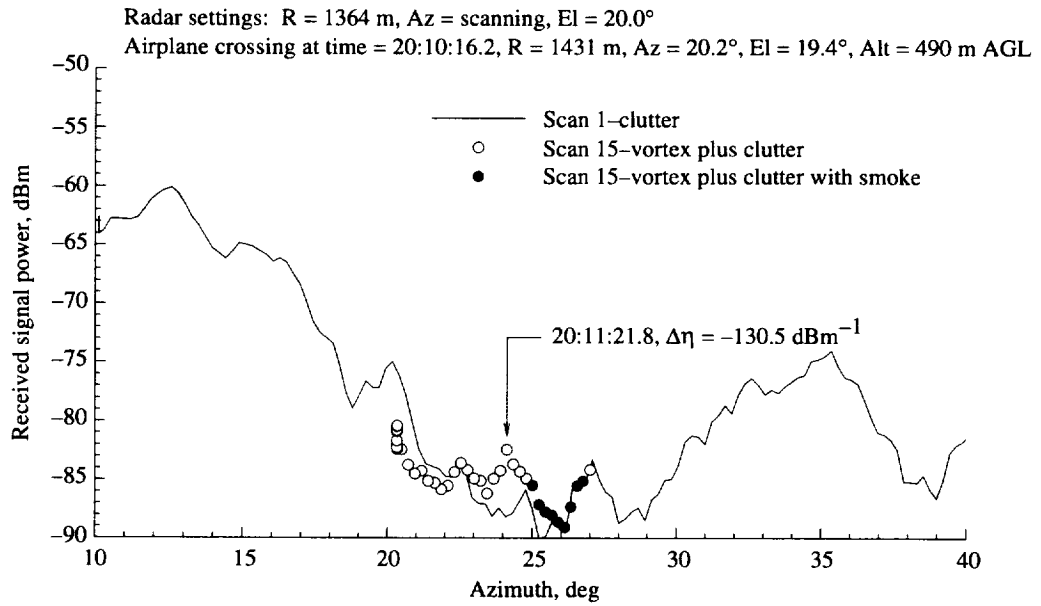

Figure A57. As for figure A56, except for azimuth scan 7.

Radar settings: R = 1366 m, Az = scanning, El = 20.0°
Airplane crossing at time = 17:27:31.7, R = 1364 m, Az = 30.0°, El = 19.7°, Alt = 475 m AGL
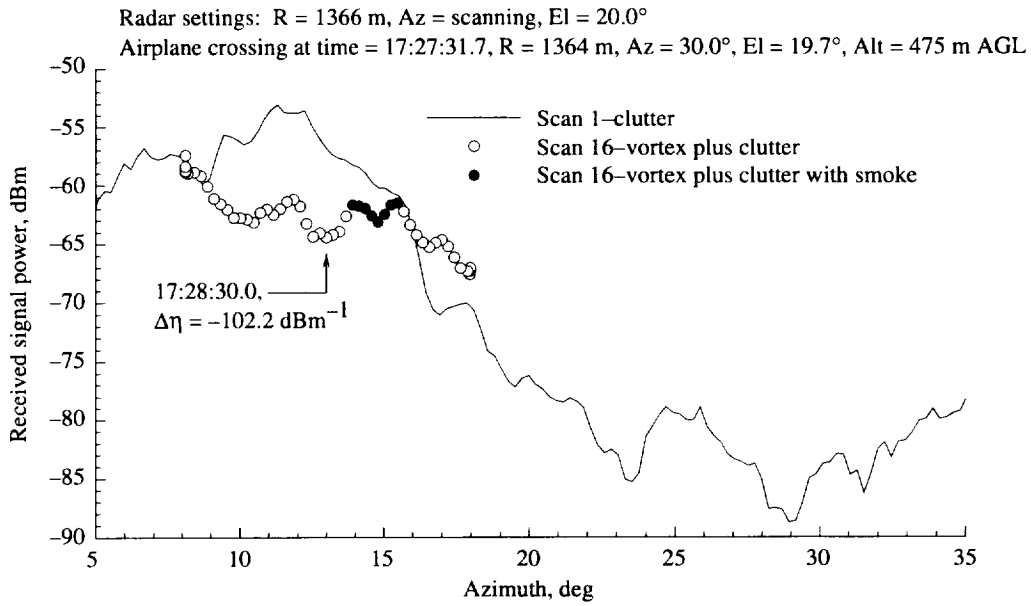
Figure A58. As for figure A56, except for azimuth scan 16.
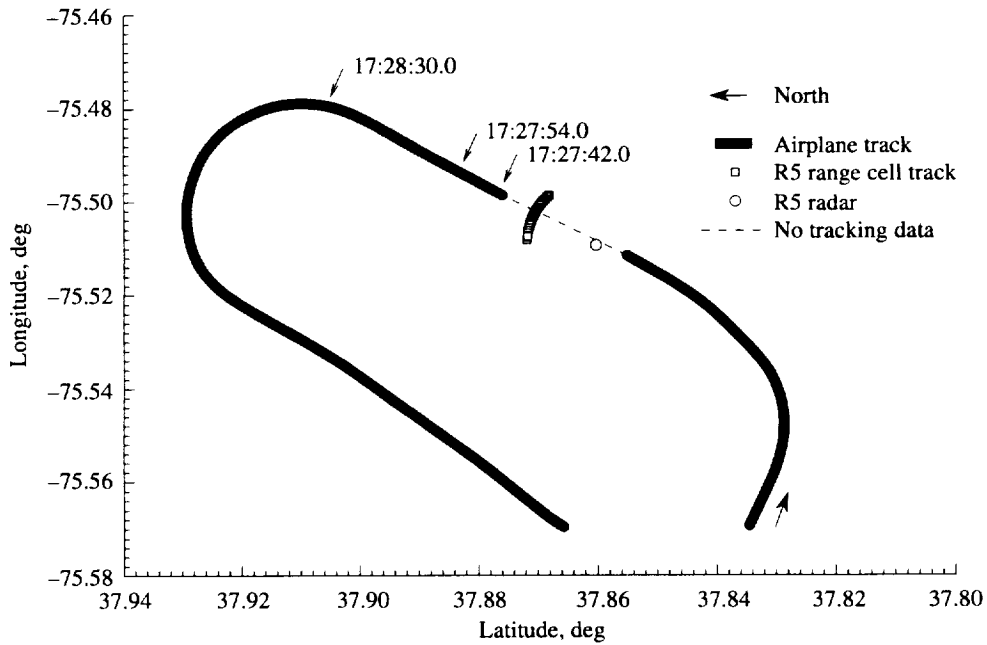
Figure A59. Pass 123 airplane and Radar 5 ground tracks; tail-on radar view of airplane wake.

Figures A60, A61, and A62 contain two azimuth scans and the ground tracks for pass 127. In scans 8 and 9, signal disturbances are seen in various parts of the scan. The disturbances not close to the smoke trails are equal in magnitude to those at the location of the smoke trails.
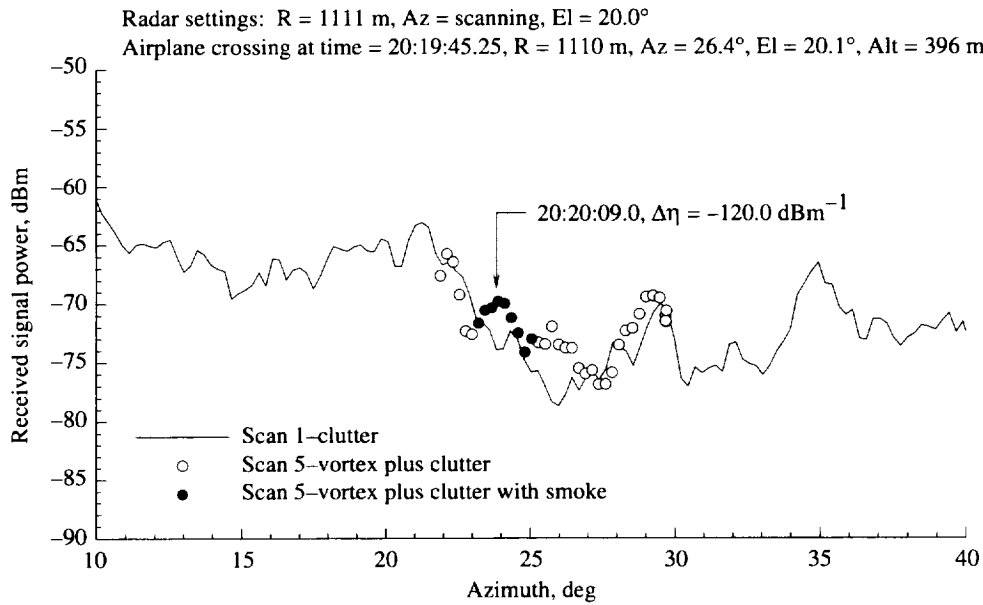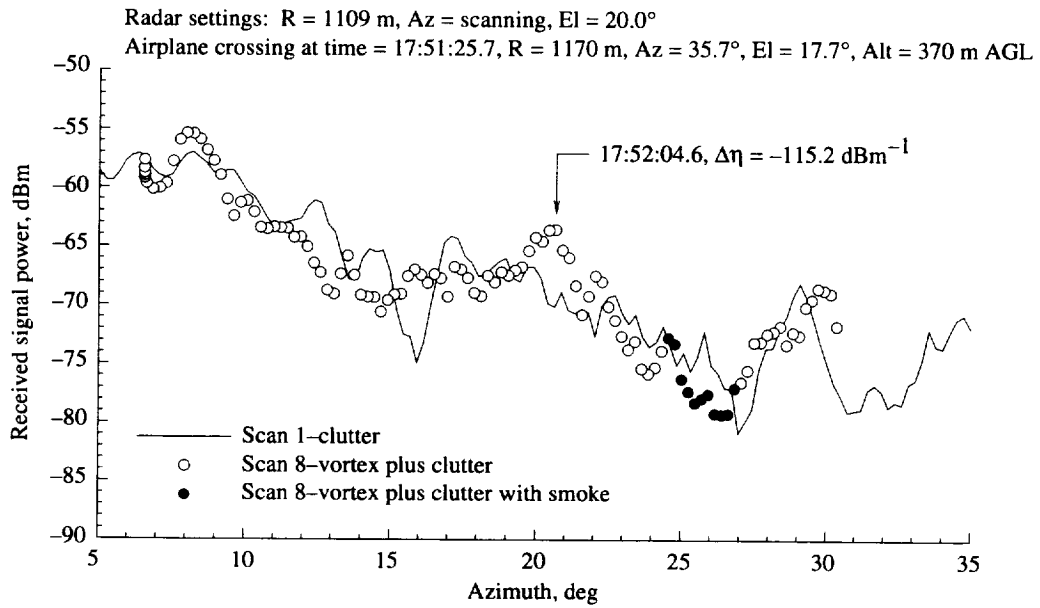

Figure A60. Total signal level vs. antenna azimuth angle compared with clutter scan for pass 127, azimuth scan 8, on 01-11-95.
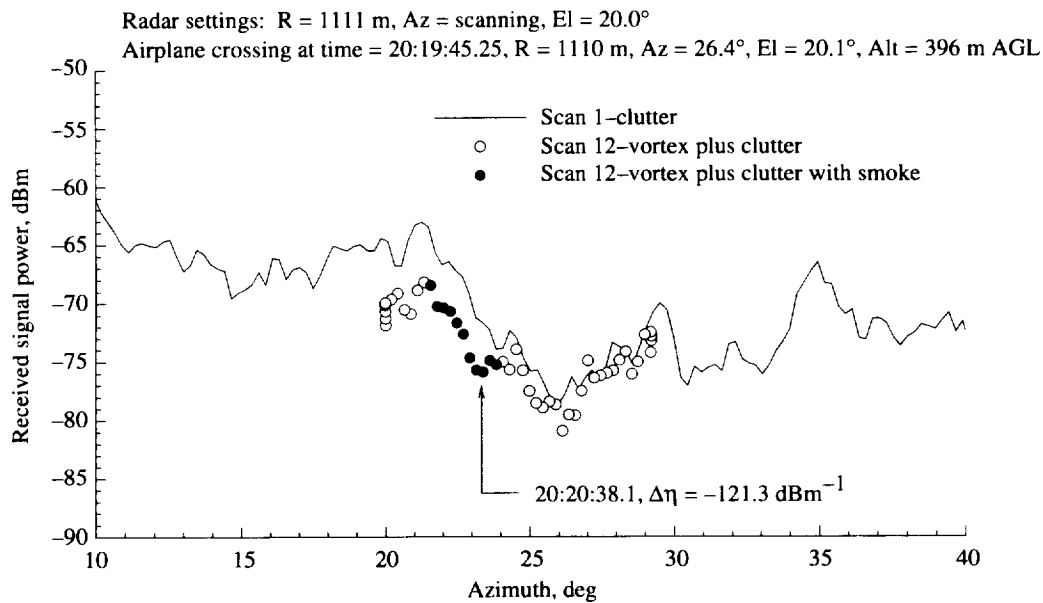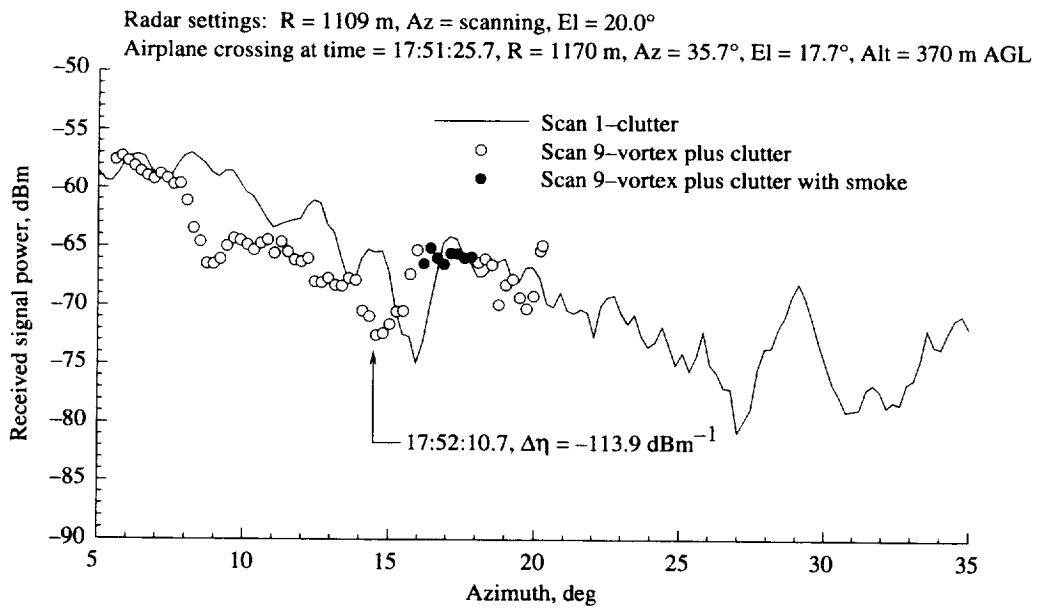

Figure A61. As for figure A60, except for azimuth scan 9.
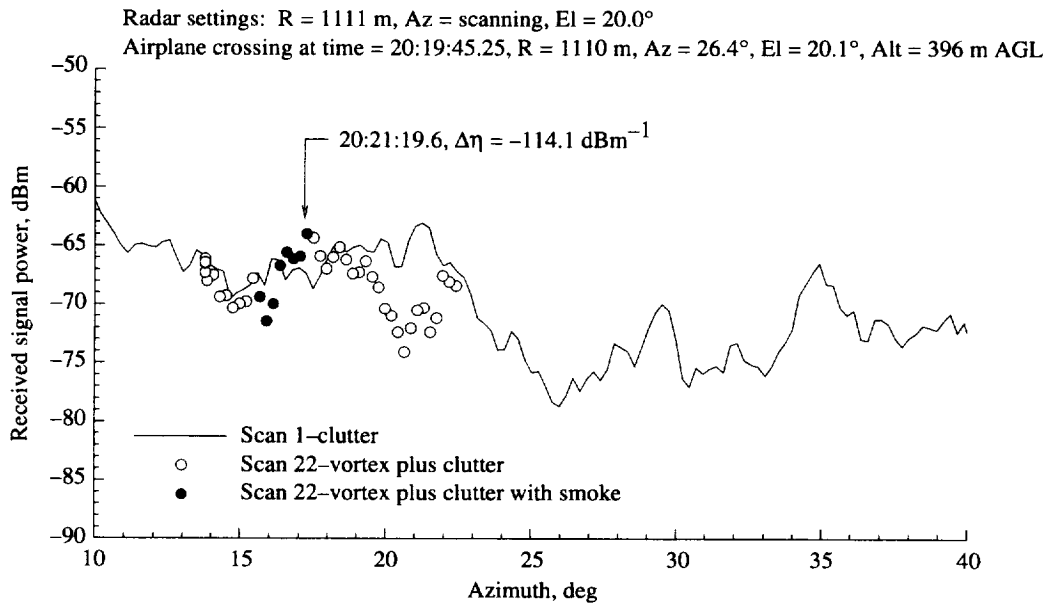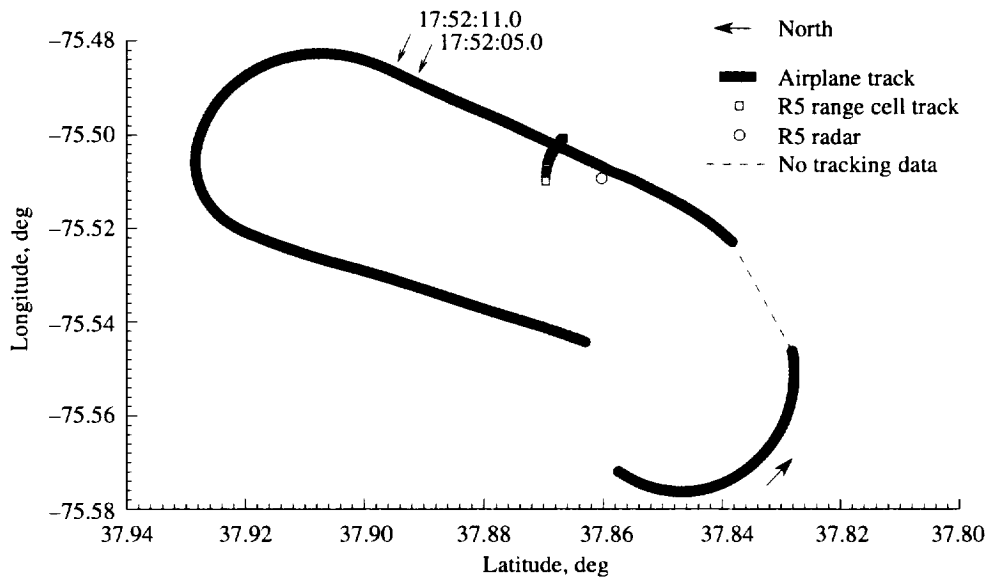
Figure A62. Pass 127 airplane and Radar 5 ground tracks; tail-on radar view of airplane wake.

Figures A63, A64, A65, A66, and A67 contain four elevation scans and the ground tracks for pass 132. In scans 7, 8, 9, and 11, a signal decrease is seen coincident with the smoke trails. During this span of 13 sec, the smoke trails have moved slightly downward, then returned to their original position.

Radar settings: R = 1259 m, Az = 145.0°, El = scanning
Airplane crossing at time = 18:34:39.0, R = 1301 m, Az = 145.0°, El = 27.1°, Alt = 608 m AGL

——— Scan 1–clutter
○ Scan 7–vortex plus clutter
● Scan 7–vortex plus clutter with smoke

18:34:57.1, Δη = –122.5 dBm^{-1}
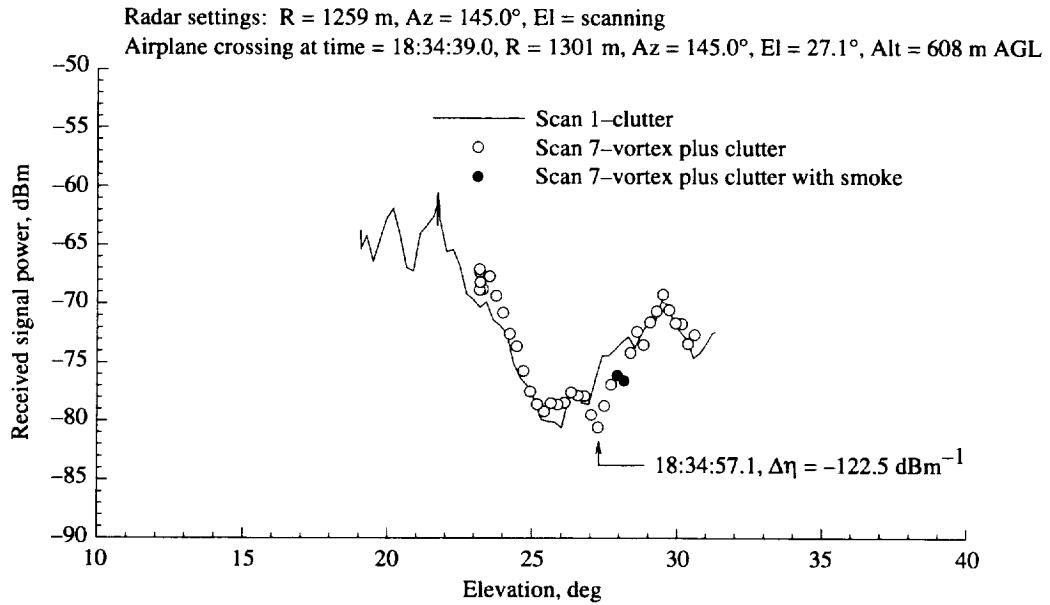
Figure A63. Total signal level vs. antenna elevation angle compared with clutter scan for pass 132, elevation scan 7, on 01-11-95.

Radar settings: R = 1259 m, Az = 145.0°, El = scanning
Airplane crossing at time = 18:34:39.0, R = 1301 m, Az = 145.0°, El = 27.1°, Alt = 608 m AGL

——— Scan 1–clutter
○ Scan 8–vortex plus clutter
● Scan 8–vortex plus clutter with smoke

18:35:01.1, Δη = –126.8 dBm^{-1}
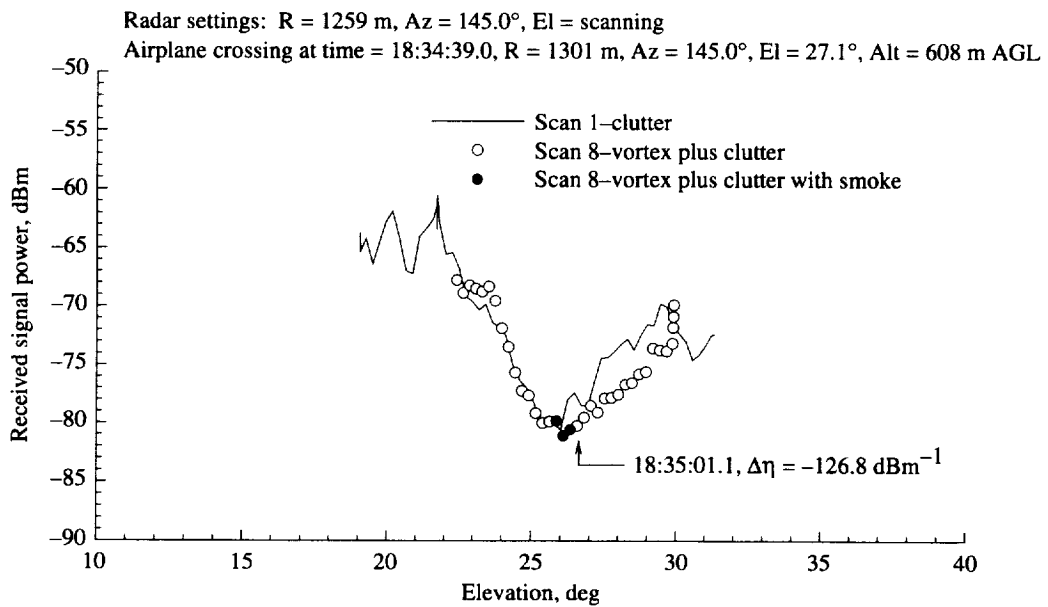
Figure A64. As for figure A63, except for elevation scan 8.

48
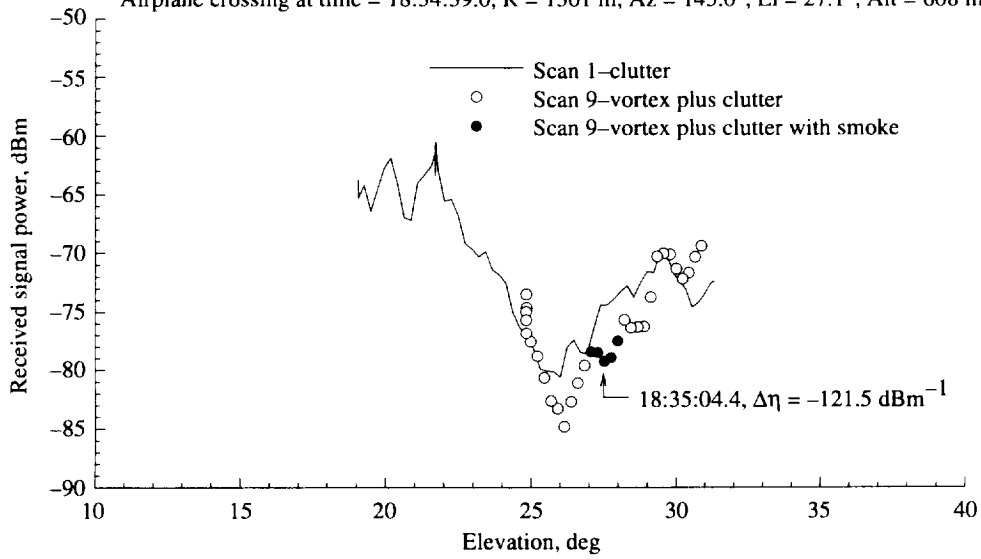
Figure A65. As for figure A63, except for elevation scan 9.
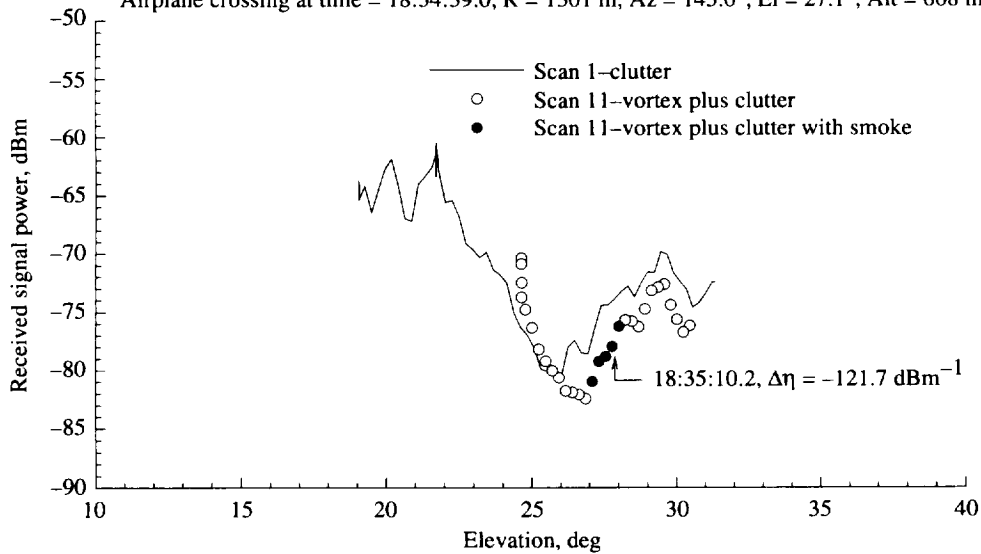
Figure A66. As for figure A63, except for elevation scan 11.
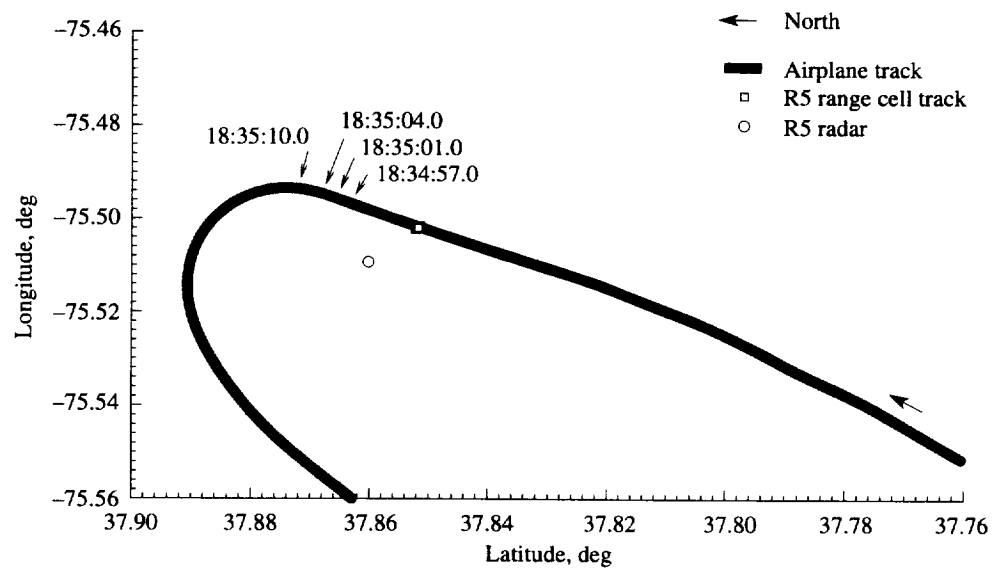
Figure A67. Pass 132 airplane and Radar 5 ground tracks; lateral radar view of airplane wake.

Figures A68, A69, and A70 contain two elevation scans and the ground tracks for pass 137. In scans 7 and 11, a signal increase is seen at the elevation of the smoke trails.

Radar settings: R = 1089 m, Az = 151.0°, El = scanning
Airplane crossing at time = 19:10:40.6, R = 1031 m, Az = 151.0°, El = 31.8°, Alt = 559 m AGL

19:10:51.2, $\Delta\eta$ = −118.9 dBm^{-1}

——— Scan 1–clutter
○ Scan 7–vortex plus clutter
● Scan 7–vortex plus clutter with smoke
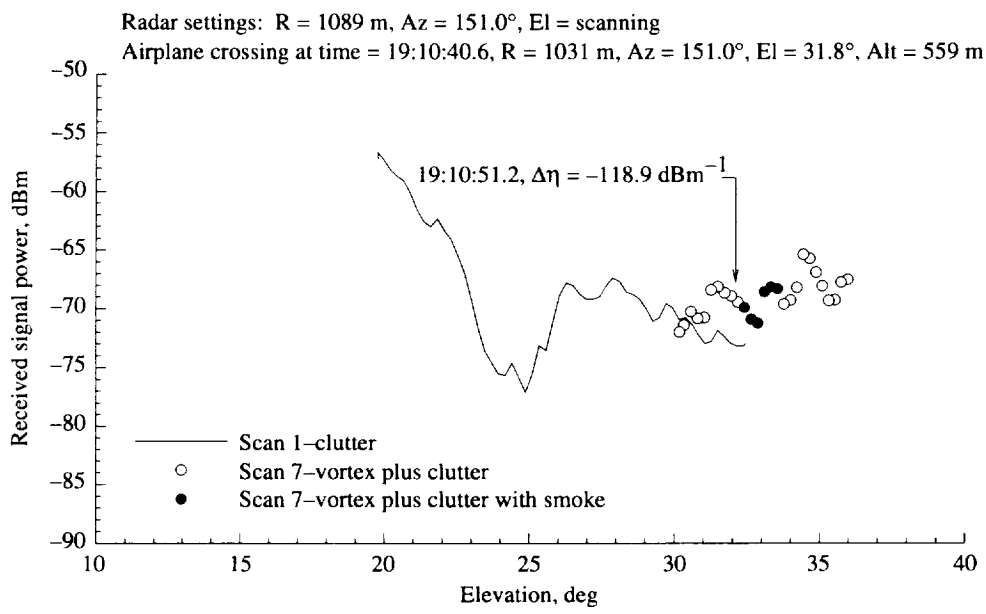
Figure A68. Total signal level vs. antenna elevation angle compared with clutter scan for pass 137, elevation scan 7, on 01-11-95.

Radar settings: R = 1089 m, Az = 151.0°, El = scanning
Airplane crossing at time = 19:10:40.6, R = 1031 m, Az = 151.0°, El = 31.8°, Alt = 559 m AGL

19:10:59.1, $\Delta\eta$ = −117.7 dBm^{-1}

——— Scan 1–clutter
○ Scan 11–vortex plus clutter
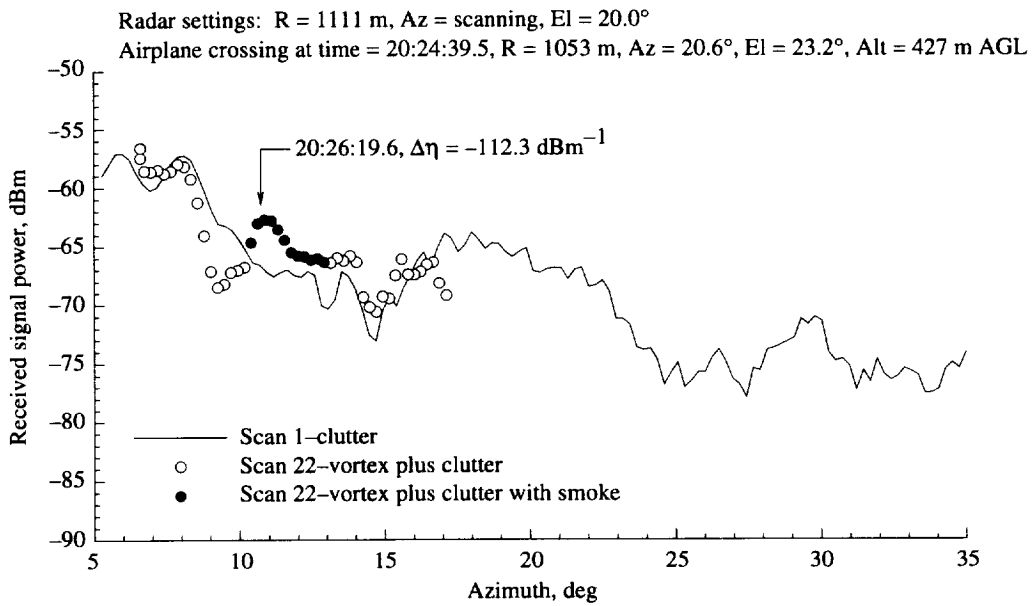● Scan 11–vortex plus clutter with smoke
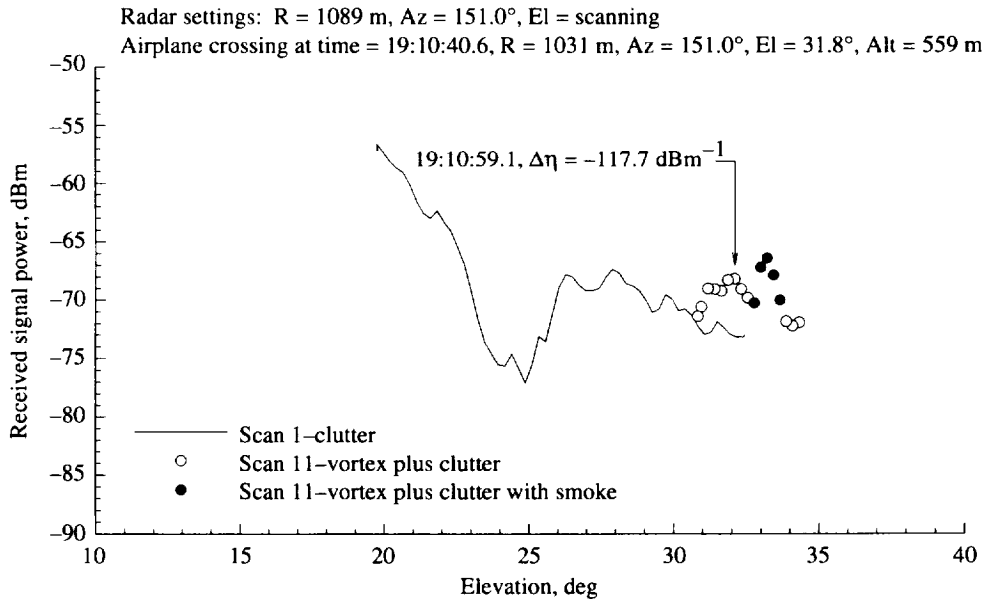
Figure A69. As for figure A68, except for elevation scan 11.
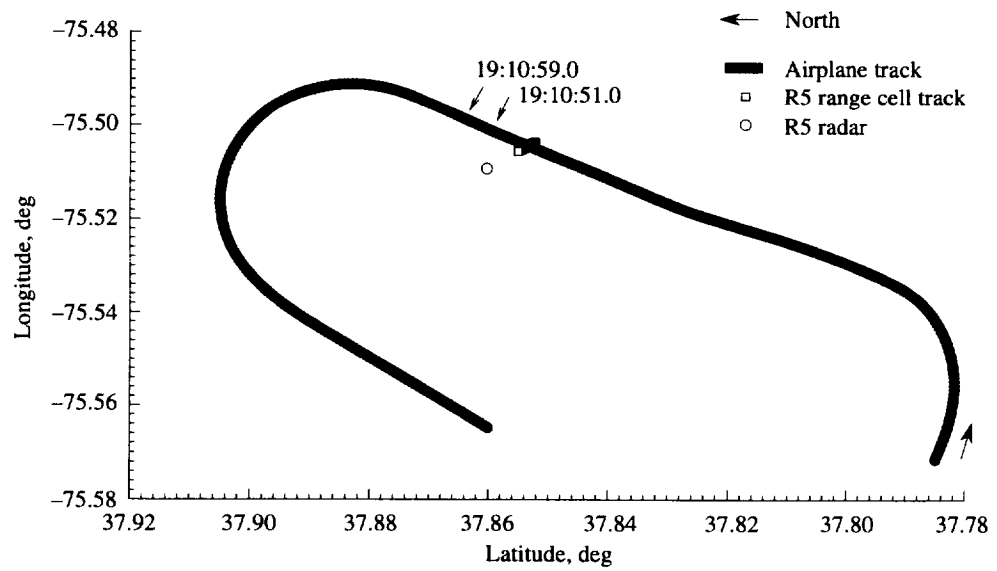
Figure A70. Pass 137 airplane and Radar 5 ground tracks; lateral radar view of airplane wake.

Figures A71, A72, A73, A74, and A75 contain four elevation scans and the ground tracks for pass 141. In scans 7, 8, 9, and 14, a signal level increase is seen at the elevation of the smoke trails.

Radar settings: R = 1089 m, Az = 151.0°, El = scanning
Airplane crossing at time = 19:37:47.3, R = 1095 m, Az = 151.0°, El = 25.6°, Alt = 489 m AGL

19:38:01.0, $\Delta\eta$ = –115.8 dBm^{-1}

——————— Scan 1–clutter
○ Scan 7–vortex plus clutter
● Scan 7–vortex plus clutter with smoke

Elevation, deg

Received signal power, dBm
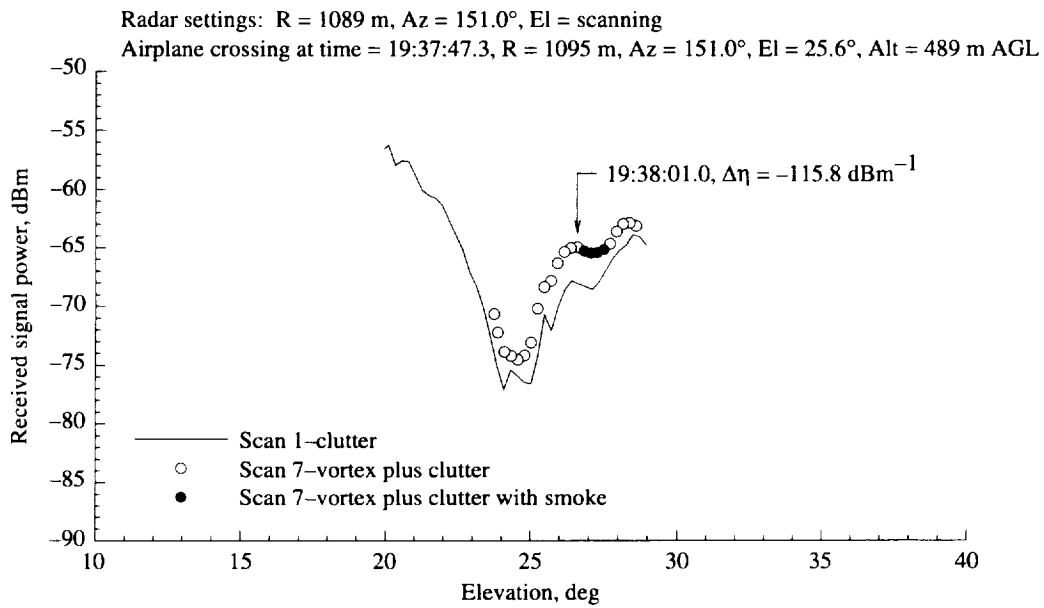
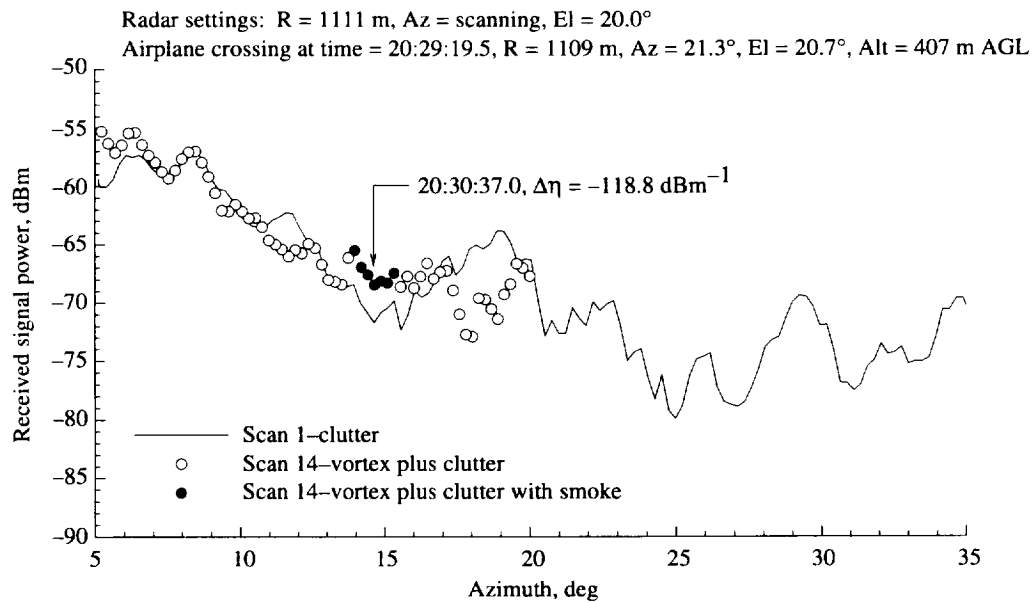Figure A71. Total signal level vs. antenna elevation angle compared with clutter scan for pass 141, elevation scan 7, on 01-11-95.

Radar settings: R = 1089 m, Az = 151.0°, El = scanning
Airplane crossing at time = 19:37:47.3, R = 1095 m, Az = 151.0°, El = 25.6°, Alt = 489 m AGL

19:38:03.7, $\Delta\eta$ = –117.7 dBm^{-1}

——————— Scan 1–clutter
○ Scan 8–vortex plus clutter
● Scan 8–vortex plus clutter with smoke

Elevation, deg

Received signal power, dBm
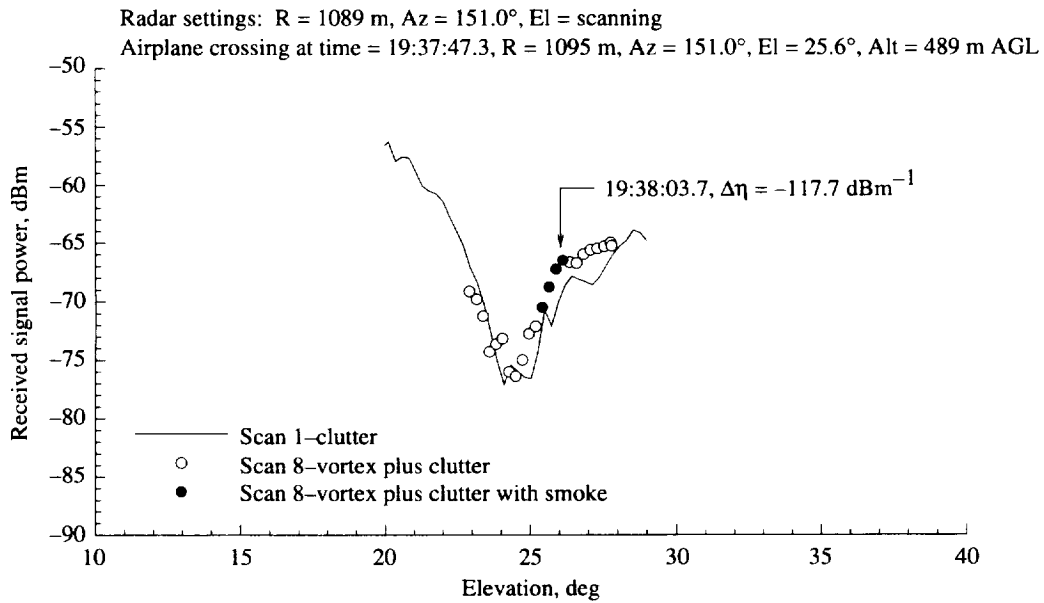
Figure A72. As for figure A71, except for elevation scan 8.

Radar settings: R = 1089 m, Az = 151.0°, El = scanning
Airplane crossing at time = 19:37:47.3, R = 1095 m, Az = 151.0°, El = 25.6°, Alt = 489 m AGL

19:38:16.8, $\Delta\eta$ = −117.0 dBm^{-1}

Scan 1–clutter
Scan 14–vortex plus clutter
Scan 14–vortex plus clutter with smoke
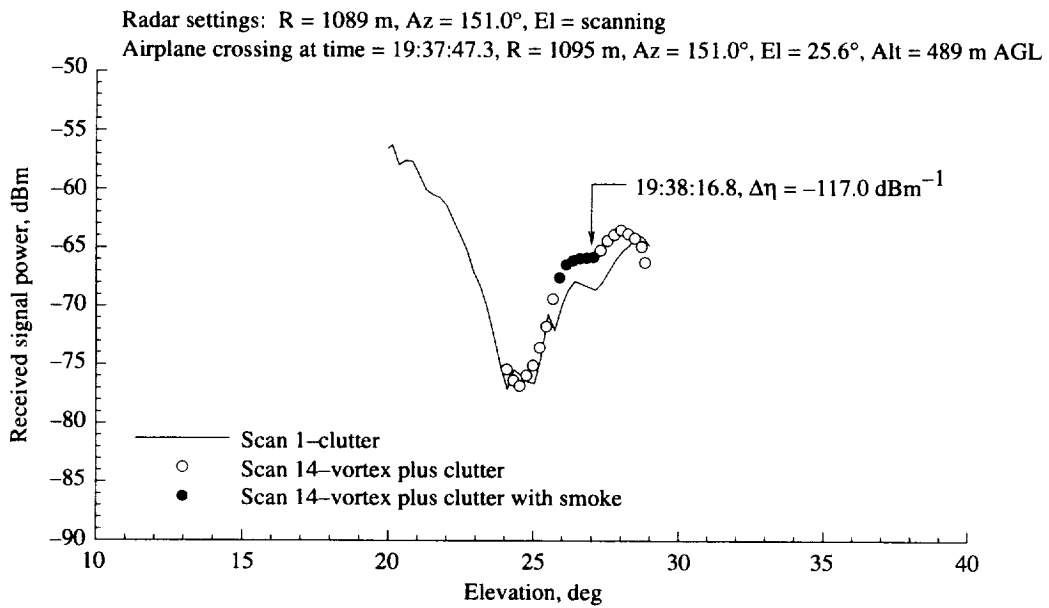
Figure A73. As for figure A71, except for elevation scan 14.

Radar settings: R = 1089 m, Az = 151.0°, El = scanning
Airplane crossing at time = 19:37:47.3, R = 1095 m, Az = 151.0°, El = 25.6°, Alt = 489 m AGL

19:38:24.8, $\Delta\eta$ = −117.4 dBm^{-1}

Scan 1–clutter
Scan 18–vortex plus clutter
Scan 18–vortex plus clutter with smoke
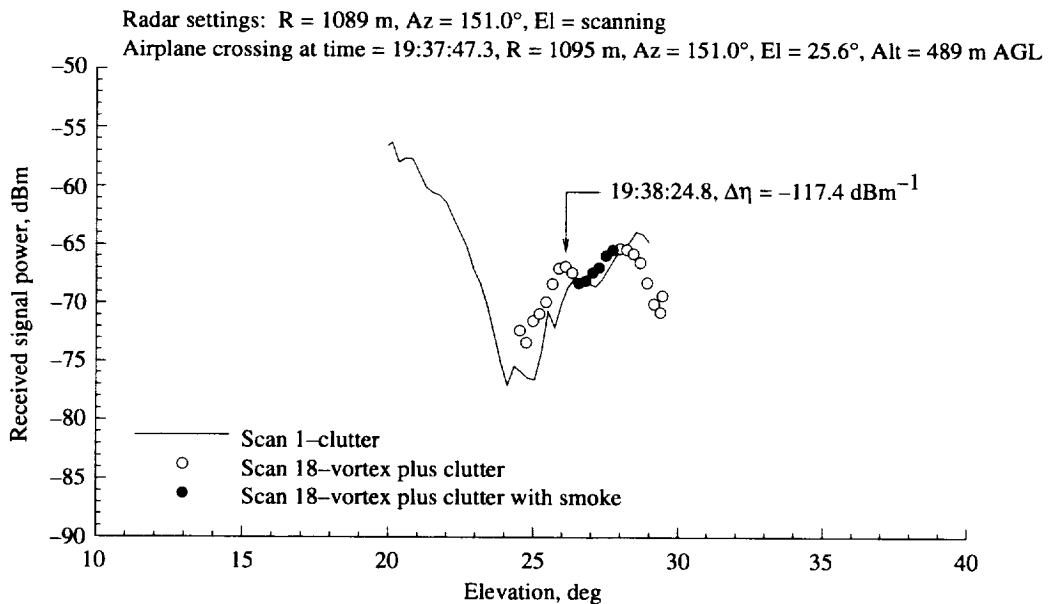
Figure A74. As for figure A71, except for elevation scan 18.
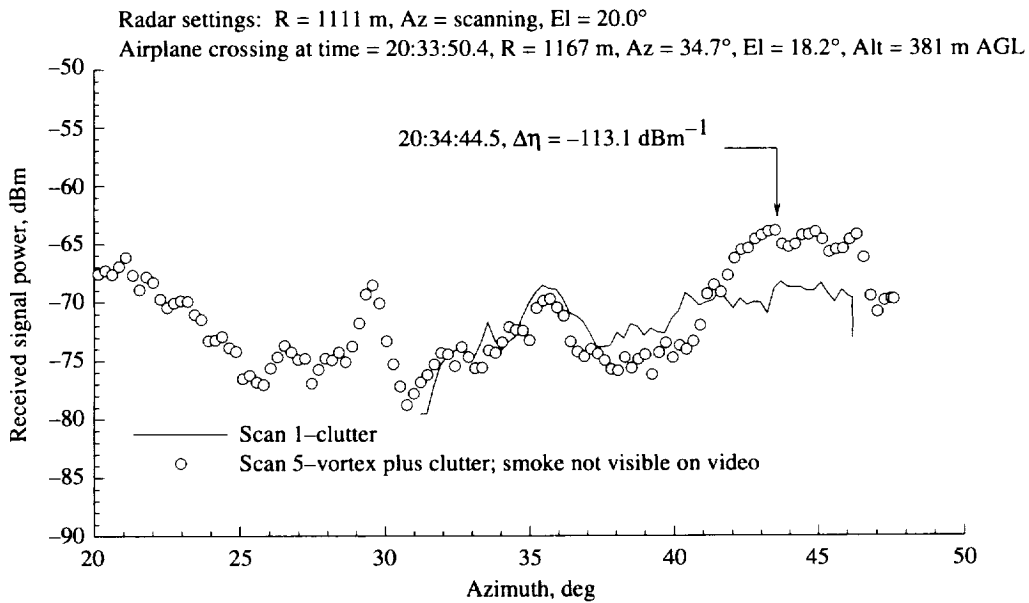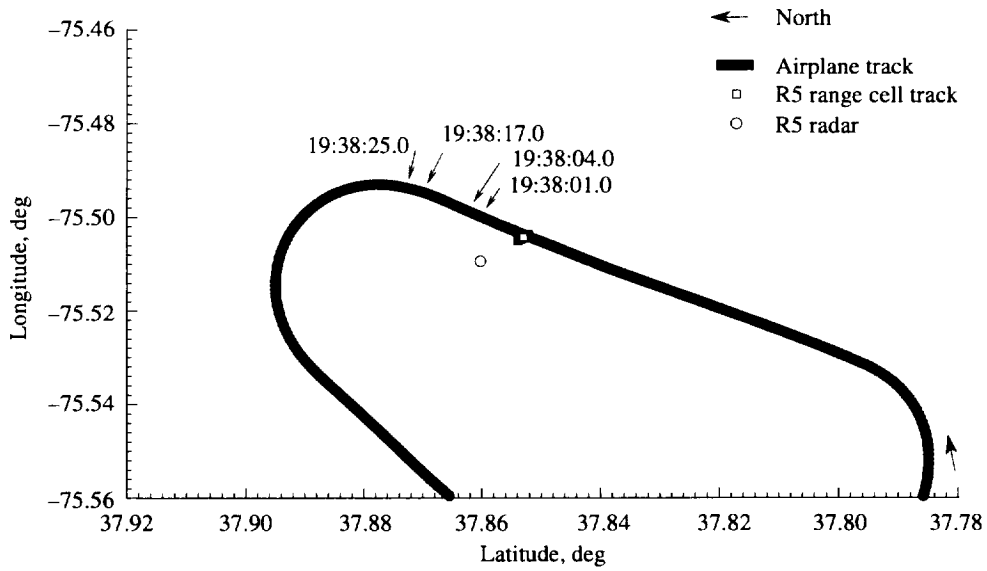
Figure A75. Pass 141 airplane and Radar 5 ground tracks; lateral radar view of airplane wake.

Figures A76, A77, and A78 contain two elevation scans and the ground tracks for pass 143. In scan 12, a signal increase is seen coincident with the smoke trails. By scan 27, the smoke had dissipated too much to locate precisely. Examining scan 27 around 28°, the elevation of the smoke trails in scan 12, one sees a signal decrease directly above that point and a signal decrease directly below. This pass was flown using 50 percent flaps, which caused the smoke trails to be visibly larger initially than the smoke trails with no flaps; the trails also dissipated faster.

Radar settings: R = 1089 m, Az = 151.0°, El = scanning
Airplane crossing at time = 19:51:49.2 R = 1133 m, Az = 151.0°, El = 25.7°, Alt = 507 m AGL

19:52:16.5, $\Delta\eta$ = -116.3 dBm^{-1}

——————— Scan 1–clutter
O   Scan 12–vortex plus clutter
●   Scan 12–vortex plus clutter with smoke
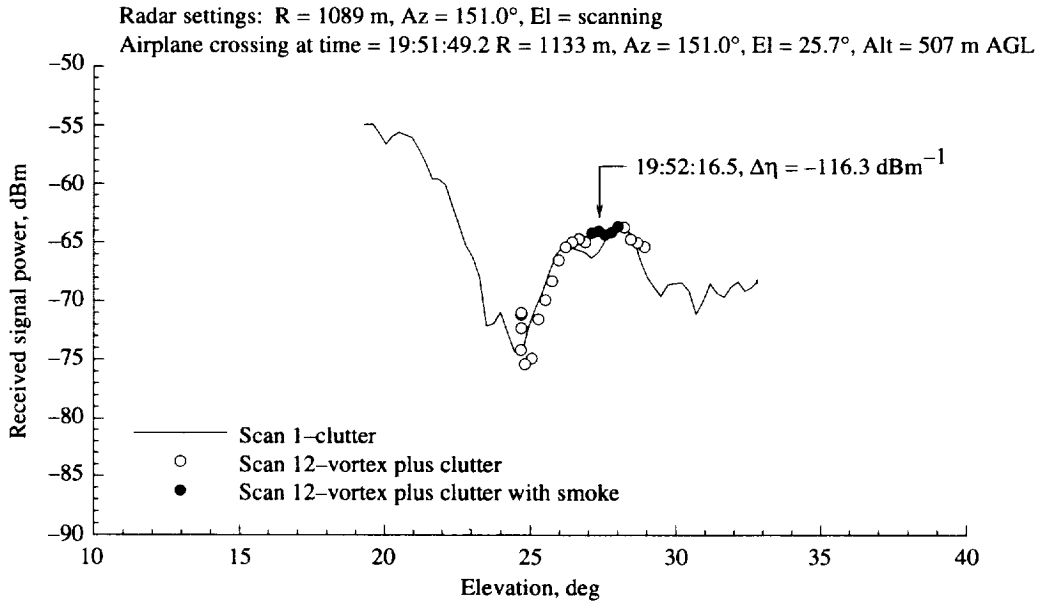
Figure A76. Total signal level vs. antenna elevation angle compared with clutter scan for pass 143, elevation scan 12, on 01-11-95.

Radar settings: R = 1089 m, Az = 151.0°, El = scanning
Airplane crossing at time = 19:51:49.2 R = 1133 m, Az = 151.0°, El = 25.7°, Alt = 507 m AGL

19:52:54.6, $\Delta\eta$ = -114.5 dBm^{-1}
(smoke no longer distinct)

——————— Scan 1–clutter
O   Scan 27–vortex plus clutter
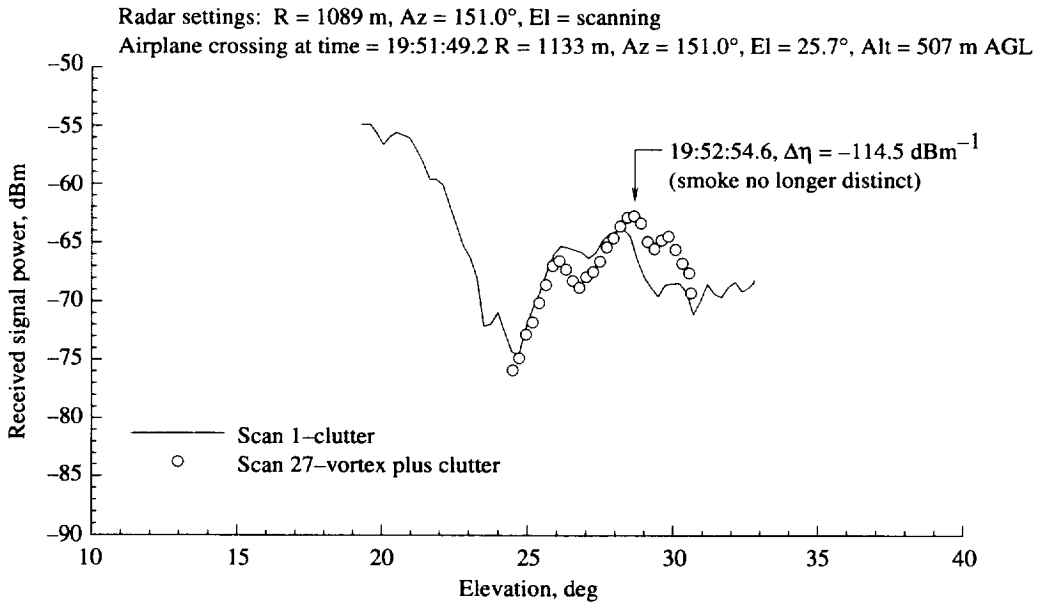
Figure A77. As for figure A76, except for elevation scan 27.

56
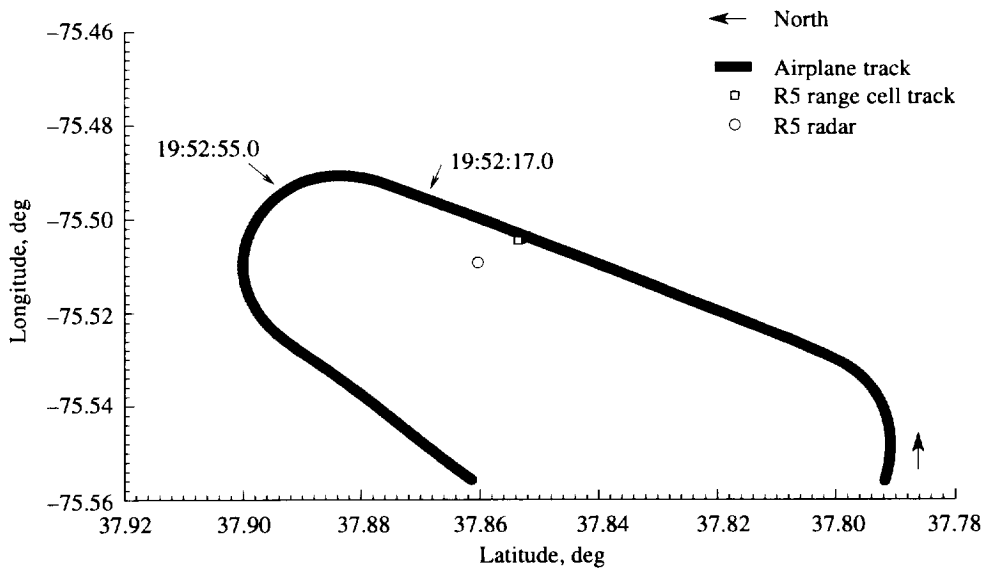
Figure A78. Pass 143 airplane and Radar 5 ground tracks; lateral radar view of airplane wake.

Figures A79 and A80 contain one elevation scan and the ground tracks for pass 149. In scan 5, a signal increase is seen just above the smoke trails. The clutter scan does not quite reach to the position of the smoke trails.

Radar settings: R = 1436 m, Az = 141.0°, El = scanning
Airplane crossing at time = 20:36:45.2, R = 1401 m, Az = 141.0°, El = 14.5°, Alt = 403 m AGL

20:36:54.6, $\Delta\eta$ = −113.1 dBm^{-1}

—— Scan 1–clutter
○ Scan 5–vortex plus clutter
● Scan 5–vortex plus clutter with smoke

Elevation, deg

Received signal power, dBm
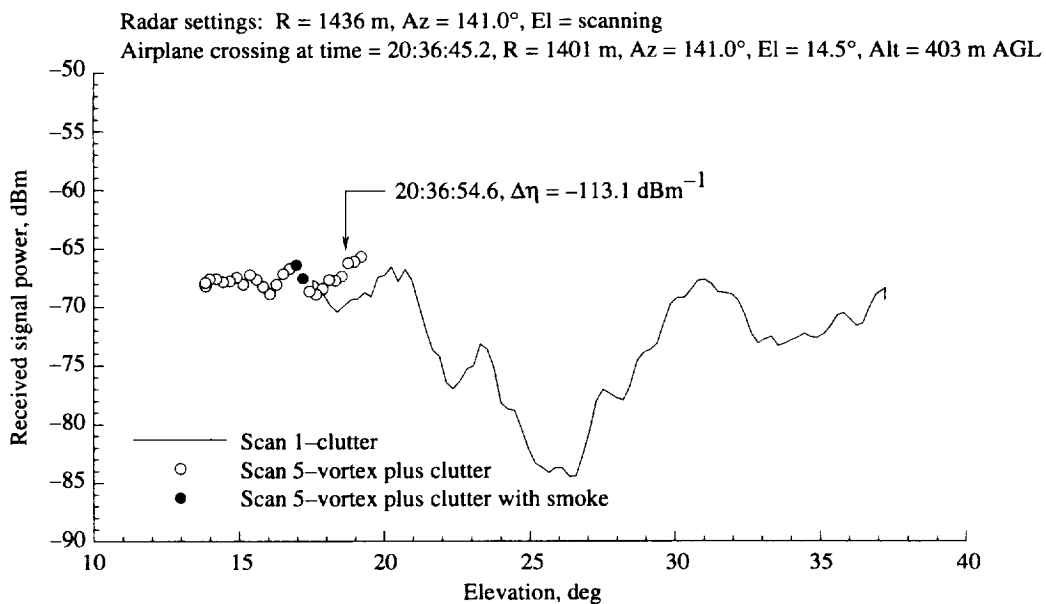
Figure A79. Total signal level vs. antenna elevation angle compared with clutter scan for pass 149, elevation scan 5, on 01-11-95.

◄— North

■ Airplane track
□ R5 range cell track
○ R5 radar

20:36:55.0

Longitude, deg

Latitude, deg
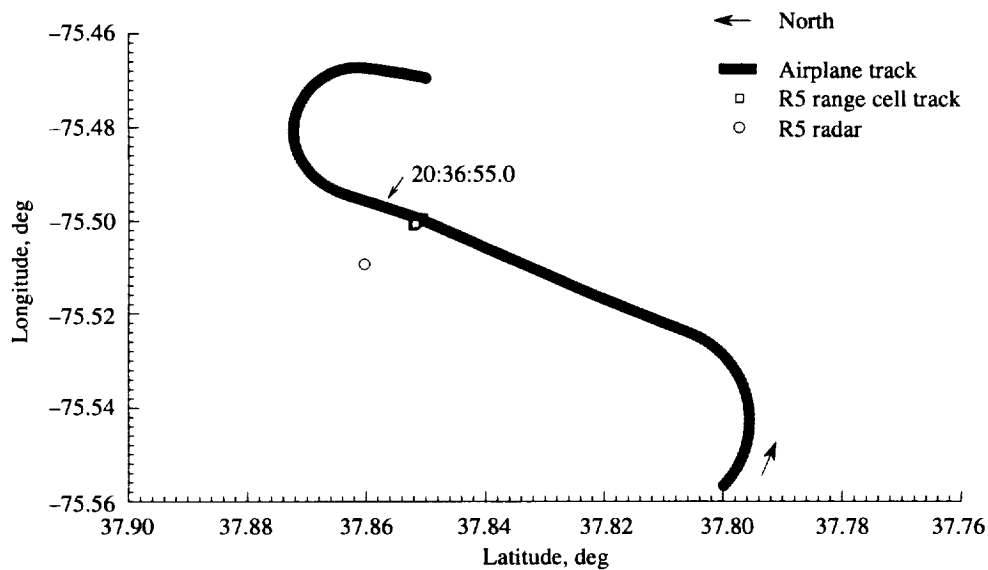
Figure A80. Pass 149 airplane and Radar 5 ground tracks; lateral radar view of airplane wake.

58

Appendix B

Meteorological Data

Wallops meteorological data were collected at 2-hr intervals. The following table contains those data recorded closest in time to the wake vortex radar recordings shown in this report.

Table B1. Meteorological Conditions at 400 m AGL

Condition	1-5-95 20:00 UTC	1-9-95 20:00 UTC	1-10-95 20:00 UTC	1-11-95 16:00 UTC	1-11-95 18:00 UTC	1-11-95 20:00 UTC
Temperature, $^\circ$C	−7.1	1.6	0.8	6.3	6.2	6.9
Pressure, mb	977.8	972.8	978.9	980.4	978.4	977.3
Water vapor mixing ratio, g/kg	0.8	2.8	2.8	5.0	3.7	4.0
Vertical gradient of water vapor mixing ratio, mg/kg/m	−0.44	0.13	0.27	−0.05	−8.24	−2.83
Cross-aircraft bearing windspeed,[1] m/s	−15.0	−1.6	−1.5	5.2	5.0	2.4

[1]Crosswind may be estimated more closely for some passes by noting change in smoke position from azimuth scan to azimuth scan in appendix A.

Appendix C

Variability of Clutter Power at Various Time Lags

This appendix presents the unsmoothed values used to create figures 5 and 6 in the text. Note that azimuth is the interpolated antenna position in degrees, SD power is the standard deviation of the change in received power after the given time lag in dBm, time refers to the time lag given in seconds, and N denotes the number of samples.

Table C2. Unsmoothed Data for Figure 5, Azimuth Scans at 20° Elevation

Azimuth	SD power	Time	N	Azimuth	SD power	Time	N	Azimuth	SD power	Time	N
10.7500	1.86516	1.75279	49	12.5000	2.27141	36.2104	98	14.2500	2.32172	72.4204	96
10.7500	2.04956	36.2105	98	12.5000	2.29427	72.4202	96	14.2500	2.16627	108.645	94
10.7500	1.99210	72.4204	96	12.5000	2.33967	108.645	94	14.2500	2.16466	144.878	92
10.7500	2.08377	108.645	94	12.5000	2.40125	144.878	92	14.2500	2.13369	181.121	90
10.7500	2.19136	144.878	92	12.5000	2.20463	181.121	90	14.5000	2.16239	4.91406	49
10.7500	2.42865	181.121	90	12.7500	2.22754	3.44523	49	14.5000	2.02886	36.2104	98
11.0000	2.09604	1.96620	49	12.7500	2.02064	36.2104	98	14.5000	2.20261	72.4202	96
11.0000	2.21790	36.2104	98	12.7500	1.95228	72.4202	96	14.5000	1.91414	108.645	94
11.0000	2.01227	72.4202	96	12.7500	1.98384	108.645	94	14.5000	2.09306	144.878	92
11.0000	2.00622	108.645	94	12.7500	2.07850	144.878	92	14.5000	2.08351	181.121	90
11.0000	2.25141	144.878	92	12.7500	2.11470	181.121	90	14.7500	2.38763	5.12317	49
11.0000	2.28617	181.121	90	13.0000	1.97259	3.65553	49	14.7500	2.33928	36.2104	98
11.2500	2.33821	2.17793	49	13.0000	1.91869	36.2105	98	14.7500	2.53594	72.4202	96
11.2500	2.38351	36.2104	98	13.0000	2.10005	72.4203	96	14.7500	2.35914	108.645	94
11.2500	2.43008	72.4202	96	13.0000	2.07644	108.645	94	14.7500	2.44110	144.878	92
11.2500	2.11737	108.645	94	13.0000	2.19186	144.878	92	14.7500	2.57510	181.121	90
11.2500	2.35072	144.878	92	13.0000	2.10890	181.121	90	15.0000	2.37466	5.33251	49
11.2500	2.42106	181.121	90	13.2500	1.92246	3.86567	49	15.0000	2.18045	36.2103	98
11.5000	2.29717	2.39070	49	13.2500	1.93279	36.2105	98	15.0000	2.18722	72.4202	96
11.5000	2.10902	36.2104	98	13.2500	2.05842	72.4204	96	15.0000	2.25001	108.645	94
11.5000	2.15305	72.4202	96	13.2500	2.15023	108.645	94	15.0000	2.29479	144.878	92
11.5000	2.11139	108.645	94	13.2500	2.26410	144.878	92	15.0000	2.30962	181.121	90
11.5000	2.09381	144.878	92	13.2500	1.90299	181.121	90	15.2500	2.23267	5.54098	49
11.5000	2.14627	181.121	90	13.5000	1.90492	4.07518	49	15.2500	1.95569	36.2105	98
11.7500	2.11190	2.60196	49	13.5000	2.17499	36.2104	98	15.2500	1.98044	72.4204	96
11.7500	2.14309	36.2105	98	13.5000	2.04002	72.4202	96	15.2500	2.26855	108.645	94
11.7500	1.93840	72.4203	96	13.5000	1.90837	108.645	94	15.2500	2.16308	144.878	92
11.7500	2.14580	108.645	94	13.5000	2.28130	144.878	92	15.2500	2.23190	181.121	90
11.7500	1.96244	144.878	92	13.5000	1.99290	181.121	90	15.5000	2.32088	5.75096	49
11.7500	2.04499	181.121	90	13.7500	2.14490	4.28508	49	15.5000	2.04636	36.2104	98
12.0000	2.49837	2.81354	49	13.7500	2.12263	36.2103	98	15.5000	2.06639	72.4202	96
12.0000	2.54577	36.2104	98	13.7500	2.09152	72.4202	96	15.5000	2.42046	108.645	94
12.0000	2.53014	72.4203	96	13.7500	2.09159	108.645	94	15.5000	2.08669	144.878	92
12.0000	2.57567	108.645	94	13.7500	2.11229	144.878	92	15.5000	2.09342	181.121	90
12.0000	2.50777	144.878	92	13.7500	1.96920	181.121	90	15.7500	2.49286	5.95982	49
12.0000	2.34607	181.121	90	14.0000	2.24227	4.49522	49	15.7500	2.21316	36.2103	98
12.2500	2.68786	3.02431	49	14.0000	2.11906	36.2103	98	15.7500	2.13951	72.4202	96
12.2500	2.64123	36.2104	98	14.0000	2.06138	72.4202	96	15.7500	2.42093	108.645	94
12.2500	2.56734	72.4202	96	14.0000	2.03237	108.645	94	15.7500	2.20631	144.878	92
12.2500	2.64848	108.645	94	14.0000	2.07835	144.878	92	15.7500	2.26484	181.121	90
12.2500	2.73508	144.878	92	14.0000	1.95188	181.121	90	16.0000	2.28421	6.16773	49
12.2500	2.57608	181.121	90	14.2500	2.27116	4.70416	49	16.0000	2.19636	36.2104	98
12.5000	2.61319	3.23453	49	14.2500	2.20321	36.2105	98	16.0000	2.16279	72.4202	96

Table C2. Continued

Azimuth	SD power	Time	N	Azimuth	SD power	Time	N	Azimuth	SD power	Time	N
16.0000	2.30214	108.645	94	18.0000	2.23119	181.121	90	20.2500	2.35691	36.2104	98
16.0000	2.22662	144.878	92	18.2500	1.95851	8.04679	49	20.2500	2.18234	72.4203	96
16.0000	2.36057	181.121	90	18.2500	2.09588	36.2103	98	20.2500	2.36903	108.645	94
16.2500	2.46903	6.37739	49	18.2500	2.06894	72.4202	96	20.2500	2.25634	144.878	92
16.2500	2.44565	36.2103	98	18.2500	2.25712	108.645	94	20.2500	2.23413	181.121	90
16.2500	2.32109	72.4202	96	18.2500	1.98776	144.878	92	20.5000	2.00195	9.92307	49
16.2500	2.63281	108.645	94	18.2500	2.06919	181.121	90	20.5000	1.96922	36.2103	98
16.2500	2.47927	144.878	92	18.5000	2.11993	8.25502	49	20.5000	1.78008	72.4202	96
16.2500	2.49600	181.121	90	18.5000	2.22502	36.2103	98	20.5000	1.87790	108.645	94
16.5000	2.41135	6.58586	49	18.5000	2.21967	72.4202	96	20.5000	2.01258	144.878	92
16.5000	2.30361	36.2104	98	18.5000	2.44996	108.645	94	20.5000	2.04464	181.121	90
16.5000	2.26556	72.4202	96	18.5000	2.07720	144.878	92	20.7500	2.09434	10.1309	49
16.5000	2.40283	108.645	94	18.5000	2.22686	181.121	90	20.7500	2.32604	36.2103	98
16.5000	2.34931	144.878	92	18.7500	2.47538	8.46325	49	20.7500	1.90241	72.4202	96
16.5000	2.31823	181.121	90	18.7500	2.49033	36.2103	98	20.7500	2.01906	108.645	94
16.7500	2.34139	6.79520	49	18.7500	2.49220	72.4202	96	20.7500	2.03952	144.878	92
16.7500	2.34247	36.2104	98	18.7500	2.79249	108.645	94	20.7500	2.11041	181.121	90
16.7500	2.13042	72.4203	96	18.7500	2.24546	144.878	92	21.0000	2.15635	10.3391	49
16.7500	2.14014	108.645	94	18.7500	2.38295	181.121	90	21.0000	2.30698	36.2103	98
16.7500	2.32302	144.878	92	19.0000	2.23142	8.67227	49	21.0000	2.01225	72.4202	96
16.7500	2.15534	181.121	90	19.0000	2.45348	36.2104	98	21.0000	2.07882	108.645	94
17.0000	2.19963	7.00367	49	19.0000	2.36988	72.4203	96	21.0000	2.05137	144.878	92
17.0000	2.24203	36.2103	98	19.0000	2.32219	108.645	94	21.0000	2.25345	181.121	90
17.0000	2.14038	72.4202	96	19.0000	2.21646	144.878	92	21.2500	2.36224	10.5473	49
17.0000	2.06668	108.645	94	19.0000	2.28427	181.121	90	21.2500	2.51769	36.2104	98
17.0000	2.22152	144.878	92	19.2500	2.22075	8.88074	49	21.2500	2.20970	72.4203	96
17.0000	2.15245	181.121	90	19.2500	2.46162	36.2103	98	21.2500	2.30993	108.645	94
17.2500	2.31773	7.21261	49	19.2500	2.58096	72.4202	96	21.2500	2.43410	144.878	92
17.2500	2.14314	36.2103	98	19.2500	2.18890	108.645	94	21.2500	2.52137	181.121	90
17.2500	2.26030	72.4202	96	19.2500	2.45270	144.878	92	21.5000	2.68235	10.7557	49
17.2500	2.21534	108.645	94	19.2500	2.16179	181.121	90	21.5000	2.69154	36.2104	98
17.2500	2.48979	144.878	92	19.5000	2.01674	9.08929	49	21.5000	2.76200	72.4203	96
17.2500	2.20666	181.121	90	19.5000	2.54149	36.2104	98	21.5000	2.44983	108.645	94
17.5000	2.27355	7.42100	49	19.5000	2.56128	72.4203	96	21.5000	2.71000	144.878	92
17.5000	2.48322	36.2104	98	19.5000	2.06426	108.645	94	21.5000	2.67825	181.121	90
17.5000	2.48383	72.4203	96	19.5000	2.53685	144.878	92	21.7500	2.45259	10.9646	49
17.5000	2.50840	108.645	94	19.5000	2.18225	181.121	90	21.7500	2.62796	36.2103	98
17.5000	2.76788	144.878	92	19.7500	2.28202	9.29696	49	21.7500	2.72681	72.4203	96
17.5000	2.39943	181.121	90	19.7500	2.60209	36.2103	98	21.7500	2.32081	108.645	94
17.7500	2.19072	7.62923	49	19.7500	2.60616	72.4202	96	21.7500	2.66703	144.878	92
17.7500	2.36958	36.2104	98	19.7500	2.45321	108.645	94	21.7500	2.39622	181.121	90
17.7500	2.44907	72.4203	96	19.7500	2.59116	144.878	92	22.0000	2.28658	11.1728	49
17.7500	2.53876	108.645	94	19.7500	2.39600	181.121	90	22.0000	2.45311	36.2103	98
17.7500	2.76777	144.878	92	20.0000	2.30604	9.50558	49	22.0000	2.39949	72.4202	96
17.7500	2.36961	181.121	90	20.0000	2.44864	36.2104	98	22.0000	2.19737	108.645	94
18.0000	2.13331	7.83881	49	20.0000	2.33088	72.4203	96	22.0000	2.54563	144.878	92
18.0000	2.29163	36.2105	98	20.0000	2.44010	108.645	94	22.0000	2.19551	181.121	90
18.0000	2.21561	72.4203	96	20.0000	2.30139	144.878	92	22.2500	2.35840	11.3799	49
18.0000	2.41825	108.645	94	20.0000	2.35884	181.121	90	22.2500	2.43920	36.2103	98
18.0000	2.28506	144.878	92	20.2500	2.27481	9.71413	49	22.2500	2.28541	72.4202	96

Azimuth	SD power	Time	N	Azimuth	SD power	Time	N	Azimuth	SD power	Time	N
22.2500	2.17720	108.645	94	24.2500	2.42736	181.121	90	26.5000	2.81562	36.2103	98
22.2500	2.45906	144.878	92	24.5000	1.93433	13.2561	49	26.5000	2.82635	72.4202	96
22.2500	2.22149	181.121	90	24.5000	2.50719	36.2102	98	26.5000	3.00614	108.645	94
22.5000	2.36893	11.5891	49	24.5000	2.54712	72.4202	96	26.5000	2.69245	144.878	92
22.5000	2.54782	36.2103	98	24.5000	2.08976	108.645	94	26.5000	2.93295	181.121	90
22.5000	2.42053	72.4202	96	24.5000	2.24105	144.878	92	26.7500	2.38122	15.1319	49
22.5000	2.12347	108.645	94	24.5000	2.29261	181.121	90	26.7500	2.68890	36.2103	98
22.5000	2.54450	144.878	92	24.7500	2.15663	13.4641	49	26.7500	2.54834	72.4203	96
22.5000	2.26830	181.121	90	24.7500	2.71225	36.2103	98	26.7500	2.88694	108.645	94
22.7500	2.19362	11.7974	49	24.7500	2.67843	72.4203	96	26.7500	2.92362	144.878	92
22.7500	2.61483	36.2104	98	24.7500	2.34477	108.645	94	26.7500	2.70678	181.121	90
22.7500	2.43429	72.4204	96	24.7500	2.47839	144.878	92	27.0000	1.94658	15.3398	49
22.7500	2.34962	108.645	94	24.7500	2.48654	181.121	90	27.0000	2.24358	36.2103	98
22.7500	2.53950	144.878	92	25.0000	2.49503	13.6728	49	27.0000	2.26469	72.4202	96
22.7500	2.35749	181.121	90	25.0000	2.92317	36.2104	98	27.0000	2.54005	108.645	94
23.0000	2.32960	12.0069	49	25.0000	2.88767	72.4202	96	27.0000	2.53661	144.878	92
23.0000	2.70857	36.2103	98	25.0000	2.67966	108.645	94	27.0000	2.19921	181.121	90
23.0000	2.68530	72.4202	96	25.0000	2.56298	144.878	92	27.2500	2.16999	15.5485	49
23.0000	2.51463	108.645	94	25.0000	2.68809	181.121	90	27.2500	2.16611	36.2103	98
23.0000	2.56579	144.878	92	25.2500	2.34083	13.8815	49	27.2500	2.14991	72.4203	96
23.0000	2.54888	181.121	90	25.2500	2.67370	36.2103	98	27.2500	2.49213	108.645	94
23.2500	2.35662	12.2144	49	25.2500	2.65273	72.4203	96	27.2500	2.31240	144.878	92
23.2500	2.40387	36.2103	98	25.2500	2.77589	108.645	94	27.2500	2.00826	181.121	90
23.2500	2.44301	72.4202	96	25.2500	2.56291	144.878	92	27.5000	2.25278	15.7568	49
23.2500	2.16176	108.645	94	25.2500	2.67715	181.121	90	27.5000	2.12020	36.2104	98
23.2500	2.32769	144.878	92	25.5000	2.19818	14.0905	49	27.5000	2.09579	72.4204	96
23.2500	2.48118	181.121	90	25.5000	2.58891	36.2103	98	27.5000	2.39171	108.645	94
23.5000	2.44369	12.4213	49	25.5000	2.59003	72.4203	96	27.5000	2.25419	144.878	92
23.5000	2.50141	36.2103	98	25.5000	2.76476	108.645	94	27.5000	2.34414	181.121	90
23.5000	2.61725	72.4202	96	25.5000	2.57136	144.878	92	27.7500	2.16381	15.9660	49
23.5000	2.17250	108.645	94	25.5000	2.50467	181.121	90	27.7500	2.25344	36.2104	98
23.5000	2.41549	144.878	92	25.7500	2.26314	14.2980	49	27.7500	2.05226	72.4204	96
23.5000	2.65927	181.121	90	25.7500	2.81632	36.2103	98	27.7500	2.33121	108.645	94
23.7500	2.24521	12.6307	49	25.7500	2.67167	72.4202	96	27.7500	2.15982	144.878	92
23.7500	2.44639	36.2103	98	25.7500	2.76420	108.645	94	27.7500	2.18028	181.121	90
23.7500	2.61225	72.4203	96	25.7500	2.53461	144.878	92	28.0000	1.98726	16.1751	49
23.7500	2.12213	108.645	94	25.7500	2.72186	181.121	90	28.0000	2.21806	36.2103	98
23.7500	2.33237	144.878	92	26.0000	2.52453	14.5066	49	28.0000	2.18075	72.4204	96
23.7500	2.66000	181.121	90	26.0000	3.08086	36.2104	98	28.0000	2.43072	108.645	94
24.0000	2.09691	12.8393	49	26.0000	2.64613	72.4203	96	28.0000	2.09819	144.878	92
24.0000	2.41241	36.2105	98	26.0000	2.79477	108.645	94	28.0000	2.43822	181.121	90
24.0000	2.51510	72.4204	96	26.0000	2.59057	144.878	92	28.2500	2.33470	16.3827	49
24.0000	1.97776	108.645	94	26.0000	2.74142	181.121	90	28.2500	2.55279	36.2103	98
24.0000	2.24989	144.878	92	26.2500	2.86904	14.7151	49	28.2500	2.73986	72.4202	96
24.0000	2.55888	181.121	90	26.2500	3.09172	36.2104	98	28.2500	2.73876	108.645	94
24.2500	2.14916	13.0487	49	26.2500	2.91152	72.4204	96	28.2500	2.38970	144.878	92
24.2500	2.41014	36.2104	98	26.2500	3.33314	108.645	94	28.2500	2.92302	181.121	90
24.2500	2.46029	72.4203	96	26.2500	2.93955	144.878	92	28.5000	2.51765	16.5917	49
24.2500	2.06258	108.645	94	26.2500	2.77300	181.121	90	28.5000	2.72886	36.2104	98
24.2500	2.22470	144.878	92	26.5000	2.66045	14.9235	49	28.5000	2.78159	72.4204	96

Azimuth	SD power	Time	N	Azimuth	SD power	Time	N	Azimuth	SD power	Time	N
28.5000	2.78169	108.645	94	30.5000	1.57424	181.121	90	32.7500	2.12017	36.2103	98
28.5000	2.50421	144.878	92	30.7500	1.55435	17.7460	50	32.7500	2.13535	72.4204	96
28.5000	2.70756	181.121	90	30.7500	1.53855	36.2104	98	32.7500	1.89470	108.645	94
28.7500	2.47978	16.7995	49	30.7500	1.55023	72.4204	96	32.7500	1.90179	144.878	92
28.7500	2.91862	36.2104	98	30.7500	1.51732	108.645	94	32.7500	1.96746	181.121	90
28.7500	2.95310	72.4204	96	30.7500	1.44304	144.878	92	33.0000	1.87308	15.8702	50
28.7500	2.82935	108.645	94	30.7500	1.45985	181.121	90	33.0000	1.92764	36.2104	98
28.7500	2.72382	144.878	92	31.0000	1.81675	17.5367	50	33.0000	1.92910	72.4203	96
28.7500	2.69224	181.121	90	31.0000	1.77823	36.2104	98	33.0000	1.71428	108.645	94
29.0000	2.27894	17.0095	49	31.0000	1.91200	72.4204	96	33.0000	1.88682	144.878	92
29.0000	2.40971	36.2104	98	31.0000	1.79865	108.645	94	33.0000	1.84792	181.121	90
29.0000	2.54449	72.4204	96	31.0000	1.85571	144.878	92	33.2500	1.73488	15.6616	50
29.0000	2.29736	108.645	94	31.0000	1.92382	181.121	90	33.2500	1.63669	36.2104	98
29.0000	2.26535	144.878	92	31.2500	2.19409	17.3290	50	33.2500	1.69646	72.4203	96
29.0000	2.40064	181.121	90	31.2500	2.19796	36.2104	98	33.2500	1.59896	108.645	94
29.2500	2.14588	17.2171	49	31.2500	2.34249	72.4203	96	33.2500	1.71617	144.878	92
29.2500	2.17864	36.2102	98	31.2500	2.23020	108.645	94	33.2500	1.72466	181.121	90
29.2500	2.38494	72.4201	96	31.2500	2.23043	144.878	92	33.5000	1.80799	15.4537	50
29.2500	2.08522	108.645	94	31.2500	2.29697	181.121	90	33.5000	1.59111	36.2104	98
29.2500	2.00556	144.878	92	31.5000	2.42048	17.1199	50	33.5000	1.65914	72.4204	96
29.2500	2.29249	181.121	90	31.5000	2.26552	36.2104	98	33.5000	1.78238	108.645	94
29.5000	2.08191	17.4248	49	31.5000	2.67827	72.4205	96	33.5000	1.80853	144.878	92
29.5000	2.09376	36.2105	98	31.5000	2.68734	108.645	94	33.5000	1.84402	181.121	90
29.5000	2.10086	72.4204	96	31.5000	2.58753	144.878	92	33.7500	1.58571	15.2445	50
29.5000	1.97794	108.645	94	31.5000	2.42337	181.121	90	33.7500	1.60406	36.2104	98
29.5000	1.97784	144.878	92	31.7500	2.79001	16.9123	50	33.7500	1.73141	72.4204	96
29.5000	2.24958	181.121	90	31.7500	2.51450	36.2104	98	33.7500	1.74133	108.645	94
29.7500	2.00679	17.6334	49	31.7500	2.72560	72.4203	96	33.7500	1.77413	144.878	92
29.7500	1.97879	36.2104	98	31.7500	2.92870	108.645	94	33.7500	1.68277	181.121	90
29.7500	1.97460	72.4204	96	31.7500	3.01868	144.878	92	34.0000	1.43708	15.0357	50
29.7500	1.89444	108.645	94	31.7500	2.58572	181.121	90	34.0000	1.71248	36.2104	98
29.7500	1.95333	144.878	92	32.0000	2.64432	16.7035	50	34.0000	1.83263	72.4204	96
29.7500	1.96484	181.121	90	32.0000	2.75692	36.2103	98	34.0000	1.67955	108.645	94
30.0000	1.75739	17.8415	49	32.0000	2.62899	72.4203	96	34.0000	1.77626	144.878	92
30.0000	1.78747	36.2103	98	32.0000	2.92169	108.645	94	34.0000	1.85462	181.121	90
30.0000	1.70370	72.4202	96	32.0000	3.05037	144.878	92	34.2500	1.76284	14.8281	50
30.0000	1.67534	108.645	94	32.0000	2.56387	181.121	90	34.2500	1.86842	36.2104	98
30.0000	1.78121	144.878	92	32.2500	2.40155	16.4954	50	34.2500	1.84960	72.4204	96
30.0000	1.81536	181.121	90	32.2500	2.45845	36.2104	98	34.2500	1.86760	108.645	94
30.2500	1.79179	18.0516	49	32.2500	2.49662	72.4203	96	34.2500	1.92526	144.878	92
30.2500	1.87977	36.2104	98	32.2500	2.73070	108.645	94	34.2500	2.03408	181.121	90
30.2500	1.66801	72.4204	96	32.2500	2.52850	144.878	92	34.5000	1.84641	14.6187	50
30.2500	1.69800	108.645	94	32.2500	2.54658	181.121	90	34.5000	2.04266	36.2104	98
30.2500	1.77537	144.878	92	32.5000	2.18188	16.2869	50	34.5000	1.96033	72.4204	96
30.2500	1.74299	181.121	90	32.5000	2.12853	36.2104	98	34.5000	2.05108	108.645	94
30.5000	1.61222	17.9545	50	32.5000	2.27307	72.4204	96	34.5000	2.02702	144.878	92
30.5000	1.69852	36.2103	98	32.5000	2.27070	108.645	94	34.5000	2.21234	181.121	90
30.5000	1.61519	72.4202	96	32.5000	2.02530	144.878	92	34.7500	1.98476	14.4112	50
30.5000	1.57807	108.645	94	32.5000	2.03593	181.121	90	34.7500	2.16953	36.2104	98
30.5000	1.65555	144.878	92	32.7500	2.09751	16.0776	50	34.7500	2.04150	72.4203	96

Table C2. Continued

Azimuth	SD power	Time	N	Azimuth	SD power	Time	N	Azimuth	SD power	Time	N
34.7500	2.19265	108.645	94	36.7500	2.61236	181.121	90	39.0000	2.47023	36.2104	98
34.7500	2.15694	144.878	92	37.0000	2.15456	12.5359	50	39.0000	2.73876	72.4204	96
34.7500	2.29498	181.121	90	37.0000	2.51455	36.2104	98	39.0000	2.53880	108.645	94
35.0000	2.12874	14.2026	50	37.0000	2.51834	72.4204	96	39.0000	2.69347	144.878	92
35.0000	2.15265	36.2103	98	37.0000	2.51200	108.645	94	39.0000	2.65328	181.121	90
35.0000	2.13170	72.4203	96	37.0000	2.52025	144.878	92	39.2500	2.49896	10.6609	50
35.0000	2.32360	108.645	94	37.0000	2.57516	181.121	90	39.2500	2.54914	36.2104	98
35.0000	2.21061	144.878	92	37.2500	2.50924	12.3284	50	39.2500	2.49481	72.4203	96
35.0000	2.32309	181.121	90	37.2500	2.60535	36.2103	98	39.2500	2.63571	108.645	94
35.2500	2.22931	13.9936	50	37.2500	2.44548	72.4203	96	39.2500	2.59576	144.878	92
35.2500	2.60300	36.2104	98	37.2500	2.70110	108.645	94	39.2500	2.77632	181.121	90
35.2500	2.54849	72.4204	96	37.2500	2.82769	144.878	92	39.5000	2.68072	25.7612	49
35.2500	2.73208	108.645	94	37.2500	2.70413	181.121	90	39.5000	2.83751	36.2103	98
35.2500	2.36396	144.878	92	37.5000	2.52463	12.1186	50	39.5000	2.71905	72.4204	96
35.2500	2.40864	181.121	90	37.5000	2.57434	36.2104	98	39.5000	2.94321	108.645	94
35.5000	2.51440	13.7862	50	37.5000	2.39290	72.4204	96	39.5000	2.76538	144.878	92
35.5000	2.82765	36.2104	98	37.5000	2.68749	108.645	94	39.5000	3.08259	181.121	90
35.5000	2.63665	72.4203	96	37.5000	2.81751	144.878	92	39.7500	2.48579	10.2429	50
35.5000	2.87108	108.645	94	37.5000	2.57792	181.121	90	39.7500	2.88077	36.2103	98
35.5000	2.62583	144.878	92	37.7500	2.27546	11.9114	50	39.7500	2.85434	72.4204	96
35.5000	2.63534	181.121	90	37.7500	2.39084	36.2103	98	39.7500	3.00077	108.645	94
35.7500	2.54446	13.5780	50	37.7500	2.36063	72.4203	96	39.7500	2.86950	144.878	92
35.7500	2.80466	36.2103	98	37.7500	2.34674	108.645	94	39.7500	3.05300	181.121	90
35.7500	2.63478	72.4203	96	37.7500	2.66535	144.878	92	40.0000	2.59655	10.0350	50
35.7500	2.87903	108.645	94	37.7500	2.33186	181.121	90	40.0000	2.87681	36.2103	98
35.7500	2.85820	144.878	92	38.0000	2.20287	11.7025	50	40.0000	2.70706	72.4203	96
35.7500	2.87628	181.121	90	38.0000	2.25717	36.2104	98	40.0000	2.96228	108.645	94
36.0000	2.29645	13.3692	50	38.0000	2.33971	72.4203	96	40.0000	2.78838	144.878	92
36.0000	2.65631	36.2103	98	38.0000	2.19804	108.645	94	40.0000	3.05321	181.121	90
36.0000	2.73439	72.4203	96	38.0000	2.52493	144.878	92	40.2500	3.41955	9.82625	50
36.0000	2.61769	108.645	94	38.0000	2.14745	181.121	90	40.2500	3.58435	36.2104	98
36.0000	3.08472	144.878	92	38.2500	2.32234	11.4939	50	40.2500	3.05840	72.4204	96
36.0000	2.89501	181.121	90	38.2500	2.34247	36.2104	98	40.2500	3.57792	108.645	94
36.2500	2.63465	13.1605	50	38.2500	2.40306	72.4203	96	40.2500	3.33658	144.878	92
36.2500	2.71954	36.2104	98	38.2500	2.40414	108.645	94	40.2500	3.36694	181.121	90
36.2500	2.83668	72.4204	96	38.2500	2.42462	144.878	92	40.5000	3.30235	9.61812	50
36.2500	2.67747	108.645	94	38.2500	2.15964	181.121	90	40.5000	3.71173	36.2103	98
36.2500	2.88103	144.878	92	38.5000	2.01604	11.2859	50	40.5000	3.17891	72.4203	96
36.2500	2.85975	181.121	90	38.5000	2.24961	36.2104	98	40.5000	3.34304	108.645	94
36.5000	2.74904	12.9532	50	38.5000	2.20473	72.4204	96	40.5000	3.22818	144.878	92
36.5000	2.83585	36.2103	98	38.5000	2.25027	108.645	94	40.5000	3.34005	181.121	90
36.5000	2.76609	72.4203	96	38.5000	2.10063	144.878	92	40.7500	3.44161	9.40875	50
36.5000	2.87773	108.645	94	38.5000	2.14571	181.121	90	40.7500	3.47264	36.2103	98
36.5000	2.94546	144.878	92	38.7500	2.24344	11.0773	50	40.7500	2.99720	72.4202	96
36.5000	2.74840	181.121	90	38.7500	2.46606	36.2103	98	40.7500	3.19796	108.645	94
36.7500	2.42683	12.7446	50	38.7500	2.31827	72.4204	96	40.7500	3.04447	144.878	92
36.7500	2.53308	36.2103	98	38.7500	2.30700	108.645	94	40.7500	3.13784	181.121	90
36.7500	2.56056	72.4202	96	38.7500	2.29038	144.878	92	41.0000	3.25637	9.20031	50
36.7500	2.55388	108.645	94	38.7500	2.42837	181.121	90	41.0000	3.01301	36.2104	98
36.7500	2.43414	144.878	92	39.0000	2.70879	10.8684	50	41.0000	2.87563	72.4204	96

Azimuth	SD power	Time	N	Azimuth	SD power	Time	N	Azimuth	SD power	Time	N
41.0000	2.77996	108.645	94	43.0000	2.58887	181.121	90	45.2500	2.12263	36.2103	98
41.0000	3.11327	144.878	92	43.2500	2.41253	7.32203	50	45.2500	2.26826	72.4203	96
41.0000	3.11469	181.121	90	43.2500	2.32940	36.2103	98	45.2500	2.33712	108.645	94
41.2500	3.13319	8.99164	50	43.2500	2.52281	72.4203	96	45.2500	2.48383	144.877	92
41.2500	3.38934	36.2104	98	43.2500	2.41275	108.645	94	45.2500	2.20208	181.121	90
41.2500	3.25812	72.4204	96	43.2500	2.11684	144.878	92	45.5000	1.88446	5.44305	50
41.2500	2.93710	108.645	94	43.2500	2.31436	181.121	90	45.5000	2.02519	36.2104	98
41.2500	3.53131	144.878	92	43.5000	2.39044	7.11445	50	45.5000	2.21742	72.4204	96
41.2500	3.31535	181.121	90	43.5000	2.15895	36.2104	98	45.5000	2.18195	108.645	94
41.5000	3.23239	8.78297	50	43.5000	2.36261	72.4204	96	45.5000	2.30025	144.878	92
41.5000	3.25762	36.2104	98	43.5000	2.33989	108.645	94	45.5000	2.13959	181.121	90
41.5000	3.21970	72.4204	96	43.5000	2.33114	144.878	92	45.7500	1.78210	5.23336	50
41.5000	3.12211	108.645	94	43.5000	2.40060	181.121	90	45.7500	2.29027	36.2103	98
41.5000	3.34478	144.878	92	43.7500	2.11531	6.90531	50	45.7500	2.28566	72.4203	96
41.5000	3.33486	181.121	90	43.7500	2.29809	36.2104	98	45.7500	2.11867	108.645	94
41.7500	2.88262	8.57477	50	43.7500	2.41371	72.4203	96	45.7500	2.37928	144.878	92
41.7500	3.07625	36.2104	98	43.7500	2.42139	108.645	94	45.7500	2.34525	181.121	90
41.7500	2.83180	72.4204	96	43.7500	2.55270	144.878	92	46.0000	1.78813	5.02422	50
41.7500	3.03364	108.645	94	43.7500	2.43465	181.121	90	46.0000	2.45375	36.2103	98
41.7500	3.05406	144.878	92	44.0000	2.41365	6.69688	50	46.0000	2.27303	72.4203	96
41.7500	3.02164	181.121	90	44.0000	2.75252	36.2103	98	46.0000	2.24005	108.645	94
42.0000	2.41600	8.36625	50	44.0000	2.78381	72.4203	96	46.0000	2.68477	144.878	92
42.0000	2.76129	36.2103	98	44.0000	2.73543	108.645	94	46.0000	2.48650	181.121	90
42.0000	2.51810	72.4203	96	44.0000	3.07832	144.878	92	46.2500	1.96769	4.81492	50
42.0000	2.61954	108.645	94	44.0000	2.84249	181.121	90	46.2500	2.69417	36.2104	98
42.0000	2.80011	144.877	92	44.2500	2.53833	6.48781	50	46.2500	2.46670	72.4204	96
42.0000	2.79156	181.121	90	44.2500	2.84194	36.2104	98	46.2500	2.59593	108.645	94
42.2500	2.72661	8.15656	50	44.2500	2.79412	72.4204	96	46.2500	2.69500	144.878	92
42.2500	2.42469	36.2104	98	44.2500	2.67267	108.645	94	46.2500	2.70540	181.121	90
42.2500	2.57478	72.4204	96	44.2500	3.06585	144.878	92	46.5000	1.85996	4.60609	50
42.2500	2.62849	108.645	94	44.2500	2.90050	181.121	90	46.5000	2.44941	36.2104	98
42.2500	2.46990	144.878	92	44.5000	2.63533	6.27906	50	46.5000	2.15258	72.4203	96
42.2500	2.66058	181.121	90	44.5000	2.98038	36.2103	98	46.5000	2.55554	108.645	94
42.5000	2.64288	7.94859	50	44.5000	2.83930	72.4203	96	46.5000	2.30811	144.877	92
42.5000	2.63643	36.2104	98	44.5000	2.61339	108.645	94	46.5000	2.55700	181.121	90
42.5000	2.42356	72.4204	96	44.5000	2.86754	144.878	92	46.7500	2.31144	4.39531	50
42.5000	2.50809	108.645	94	44.5000	2.90864	181.121	90	46.7500	2.59643	36.2103	98
42.5000	2.64768	144.878	92	44.7500	2.65179	6.06969	50	46.7500	2.59757	72.4204	96
42.5000	2.71414	181.121	90	44.7500	2.82154	36.2104	98	46.7500	2.73674	108.645	94
42.7500	2.39252	7.74031	50	44.7500	2.78926	72.4204	96	46.7500	2.42758	144.878	92
42.7500	2.82037	36.2104	98	44.7500	2.57978	108.645	94	46.7500	2.92744	181.121	90
42.7500	2.29588	72.4203	96	44.7500	3.01883	144.878	92	47.0000	2.47547	4.18617	50
42.7500	2.56049	108.645	94	44.7500	2.86183	181.121	90	47.0000	2.70141	36.2103	98
42.7500	2.67069	144.878	92	45.0000	2.30119	5.86078	50	47.0000	2.63341	72.4203	96
42.7500	2.57400	181.121	90	45.0000	2.46114	36.2104	98	47.0000	2.89840	108.645	94
43.0000	2.51329	7.53086	50	45.0000	2.41526	72.4204	96	47.0000	2.58192	144.878	92
43.0000	2.81036	36.2103	98	45.0000	2.36013	108.645	94	47.0000	2.99951	181.121	90
43.0000	2.38392	72.4203	96	45.0000	2.81441	144.878	92	47.2500	2.50834	3.97563	50
43.0000	2.66691	108.645	94	45.0000	2.48566	181.121	90	47.2500	2.56408	36.2104	98
43.0000	2.52507	144.878	92	45.2500	2.00555	5.65234	50	47.2500	2.44458	72.4204	96

Table C2. Concluded

Azimuth	SD power	Time	N	Azimuth	SD power	Time	N
47.2500	2.62096	108.645	94	48.5000	1.99855	72.4204	96
47.2500	2.51515	144.878	92	48.5000	2.28518	108.645	94
47.2500	2.50629	181.121	90	48.5000	2.26599	144.878	92
47.5000	2.44029	3.76633	50	48.5000	2.41984	181.121	90
47.5000	2.48604	36.2103	98	48.7500	1.94497	2.71344	50
47.5000	2.53893	72.4202	96	48.7500	2.73009	36.2103	98
47.5000	2.74956	108.645	94	48.7500	2.38999	72.4203	96
47.5000	2.48477	144.878	92	48.7500	2.38837	108.645	94
47.5000	2.61432	181.121	90	48.7500	2.53360	144.878	92
47.7500	2.08293	3.55625	50	48.7500	2.52054	181.121	90
47.7500	2.10234	36.2103	98	49.0000	1.86157	2.50195	50
47.7500	2.20993	72.4202	96	49.0000	2.48001	36.2103	98
47.7500	2.49158	108.645	94	49.0000	2.20841	72.4202	96
47.7500	2.39393	144.877	92	49.0000	2.14510	108.645	94
47.7500	2.48069	181.121	90	49.0000	2.40405	144.877	92
48.0000	1.82711	3.34508	50	49.0000	2.27523	181.121	90
48.0000	2.03055	36.2103	98	49.2500	2.00424	2.28930	50
48.0000	1.95340	72.4203	96	49.2500	2.26084	36.2103	98
48.0000	2.32953	108.645	94	49.2500	1.93743	72.4202	96
48.0000	2.33798	144.877	92	49.2500	1.97363	108.645	94
48.0000	2.43321	181.121	90	49.2500	2.03616	144.877	92
48.2500	1.87692	3.13539	50	49.2500	2.26058	181.121	90
48.2500	1.88965	36.2104	98	49.5000	2.28072	2.07836	50
48.2500	1.85487	72.4203	96	49.5000	2.45436	36.2104	98
48.2500	2.07192	108.645	94	49.5000	2.09427	72.4204	96
48.2500	2.20506	144.878	92	49.5000	2.39108	108.645	94
48.2500	2.27829	181.121	90	49.5000	2.16974	144.878	92
48.5000	1.80633	2.92398	50	49.5000	2.43425	181.121	90
48.5000	2.18713	36.2104	98				

Table C3. Unsmoothed Data for Figure 6, Elevation Scans at 141° Azimuth

Elevation	SD power	Time	N	Elevation	SD power	Time	N	Elevation	SD power	Time	N
11.0000	2.32381	2.12925	46	13.0000	2.65455	74.5643	90	15.0000	2.50956	149.177	86
11.0000	2.58288	37.2756	92	13.0000	2.37214	111.867	88	15.0000	2.70711	186.477	84
11.0000	2.70195	74.5643	90	13.0000	2.31525	149.177	86	15.2500	2.31699	5.82201	46
11.0000	2.80817	111.867	88	13.0000	2.59538	186.477	84	15.2500	2.53601	37.2758	92
11.0000	2.89228	149.177	86	13.2500	2.00581	4.09256	46	15.2500	2.70104	74.5645	90
11.0000	2.72977	186.478	84	13.2500	2.22633	37.2757	92	15.2500	2.80818	111.867	88
11.2500	2.20989	2.34868	46	13.2500	2.47987	74.5644	90	15.2500	2.72992	149.177	86
11.2500	2.42677	37.2756	92	13.2500	2.19303	111.867	88	15.2500	2.83365	186.478	84
11.2500	2.69642	74.5642	90	13.2500	2.28109	149.177	86	15.5000	2.52749	6.03991	46
11.2500	2.77951	111.867	88	13.2500	2.65120	186.478	84	15.5000	2.78995	37.2757	92
11.2500	2.82822	149.177	86	13.5000	2.03202	4.30825	46	15.5000	2.77034	74.5643	90
11.2500	2.93491	186.478	84	13.5000	2.07059	37.2756	92	15.5000	2.76811	111.867	88
11.5000	2.76370	2.56726	46	13.5000	2.37392	74.5643	90	15.5000	2.73609	149.177	86
11.5000	2.66818	37.2756	92	13.5000	2.17167	111.867	88	15.5000	2.85793	186.477	84
11.5000	2.99206	74.5644	90	13.5000	2.29192	149.177	86	15.7500	2.52668	6.25594	46
11.5000	3.02834	111.867	88	13.5000	2.44281	186.477	84	15.7500	2.60113	37.2756	92
11.5000	3.06946	149.177	86	13.7500	1.80945	4.52480	46	15.7500	2.45547	74.5642	90
11.5000	3.17619	186.478	84	13.7500	2.05498	37.2756	92	15.7500	2.51473	111.866	88
11.7500	2.37101	2.78550	46	13.7500	2.19919	74.5643	90	15.7500	2.56782	149.177	86
11.7500	2.40330	37.2757	92	13.7500	2.23598	111.867	88	15.7500	2.71260	186.477	84
11.7500	2.86534	74.5646	90	13.7500	2.26423	149.177	86	16.0000	2.49608	6.47079	46
11.7500	2.87777	111.867	88	13.7500	2.54395	186.477	84	16.0000	2.21768	37.2757	92
11.7500	3.06539	149.177	86	14.0000	2.16068	4.74168	46	16.0000	2.31184	74.5644	90
11.7500	3.05642	186.478	84	14.0000	2.05103	37.2757	92	16.0000	2.36949	111.867	88
12.0000	2.23877	3.00391	46	14.0000	2.26210	74.5645	90	16.0000	2.62141	149.177	86
12.0000	2.27412	37.2757	92	14.0000	2.11032	111.867	88	16.0000	2.44945	186.478	84
12.0000	2.54743	74.5644	90	14.0000	2.20355	149.177	86	16.2500	2.40801	6.68665	46
12.0000	2.64662	111.867	88	14.0000	2.54909	186.478	84	16.2500	1.99775	37.2758	92
12.0000	2.57474	149.177	86	14.2500	2.00104	4.95890	46	16.2500	2.04234	74.5646	90
12.0000	2.63877	186.478	84	14.2500	2.15411	37.2758	92	16.2500	2.09931	111.867	88
12.2500	2.28226	3.22266	46	14.2500	2.37668	74.5645	90	16.2500	2.36327	149.177	86
12.2500	2.38832	37.2756	92	14.2500	2.16768	111.867	88	16.2500	2.35939	186.478	84
12.2500	2.60899	74.5643	90	14.2500	2.13129	149.177	86	16.5000	2.38683	6.90234	46
12.2500	2.51605	111.867	88	14.2500	2.46714	186.478	84	16.5000	2.27087	37.2757	92
12.2500	2.74268	149.177	86	14.5000	2.06180	5.17527	46	16.5000	2.18753	74.5644	90
12.2500	2.56129	186.478	84	14.5000	2.17794	37.2757	92	16.5000	2.27776	111.867	88
12.5000	1.82621	3.44005	46	14.5000	2.45819	74.5645	90	16.5000	2.27539	149.177	86
12.5000	2.33229	37.2756	92	14.5000	2.29535	111.867	88	16.5000	2.46454	186.477	84
12.5000	2.49517	74.5644	90	14.5000	2.18385	149.177	86	16.7500	2.49291	7.11906	46
12.5000	2.42011	111.867	88	14.5000	2.38802	186.478	84	16.7500	2.50448	37.2757	92
12.5000	2.62661	149.177	86	14.7500	1.66934	5.39062	46	16.7500	2.27816	74.5645	90
12.5000	2.47608	186.478	84	14.7500	2.29872	37.2756	92	16.7500	2.36159	111.867	88
12.7500	1.59473	3.65744	46	14.7500	2.14376	74.5642	90	16.7500	2.47069	149.177	86
12.7500	2.33180	37.2756	92	14.7500	2.24935	111.866	88	16.7500	2.26162	186.478	84
12.7500	2.60498	74.5643	90	14.7500	2.15551	149.177	86	17.0000	2.27341	7.33407	46
12.7500	2.44089	111.867	88	14.7500	2.23979	186.477	84	17.0000	2.34902	37.2756	92
12.7500	2.50663	149.177	86	15.0000	2.21196	5.60785	46	17.0000	2.31000	74.5643	90
12.7500	2.59382	186.478	84	15.0000	2.64323	37.2756	92	17.0000	2.20746	111.867	88
13.0000	1.75989	3.87534	46	15.0000	2.67103	74.5644	90	17.0000	2.26897	149.177	86
13.0000	2.20894	37.2757	92	15.0000	2.59592	111.867	88	17.0000	2.17592	186.477	84

Table C3. Continued

Elevation	SD power	Time	N	Elevation	SD power	Time	N	Elevation	SD power	Time	N
17.2500	1.97206	7.54908	46	19.2500	2.18672	74.5643	90	21.2500	2.59979	149.177	86
17.2500	2.11671	37.2756	92	19.2500	2.46618	111.867	88	21.2500	2.59357	186.478	84
17.2500	2.11025	74.5643	90	19.2500	2.29948	149.177	86	21.5000	2.83405	11.2143	46
17.2500	2.05280	111.867	88	19.2500	2.25233	186.477	84	21.5000	2.59814	37.2757	92
17.2500	2.07866	149.177	86	19.5000	2.27073	9.49015	46	21.5000	2.55869	74.5645	90
17.2500	2.14443	186.477	84	19.5000	2.10610	37.2758	92	21.5000	2.88320	111.867	88
17.5000	2.19408	7.76613	46	19.5000	2.40155	74.5646	90	21.5000	2.95580	149.177	86
17.5000	2.22957	37.2757	92	19.5000	2.67426	111.867	88	21.5000	3.07140	186.477	84
17.5000	2.24129	74.5645	90	19.5000	2.63208	149.177	86	21.7500	2.74884	11.4292	46
17.5000	2.37595	111.867	88	19.5000	2.53744	186.478	84	21.7500	2.61833	37.2757	92
17.5000	2.56729	149.177	86	19.7500	2.12386	9.70584	46	21.7500	2.67050	74.5643	90
17.5000	2.41633	186.478	84	19.7500	2.17837	37.2757	92	21.7500	2.88985	111.867	88
17.7500	2.44268	7.98064	46	19.7500	2.41177	74.5645	90	21.7500	2.98649	149.177	86
17.7500	2.38442	37.2758	92	19.7500	2.43249	111.867	88	21.7500	3.14394	186.477	84
17.7500	2.26207	74.5646	90	19.7500	2.43089	149.177	86	22.0000	2.92587	11.6456	46
17.7500	2.46570	111.867	88	19.7500	2.28623	186.478	84	22.0000	2.75511	37.2758	92
17.7500	2.63695	149.177	86	20.0000	2.11597	9.92086	46	22.0000	3.19519	74.5645	90
17.7500	2.53900	186.478	84	20.0000	2.15170	37.2758	92	22.0000	3.17371	111.867	88
18.0000	2.22817	8.19616	46	20.0000	2.16860	74.5645	90	22.0000	3.22492	149.177	86
18.0000	2.37708	37.2757	92	20.0000	2.24694	111.867	88	22.0000	3.25094	186.477	84
18.0000	2.12843	74.5644	90	20.0000	2.14410	149.177	86	22.2500	3.09555	11.8609	46
18.0000	2.62219	111.867	88	20.0000	2.20804	186.477	84	22.2500	3.14154	37.2759	92
18.0000	2.51495	149.177	86	20.2500	2.26585	10.1377	46	22.2500	3.48684	74.5647	90
18.0000	2.60632	186.477	84	20.2500	2.10446	37.2757	92	22.2500	3.53491	111.867	88
18.2500	2.39814	8.41168	46	20.2500	2.20728	74.5644	90	22.2500	3.48927	149.177	86
18.2500	2.58818	37.2756	92	20.2500	2.29735	111.867	88	22.2500	3.23747	186.478	84
18.2500	2.47447	74.5644	90	20.2500	2.23104	149.177	86	22.5000	3.23597	12.0764	46
18.2500	2.84696	111.867	88	20.2500	2.45340	186.477	84	22.5000	3.28472	37.2758	92
18.2500	2.91358	149.177	86	20.5000	2.21801	10.3524	46	22.5000	3.56813	74.5646	90
18.2500	2.96067	186.477	84	20.5000	2.07687	37.2758	92	22.5000	3.39146	111.867	88
18.5000	2.09772	8.62891	46	20.5000	2.12900	74.5646	90	22.5000	3.63685	149.177	86
18.5000	2.27754	37.2758	92	20.5000	2.16907	111.867	88	22.5000	3.36358	186.477	84
18.5000	2.40242	74.5646	90	20.5000	2.37235	149.177	86	22.7500	2.71642	12.2926	46
18.5000	2.43737	111.867	88	20.5000	2.16237	186.478	84	22.7500	3.05833	37.2757	92
18.5000	2.55501	149.177	86	20.7500	2.43980	10.5672	46	22.7500	3.18670	74.5643	90
18.5000	2.54356	186.477	84	20.7500	2.34942	37.2757	92	22.7500	2.98198	111.867	88
18.7500	2.11208	8.84273	46	20.7500	2.27138	74.5645	90	22.7500	3.07166	149.177	86
18.7500	2.23162	37.2759	92	20.7500	2.26434	111.867	88	22.7500	2.95919	186.477	84
18.7500	2.22747	74.5647	90	20.7500	2.46787	149.177	86	23.0000	2.17277	12.5071	46
18.7500	2.40848	111.867	88	20.7500	2.12081	186.477	84	23.0000	2.45792	37.2758	92
18.7500	2.39579	149.177	86	21.0000	2.60425	10.7835	46	23.0000	2.80833	74.5646	90
18.7500	2.45572	186.478	84	21.0000	2.59706	37.2758	92	23.0000	2.55387	111.867	88
19.0000	2.30336	9.05910	46	21.0000	2.45155	74.5645	90	23.0000	2.40031	149.177	86
19.0000	2.38883	37.2758	92	21.0000	2.53022	111.867	88	23.0000	2.15434	186.478	84
19.0000	2.23674	74.5646	90	21.0000	2.57298	149.177	86	23.2500	2.08375	12.7227	46
19.0000	2.57643	111.867	88	21.0000	2.42104	186.477	84	23.2500	2.02286	37.2757	92
19.0000	2.44845	149.177	86	21.2500	2.70147	10.9990	46	23.2500	2.24215	74.5645	90
19.0000	2.50349	186.477	84	21.2500	2.61978	37.2759	92	23.2500	2.17185	111.867	88
19.2500	2.24373	9.27446	46	21.2500	2.52862	74.5647	90	23.2500	2.14499	149.177	86
19.2500	2.19890	37.2756	92	21.2500	2.61780	111.867	88	23.2500	1.90407	186.477	84

Elevation	SD power	Time	N	Elevation	SD power	Time	N	Elevation	SD power	Time	N
23.5000	1.83014	12.9375	46	25.5000	2.56255	74.5643	90	27.5000	2.76491	149.177	86
23.5000	1.91421	37.2759	92	25.5000	2.51851	111.867	88	27.5000	3.00388	186.478	84
23.5000	1.85831	74.5646	90	25.5000	3.00053	149.177	86	27.7500	2.48936	16.5992	46
23.5000	1.93411	111.867	88	25.5000	2.72823	186.477	84	27.7500	2.39698	37.2758	92
23.5000	1.89481	149.177	86	25.7500	2.27306	14.8762	46	27.7500	2.52084	74.5645	90
23.5000	2.02111	186.477	84	25.7500	2.24165	37.2758	92	27.7500	2.51375	111.867	88
23.7500	1.89848	13.1535	46	25.7500	2.14656	74.5646	90	27.7500	2.58899	149.177	86
23.7500	1.93395	37.2758	92	25.7500	2.30155	111.867	88	27.7500	2.94195	186.477	84
23.7500	2.06877	74.5645	90	25.7500	2.52276	149.177	86	28.0000	2.63792	16.8156	46
23.7500	1.94346	111.867	88	25.7500	2.30743	186.478	84	28.0000	2.54471	37.2757	92
23.7500	1.98301	149.177	86	26.0000	2.44933	15.0919	46	27.5000	2.76491	149.177	86
23.7500	2.09248	186.478	84	26.0000	2.14632	37.2758	92	28.0000	2.52119	74.5645	90
24.0000	2.09002	13.3680	46	26.0000	2.23650	74.5645	90	28.0000	2.44880	111.867	88
24.0000	1.97522	37.2757	92	26.0000	2.37250	111.867	88	28.0000	2.50819	149.177	86
24.0000	2.03979	74.5645	90	26.0000	2.41231	149.177	86	28.0000	2.80180	186.477	84
24.0000	1.90833	111.867	88	26.0000	2.35729	186.477	84	28.2500	2.48372	17.0306	46
24.0000	2.06047	149.177	86	26.2500	2.42278	15.3072	46	28.2500	2.73717	37.2758	92
24.0000	2.05309	186.477	84	26.2500	2.30841	37.2758	92	28.2500	2.45817	74.5647	90
24.2500	2.32826	13.5839	46	26.2500	2.73572	74.5644	90	28.2500	2.47413	111.867	88
24.2500	2.06268	37.2757	92	26.2500	2.65616	111.867	88	28.2500	2.23322	149.177	86
24.2500	2.30623	74.5645	90	26.2500	2.68207	149.177	86	28.2500	2.68972	186.478	84
24.2500	2.21540	111.867	88	26.2500	2.79553	186.477	84	28.5000	2.27642	17.2468	46
24.2500	2.19222	149.177	86	26.5000	2.61729	15.5226	46	28.5000	2.31783	37.2758	92
24.2500	2.20014	186.477	84	26.5000	2.72758	37.2757	92	28.5000	2.22775	74.5646	90
24.5000	2.16705	13.7998	46	26.5000	2.76165	74.5644	90	28.5000	2.26971	111.867	88
24.5000	2.09152	37.2758	92	26.5000	2.70009	111.867	88	28.5000	2.12176	149.177	86
24.5000	2.38300	74.5646	90	26.5000	2.69421	149.177	86	28.5000	2.49486	186.477	84
24.5000	2.49389	111.867	88	26.5000	3.04577	186.477	84	28.7500	2.12638	17.4620	46
24.5000	2.26835	149.177	86	26.7500	2.42550	15.7383	46	28.7500	2.09511	37.2758	92
24.5000	2.32639	186.478	84	26.7500	2.62683	37.2758	92	28.7500	2.07427	74.5645	90
24.7500	2.39790	14.0151	46	26.7500	2.68472	74.5645	90	28.7500	2.11951	111.867	88
24.7500	2.39600	37.2758	92	26.7500	2.69267	111.867	88	28.7500	2.02379	149.177	86
24.7500	2.89053	74.5646	90	26.7500	2.57109	149.177	86	28.7500	2.33349	186.477	84
24.7500	2.82226	111.867	88	26.7500	2.86596	186.477	84	29.0000	1.75109	17.6773	46
24.7500	2.78869	149.177	86	27.0000	2.47767	15.9535	46	29.0000	1.71580	37.2757	92
24.7500	2.61376	186.478	84	27.0000	2.61325	37.2759	92	29.0000	1.91607	74.5643	90
25.0000	2.68991	14.2296	46	27.0000	2.97303	74.5646	90	29.0000	1.74654	111.867	88
25.0000	2.65187	37.2757	92	27.0000	2.83325	111.867	88	29.0000	1.69657	149.177	86
25.0000	2.95023	74.5645	90	27.0000	2.91111	149.177	86	29.0000	1.99417	186.477	84
25.0000	2.99280	111.867	88	27.0000	3.08173	186.478	84	29.2500	1.96152	17.8930	46
25.0000	3.23161	149.177	86	27.2500	2.71359	16.1690	46	29.2500	1.88029	37.2758	92
25.0000	2.90655	186.477	84	27.2500	2.39299	37.2758	92	29.2500	1.90467	74.5646	90
25.2500	2.50127	14.4457	46	27.2500	2.88414	74.5645	90	29.2500	1.73885	111.867	88
25.2500	2.56746	37.2758	92	27.2500	2.81602	111.867	88	29.2500	1.91939	149.178	86
25.2500	2.70922	74.5645	90	27.2500	3.01422	149.177	86	29.2500	1.83655	186.478	84
25.2500	2.59837	111.867	88	27.2500	2.96609	186.477	84	29.5000	2.18635	18.1080	46
25.2500	3.17174	149.177	86	27.5000	2.70133	16.3842	46	29.5000	2.19599	37.2759	92
25.2500	2.95931	186.477	84	27.5000	2.45628	37.2758	92	29.5000	1.84893	74.5646	90
25.5000	2.56110	14.6613	46	27.5000	2.81656	74.5646	90	29.5000	1.85282	111.867	88
25.5000	2.54068	37.2757	92	27.5000	2.72799	111.867	88	29.5000	1.96238	149.177	86

Elevation	SD power	Time	N	Elevation	SD power	Time	N	Elevation	SD power	Time	N
29.5000	1.92729	186.477	84	31.7500	2.50172	74.5647	90	33.7500	2.47839	149.177	86
29.7500	2.32000	18.3234	46	31.7500	2.47130	111.867	88	33.7500	2.40181	186.477	84
29.7500	2.45276	37.2758	92	31.7500	2.50737	149.177	86	34.0000	2.12490	15.2911	47
29.7500	2.17774	74.5645	90	31.7500	2.70365	186.477	84	34.0000	2.39253	37.2757	92
29.7500	1.95841	111.867	88	32.0000	2.69618	17.0140	47	34.0000	2.22579	74.5645	90
29.7500	2.33490	149.177	86	32.0000	2.33118	37.2759	92	34.0000	2.11691	111.867	88
29.7500	2.20236	186.477	84	32.0000	2.49659	74.5648	90	34.0000	2.40407	149.177	86
30.0000	1.99879	18.5394	46	32.0000	2.70651	111.867	88	34.0000	2.22294	186.477	84
30.0000	2.06069	37.2758	92	32.0000	2.75199	149.177	86	34.2500	2.33671	15.0750	47
30.0000	2.13675	74.5645	90	32.0000	2.73043	186.477	84	34.2500	2.24826	37.2759	92
30.0000	2.04409	111.867	88	32.2500	2.34006	16.7987	47	34.2500	2.23158	74.5647	90
30.0000	2.15309	149.177	86	32.2500	2.09592	37.2758	92	34.2500	2.25340	111.867	88
30.0000	2.02919	186.478	84	32.2500	2.19139	74.5645	90	34.2500	2.42304	149.177	86
30.2500	2.12804	18.5221	47	32.2500	2.21647	111.867	88	34.2500	2.28582	186.477	84
30.2500	2.13565	37.2758	92	32.2500	2.25556	149.177	86	34.5000	2.42073	14.8612	47
30.2500	2.32438	74.5645	90	32.2500	2.19589	186.477	84	34.5000	2.37080	37.2759	92
30.2500	2.28531	111.867	88	32.5000	2.00349	16.5836	47	34.5000	2.59704	74.5646	90
30.2500	2.19559	149.177	86	32.5000	1.86397	37.2758	92	34.5000	2.50874	111.867	88
30.2500	2.16736	186.477	84	32.5000	2.09818	74.5645	90	34.5000	2.43357	149.177	86
30.5000	2.34813	37.2758	92	32.5000	2.16529	111.867	88	34.5000	2.69120	186.477	84
30.5000	2.47805	74.5647	90	32.5000	2.06493	149.177	86	34.7500	2.16964	14.6454	47
30.5000	2.41668	111.867	88	32.5000	1.93139	186.477	84	34.7500	2.39065	37.2758	92
30.5000	2.35914	149.177	86	32.7500	1.78251	16.3675	47	34.7500	2.58675	74.5645	90
30.5000	2.37003	186.477	84	32.7500	2.09957	37.2757	92	34.7500	2.45484	111.867	88
30.7500	2.46761	18.0924	47	32.7500	2.27029	74.5645	90	34.7500	2.60509	149.177	86
30.7500	2.41268	37.2759	92	32.7500	2.10295	111.867	88	34.7500	2.58466	186.477	84
30.7500	2.45238	74.5646	90	32.7500	2.15335	149.177	86	35.0000	1.93490	14.4285	47
30.7500	2.59586	111.867	88	32.7500	2.14428	186.477	84	35.0000	2.06380	37.2758	92
30.7500	2.51228	149.177	86	33.0000	1.57585	16.1533	47	35.0000	2.17773	74.5645	90
30.7500	2.62384	186.477	84	33.0000	2.06602	37.2759	92	35.0000	2.27162	111.867	88
31.0000	2.36166	17.8763	47	33.0000	2.23595	74.5648	90	35.0000	2.35068	149.177	86
31.0000	2.38907	37.2758	92	33.0000	2.09109	111.867	88	35.0000	2.23985	186.477	84
31.0000	2.27226	74.5646	90	33.0000	2.04792	149.177	86	35.2500	1.65398	14.2149	47
31.0000	2.56105	111.867	88	33.0000	1.95818	186.477	84	35.2500	1.91264	37.2759	92
31.0000	2.34190	149.177	86	33.2500	1.83380	15.9368	47	35.2500	1.96275	74.5647	90
31.0000	2.68665	186.477	84	33.2500	2.14971	37.2759	92	35.2500	2.09523	111.867	88
31.2500	2.15018	17.6609	47	33.2500	2.29541	74.5646	90	35.2500	2.03274	149.177	86
31.2500	1.92913	37.2758	92	33.2500	2.16961	111.867	88	35.2500	2.08386	186.477	84
31.2500	2.09822	74.5646	90	33.2500	2.12329	149.177	86	35.5000	1.69852	13.9985	47
31.2500	2.17578	111.867	88	33.2500	2.13894	186.477	84	35.5000	2.14738	37.2760	92
31.2500	2.08571	149.177	86	33.5000	2.01601	15.7217	47	35.5000	2.10154	74.5648	90
31.2500	2.40131	186.477	84	33.5000	2.44062	37.2758	92	35.5000	2.31277	111.867	88
31.5000	2.20637	17.4446	47	33.5000	2.44405	74.5646	90	35.5000	2.18529	149.177	86
31.5000	2.04340	37.2757	92	33.5000	2.36170	111.867	88	35.5000	2.29844	186.477	84
31.5000	2.25407	74.5644	90	33.5000	2.34799	149.177	86	35.7500	1.86387	13.7822	47
31.5000	2.08119	111.867	88	33.5000	2.44003	186.477	84	35.7500	2.17278	37.2760	92
31.5000	2.22270	149.177	86	33.7500	1.95472	15.5062	47	35.7500	2.28430	74.5647	90
31.5000	2.38023	186.477	84	33.7500	2.39177	37.2758	92	35.7500	2.40369	111.867	88
31.7500	2.44271	17.2311	47	33.7500	2.36540	74.5646	90	35.7500	2.39580	149.177	86
31.7500	2.28150	37.2758	92	33.7500	2.22059	111.867	88	35.7500	2.29662	186.477	84

Elevation	SD power	Time	N	Elevation	SD power	Time	N	Elevation	SD power	Time	N
36.0000	2.07122	13.5680	47	38.0000	1.86754	74.5648	90	40.0000	2.02201	149.177	86
36.0000	2.19793	37.2758	92	38.0000	1.96027	111.867	88	40.0000	2.05538	186.477	84
36.0000	2.34215	74.5646	90	38.0000	1.93649	149.177	86	40.2500	1.81510	9.90459	47
36.0000	2.45224	111.867	88	38.0000	2.03208	186.477	84	40.2500	2.17578	37.2761	92
36.0000	2.53873	149.177	86	38.2500	1.85977	11.6288	47	40.2500	2.00956	74.5648	90
36.0000	2.22728	186.477	84	38.2500	1.92038	37.2759	92	40.2500	2.18393	111.867	88
36.2500	2.20568	13.3529	47	38.2500	1.93919	74.5646	90	40.2500	2.23266	149.177	86
36.2500	1.95919	37.2758	92	38.2500	2.07329	111.867	88	40.2500	2.10501	186.477	84
36.2500	2.03585	74.5646	90	38.2500	2.09824	149.177	86	40.5000	1.87643	9.68833	47
36.2500	2.12292	111.867	88	38.2500	2.22240	186.477	84	40.5000	2.27792	37.2760	92
36.2500	2.28458	149.177	86	38.5000	1.75476	11.4132	47	40.5000	2.33760	74.5647	90
36.2500	2.06339	186.477	84	38.5000	1.78582	37.2758	92	40.5000	2.51688	111.867	88
36.5000	2.33931	13.1378	47	38.5000	2.04360	74.5646	90	40.5000	2.55063	149.177	86
36.5000	2.22926	37.2760	92	38.5000	1.85193	111.867	88	40.5000	2.22115	186.477	84
36.5000	2.13948	74.5648	90	38.5000	2.03898	149.177	86	40.7500	2.40458	9.47141	47
36.5000	2.18281	111.867	88	38.5000	2.28428	186.477	84	40.7500	2.64356	37.2759	92
36.5000	2.37382	149.177	86	38.7500	2.00531	11.1990	47	40.7500	2.47962	74.5646	90
36.5000	2.31519	186.477	84	38.7500	1.99410	37.2759	92	40.7500	2.71619	111.867	88
36.7500	1.90993	12.9242	47	38.7500	2.18868	74.5648	90	40.7500	2.73682	149.177	86
36.7500	2.12173	37.2760	92	38.7500	2.10535	111.867	88	40.7500	2.26564	186.477	84
36.7500	2.19281	74.5648	90	38.7500	2.19790	149.177	86	41.0000	2.27262	9.25698	47
36.7500	2.19430	111.867	88	38.7500	2.26932	186.477	84	41.0000	2.40781	37.2760	92
36.7500	2.40366	149.177	86	39.0000	1.85264	10.9832	47	41.0000	2.38365	74.5647	90
36.7500	2.36214	186.477	84	39.0000	2.14022	37.2760	92	41.0000	2.54422	111.867	88
37.0000	1.66087	12.7071	47	39.0000	2.16682	74.5647	90	41.0000	2.58041	149.177	86
37.0000	1.83646	37.2758	92	39.0000	2.18089	111.867	88	41.0000	2.16951	186.477	84
37.0000	2.08804	74.5645	90	39.0000	2.31812	149.177	86	41.2500	2.17859	9.04338	47
37.0000	1.98786	111.867	88	39.0000	2.32595	186.477	84	41.2500	2.10069	37.2761	92
37.0000	2.19214	149.177	86	39.2500	1.99371	10.7676	47	41.2500	2.08058	74.5649	90
37.0000	2.09487	186.477	84	39.2500	2.31769	37.2760	92	41.2500	2.10933	111.867	88
37.2500	1.54583	12.4912	47	39.2500	2.30189	74.5647	90	41.2500	2.21139	149.177	86
37.2500	1.72658	37.2758	92	39.2500	2.41932	111.867	88	41.2500	1.90568	186.477	84
37.2500	1.76455	74.5646	90	39.2500	2.51968	149.177	86	41.5000	2.03319	8.82497	47
37.2500	1.75070	111.867	88	39.2500	2.59953	186.477	84	41.5000	1.85463	37.2761	92
37.2500	1.87482	149.177	86	39.5000	2.01382	10.5505	47	41.5000	1.84242	74.5647	90
37.2500	1.98434	186.477	84	39.5000	2.42615	37.2759	92	41.5000	1.92506	111.867	88
37.5000	1.47322	12.2758	47	39.5000	2.34328	74.5647	90	41.5000	2.10780	149.177	86
37.5000	1.66663	37.2758	92	39.5000	2.33342	111.867	88	41.5000	1.87337	186.477	84
37.5000	1.78192	74.5646	90	39.5000	2.52694	149.177	86	41.7500	2.27122	8.61004	47
37.5000	1.62740	111.867	88	39.5000	2.58542	186.477	84	41.7500	1.99763	37.2761	92
37.5000	1.78668	149.177	86	39.7500	1.91915	10.3371	47	41.7500	2.11819	74.5647	90
37.5000	1.90974	186.477	84	39.7500	2.16891	37.2760	92	41.7500	2.03327	111.867	88
37.7500	1.71627	12.0600	47	39.7500	2.10368	74.5647	90	41.7500	2.09141	149.177	86
37.7500	2.01816	37.2759	92	39.7500	2.02191	111.867	88	41.7500	2.04325	186.477	84
37.7500	2.05387	74.5648	90	39.7500	2.08900	149.177	86	42.0000	2.24431	8.39528	47
37.7500	1.78830	111.867	88	39.7500	2.13154	186.477	84	42.0000	2.01588	37.2760	92
37.7500	1.84680	149.177	86	40.0000	1.74178	10.1201	47	42.0000	2.21976	74.5648	90
37.7500	2.05861	186.477	84	40.0000	2.17215	37.2760	92	42.0000	2.05433	111.867	88
38.0000	1.81079	11.8447	47	40.0000	1.87251	74.5648	90	42.0000	2.05759	149.177	86
38.0000	2.01393	37.2760	92	40.0000	2.05009	111.867	88	42.0000	2.37996	186.477	84

Elevation	SD power	Time	N	Elevation	SD power	Time	N	Elevation	SD power	Time	N
42.2500	2.23834	8.17869	47	44.2500	1.96497	74.5646	90	46.2500	2.25860	149.177	86
42.2500	2.07615	37.2761	92	44.2500	2.18820	111.867	88	46.2500	2.34307	186.477	84
42.2500	2.31157	74.5648	90	44.2500	1.95801	149.177	86	46.5000	1.67766	4.50681	47
42.2500	2.25151	111.867	88	44.2500	2.22881	186.477	84	46.5000	1.76923	37.2760	92
42.2500	2.18406	149.177	86	44.5000	1.97823	6.23770	47	46.5000	1.81727	74.5648	90
42.2500	2.50456	186.478	84	44.5000	2.29025	37.2760	92	46.5000	1.88966	111.867	88
42.5000	2.40371	7.96443	47	44.5000	2.18791	74.5646	90	46.5000	1.81333	149.177	86
42.5000	2.23899	37.2762	92	44.5000	2.51754	111.867	88	46.5000	2.09382	186.477	84
42.5000	2.48056	74.5648	90	44.5000	2.17772	149.177	86	46.7500	2.05385	4.29023	47
42.5000	2.22206	111.867	88	44.5000	2.26327	186.477	84	46.7500	1.97608	37.2760	92
42.5000	2.07061	149.177	86	44.7500	1.94413	6.02194	47	46.7500	2.01030	74.5646	90
42.5000	2.33675	186.477	84	44.7500	2.14954	37.2760	92	46.7500	2.10872	111.867	88
42.7500	2.10220	7.74701	47	44.7500	2.06206	74.5648	90	46.7500	1.89686	149.177	86
42.7500	2.03456	37.2761	92	44.7500	2.31294	111.867	88	46.7500	2.14636	186.477	84
42.7500	2.18846	74.5648	90	44.7500	2.15804	149.177	86	47.0000	2.75851	4.07447	47
42.7500	1.91943	111.867	88	44.7500	2.25576	186.477	84	47.0000	2.38565	37.2760	92
42.7500	1.97679	149.177	86	45.0000	2.10127	5.80552	47	47.0000	2.29672	74.5648	90
42.7500	2.06198	186.477	84	45.0000	2.23375	37.2761	92	47.0000	2.55537	111.867	88
43.0000	1.64673	7.53208	47	45.0000	2.09756	74.5648	90	47.0000	2.28966	149.177	86
43.0000	1.94435	37.2759	92	45.0000	2.15114	111.867	88	47.0000	2.69269	186.477	84
43.0000	2.17039	74.5645	90	45.0000	2.02251	149.177	86	47.2500	2.73814	3.85688	47
43.0000	1.91268	111.867	88	45.0000	2.28942	186.477	84	47.2500	2.49253	37.2761	92
43.0000	2.00996	149.177	86	45.2500	2.10540	5.58910	47	47.2500	2.37879	74.5648	90
43.0000	2.14281	186.477	84	45.2500	2.09056	37.2761	92	47.2500	2.60845	111.867	88
43.2500	2.01651	7.31732	47	45.2500	2.06104	74.5647	90	47.2500	2.35623	149.177	86
43.2500	1.99107	37.2760	92	45.2500	1.98111	111.867	88	47.2500	2.57089	186.477	84
43.2500	2.22791	74.5646	90	45.2500	1.99590	149.177	86	47.5000	2.24505	3.63863	47
43.2500	2.09782	111.867	88	45.2500	2.12784	186.477	84	47.5000	2.26604	37.2760	92
43.2500	2.21668	149.177	86	45.5000	2.06554	5.37367	47	47.5000	2.43110	74.5647	90
43.2500	2.19419	186.477	84	45.5000	2.05191	37.2760	92	47.5000	2.52940	111.867	88
43.5000	2.06917	7.10040	47	45.5000	2.26338	74.5647	90	47.5000	2.47309	149.177	86
43.5000	1.84265	37.2760	92	45.5000	1.98031	111.867	88	47.5000	2.29898	186.477	84
43.5000	1.94729	74.5648	90	45.5000	1.71305	149.177	86	47.7500	2.30792	3.42221	47
43.5000	2.01772	111.867	88	45.5000	2.17886	186.477	84	47.7500	2.37559	37.2760	92
43.5000	2.10317	149.177	86	45.7500	2.12863	5.15708	47	47.7500	2.51875	74.5647	90
43.5000	2.15751	186.478	84	45.7500	2.20227	37.2760	92	47.7500	2.57100	111.867	88
43.7500	1.84100	6.88514	47	45.7500	2.49759	74.5646	90	47.7500	2.59602	149.177	86
43.7500	1.85826	37.2762	92	45.7500	2.09073	111.867	88	47.7500	2.46438	186.477	84
43.7500	2.04470	74.5649	90	45.7500	2.00952	149.177	86	48.0000	2.19221	3.20296	47
43.7500	1.94306	111.867	88	45.7500	2.26171	186.477	84	48.0000	2.55131	37.2760	92
43.7500	1.85652	149.178	86	46.0000	2.12534	4.93999	47	48.0000	2.66369	74.5646	90
43.7500	2.10824	186.478	84	46.0000	2.45143	37.2761	92	48.0000	2.58880	111.867	88
44.0000	1.74196	6.66872	47	46.0000	2.58729	74.5648	90	48.0000	2.61526	149.177	86
44.0000	1.84750	37.2760	92	46.0000	2.33249	111.867	88	48.0000	2.45505	186.477	84
44.0000	1.96819	74.5647	90	46.0000	2.35813	149.177	86	48.2500	2.39608	2.98637	47
44.0000	1.73328	111.867	88	46.0000	2.35391	186.477	84	48.2500	2.51862	37.2760	92
44.0000	1.69309	149.177	86	46.2500	2.02102	4.72424	47	48.2500	2.82599	74.5647	90
44.0000	2.01649	186.477	84	46.2500	2.05208	37.2761	92	48.2500	2.48604	111.867	88
44.2500	1.77672	6.45329	47	46.2500	2.47868	74.5647	90	48.2500	2.58829	149.177	86
44.2500	2.05313	37.2759	92	46.2500	2.26085	111.867	88	48.2500	2.55372	186.477	84

Table C3. Concluded

Elevation	SD power	Time	N
48.5000	2.30379	2.76762	47
48.5000	2.41135	37.2761	92
48.5000	2.73418	74.5647	90
48.5000	2.46775	111.867	88
48.5000	2.32684	149.177	86
48.5000	2.72334	186.477	84
48.7500	2.51315	2.54820	47
48.7500	2.43093	37.2760	92
48.7500	2.50799	74.5646	90
48.7500	2.49898	111.867	88
48.7500	2.39004	149.177	86
48.7500	2.85537	186.477	84
49.0000	2.18739	2.32962	47
49.0000	2.18251	37.2761	92
49.0000	2.35100	74.5647	90
49.0000	2.29388	111.867	88
49.0000	2.17371	149.177	86
49.0000	2.47091	186.477	84
49.2500	2.06427	2.10971	47
49.2500	2.28680	37.2759	92
49.2500	2.43249	74.5645	90
49.2500	2.18969	111.867	88
49.2500	2.26681	149.177	86
49.2500	2.53466	186.477	84

References

1. Hardy, Kenneth R.; and Gage, Kenneth S.: The History of Radar Studies of the Clear Atmosphere. *Radar in Meteorology—Battan Memorial and 40th Anniversary Radar Meteorology Conference*, David Atlas, ed., AMS, 1990, pp. 130–142.

2. Tatarski, V. I. (R. A. Silverman, transl.): *Wave Propagation in a Turbulent Medium.* McGraw-Hill Book Co., Inc., 1961.

3. Sauvageot, Henri: *Radar Meteorology.* Artech House, 1991.

4. Spiegel, E. A.; and Veronis, G.: On the Boussinesq Approximation for a Compressible Fluid. *J. Astrophys.*, vol. 131, 1960, pp. 442–447.

5. Proctor, Fred H.: Numerical Simulation of Wake Vortices Measured During the Idaho Falls and Memphis Field Programs. AIAA-96-2496, Jan. 1996.

6. Marshall, Robert E.; and Scales, Wayne: *Wake Vortex Radar Reflectivity.* RTI/4500/041-03S, Research Triangle Inst. (RTI), Mar. 1996.

7. Ottersten, H.: Radar Backscattering From the Turbulent Clear Atmosphere. *Radio Sci.*, vol. 4, pp. 1251–1255.

8. Gilson, W. H.: *Radar Measurements of Aircraft Wakes.* Proj. Rep. AAW-11, Lincoln Lab., F19628-90-C-0002, U.S. Air Force, Sept. 1992.

9. Nespor, Jerald D.; Hudson, B.; Stegall, R. L.; and Freedman, Jerome E.: Doppler Radar Detection of Vortex Hazard Indicators. *Airborne Windshear Detection and Warning Systems—Fifth and Final Combined Manufacturers' and Technologists' Conference*, Part 2, Victor E. Delnore, compiler, NASA CP-10139, DOT/FAA/RD-94-14-PT-2, July 1994, pp. 651–688.

10. Wonnacott, Ronald J.; and Wonnacott, Thomas H.: *Introductory Statistics.* John Wiley & Sons, 1985.

REPORT DOCUMENTATION PAGE

1. AGENCY USE ONLY (Leave blank)	2. REPORT DATE November 1997	3. REPORT TYPE AND DATES COVERED Technical Paper

4. TITLE AND SUBTITLE
Measured Changes in C-Band Radar Reflectivity of Clear Air Caused by Aircraft Wake Vortices

5. FUNDING NUMBERS
WU 548-10-41-01

6. AUTHOR(S)
Anne I. Mackenzie

7. PERFORMING ORGANIZATION NAME(S) AND ADDRESS(ES)
NASA Langley Research Center
Hampton, VA 23681-2199

8. PERFORMING ORGANIZATION REPORT NUMBER
L-17618

9. SPONSORING/MONITORING AGENCY NAME(S) AND ADDRESS(ES)
National Aeronautics and Space Administration
Washington, DC 20546-0001

10. SPONSORING/MONITORING AGENCY REPORT NUMBER
NASA TP-3671

11. SUPPLEMENTARY NOTES

12a. DISTRIBUTION/AVAILABILITY STATEMENT
Unclassified–Unlimited
Subject Category 32
Availability: NASA CASI (301) 621-0390

12b. DISTRIBUTION CODE

13. ABSTRACT (Maximum 200 words)
Wake vortices from a C-130 airplane were observed at the NASA Wallops Flight Facility with a ground-based, monostatic C-band radar and an antenna-mounted boresight video camera. The airplane wake was viewed from a distance of approximately 1 km, and radar scanning was adjusted to cross a pair of marker smoke trails generated by the C-130. For each airplane pass, changes in radar reflectivity were calculated by subtracting the signal magnitudes during an initial clutter scan from the signal magnitudes during vortex-plus-clutter scans. The results showed both increases and decreases in reflectivity on and near the smoke trails in a characteristic sinusoidal pattern of heightened reflectivity in the center and lessened reflectivity at the sides. Reflectivity changes in either direction varied from -131 to -102 dBm^{-1}; the vortex-plus-clutter to noise ratio varied from 20 to 41 dB. The radar recordings lasted 2.5 min each; evidence of wake vortices was found for up to 2 min after the passage of the airplane. Ground and aircraft clutter were eliminated as possible sources of the disturbance by noting the occurrence of vortex signatures at different positions relative to the ground and the airplane. This work supports the feasibility of vortex detection by radar, and it is recommended that future radar vortex detection be done with Doppler systems.

14. SUBJECT TERMS
Wake vortex detection; C-band radar; Bragg scattering; Clear-air reflectivity

15. NUMBER OF PAGES
80

16. PRICE CODE
A05

17. SECURITY CLASSIFICATION OF REPORT Unclassified	18. SECURITY CLASSIFICATION OF THIS PAGE Unclassified	19. SECURITY CLASSIFICATION OF ABSTRACT Unclassified	20. LIMITATION OF ABSTRACT